ANNALS OF THE OBSERVATORY OF LUND. No. 18:1

THREE-DIMENSIONAL GALACTIC STELLAR ORBITS

BY

A. OLLONGREN

THREE-DIMENSIONAL GALACTIC STELLAR ORBITS

A. OLLONGREN

TABLE OF ERRATA

Page	column	line	formula	read:
10	1		(1.1)	$\dot{p}_i = -\frac{\partial H}{\partial q_i}$ $(i = 1, 2, \ldots, n)$
12	2		(2.2)	$-\infty$ for lower limit of integral
23	1			under subtitle of Figure 5: F (non)-isolating
28	2	1		Figure 6
30	2		(12.2)	second term in definition of g_{22}: $\frac{1}{J^2}\left(\frac{\partial F}{\partial z}\right)^2$
30	2		(12.4)	third term in definition of K: $\frac{1}{2} J^2 g_{11} p_\mu{}^2$
31	3	3		insert F before "only"
31	1		(5)	$U = \frac{1}{2}\frac{h^2}{e^{2r}\cos^2\varphi} + \Phi(r)$
31	1			OFF-CENTRE ELLIPTIC COORDINATES: (see footnote page 27)
34			(15.8)	second term in definition of Q_{II}: P_a/P_b
35	2	6		(15.11)
42	2	6		velocity components
55	1	52		$\ddot{y} = +a$
56	1	52		$I = (\sqrt{\lvert \Pi/Z \rvert})_{z=0}$
63	1			G. HAMEL 1949, "Theoretische Mechanik", Springer-Verlag, Berlin, Göttingen, Heidelberg.

THREE-DIMENSIONAL GALACTIC STELLAR ORBITS

BY A. OLLONGREN

The properties of three-dimensional orbits of stars in the galactic system are studied with the objective of gaining more insight into the dynamical properties of the system as a whole. The galactic potential function is taken to be a known time-independent function with both an axis and a plane of symmetry. By means of the integral of angular momentum the problem is reduced to the two-dimensional one of motion in the meridional plane. This is then solved by numerical integration.

One reason for undertaking the computation of these orbits was the discrepancy between the inequality of the meridional velocity dispersions, observed for high-velocity as well as for low-velocity stars, and a theorem of JEANS. Under the assumption that there are only two integrals of motion, this theorem predicts circular symmetry of the meridional velocity distribution for any axisymmetric stellar system in dynamical equilibrium. The present computations show that in the galactic field of force there is no conversion between the two meridional components of the motion. They give empirical evidence for the existence of a third integral of motion, though no explicit form has been found for this integral.

Analytical solutions can be obtained if the potential has a special form admitting separation of variables in a suitable coordinate system. The most general separable case is that of elliptic coordinates; in this case the third integral of motion is quadratic in the velocities. In practice separation is always possible for low velocities, but the method cannot be applied to the high-velocity orbits treated in the present paper.

The numerical computations are concerned with only one family of orbits (i.e. one value of the area constant and one energy). A detailed phenomenology for the meridional motion of one class of orbits within this family is given; all orbits of this class have been called box-type orbits, because the meridional trajectory, which is topologically equivalent to a Lissajous figure, fills a region in the meridional plane having the shape of a box with rectangular corners. An existence theorem is given for those box-type orbits which can be described in a curvilinear orthogonal coordinate system. The computed box-type orbits, however, are shown to be more general. The properties of the box-type orbits are also discussed by means of the inclination diagram, in which the inclinations of successive intersections of the orbit with the axis $z = 0$ are plotted as a function along this axis. Evidence for the existence of a third integral of motion is provided by the characteristics of the box-type orbits in the inclination diagram. A more general discussion of the inclination diagram reveals the existence of other types of orbits in the same family. They are not discussed in the present paper.

The conclusions are necessarily provisional, since they are based on only one family of orbits and only one type within that family. However, since the box-type constituents of a family form a non-trivial class of orbits, and since this class is increasingly important for families of smaller energy than considered here, the inference can be drawn that, contrary to JEANS' theorem, a triaxial distribution of velocities is possible in the field of force in the galactic system.

I. The need for numerical orbit computations

In his book "Introduction to the Mechanics of Stellar Systems", RUDOLF KURTH (1957) writes (p. 140): "...there is very little known about the trajectories of the elements of mass in stationary models with rotational symmetry.... The general case will again be a rozette-like orbit; the other possibilities are all special cases. *No investigations seem to have yet been made into the general character of the orbits outside the equatorial plane.*"

The investigation into the properties of the mentioned trajectories was undertaken independently by CONTOPOULOS (1957, 1958) and by the author in collaboration with INGRID TORGÅRD.

In his work CONTOPOULOS has limited himself to the case of orbits with relatively low energies; he was forced to do this because the potential function which he used is a good representation of the actual potential function of the galactic system only in a limited region around the orbit of the sun. In collaboration with P. O. LINDBLAD, and by means of the electronic computer BESK, he has performed numerical integrations for two orbits. The amplitudes of these orbits in two mutually perpendicular directions are all smaller than 0.5 kpc; some relevant data for these orbits are given in section 10 of the present work. On the basis of his theory of the formal third integral of motion, CONTOPOULOS has succeeded in explaining analytically the properties of the numerically computed trajectories.

However, for the more interesting case of the high-

velocity stars, which have large meridional amplitudes, the method of CONTOPOULOS cannot be used. The present investigation was undertaken to determine the general characteristics of three-dimensional orbits of *higher* energy. To attain this objective, a rather extensive series of numerical computations was performed, also by means of the BESK. The results of a number of these computations are discussed in this thesis.

1. *The fundamental problem of stellar dynamics*

Let $(q_1, q_2, \ldots, q_n)$ specify the n generalised coordinates of a conservative dynamical system with n degrees of freedom, and let $(p_1, p_2, \ldots, p_n)$ be their conjugate momenta; the state of the system is defined by the *representative point* of the system in the phase space: $(q_1, q_2, \ldots, q_n, p_1, p_2, \ldots, p_n)$. The representative point describes a *path* in the phase space, which satisfies the canonical equations of motion

$$\dot{q}_i = \frac{\partial H}{\partial p_i} \quad \dot{p}_i - = \frac{\partial H}{\partial q_i} \; (i = 1, 2, \ldots, n), \qquad (1.1)$$

in which H is the Hamiltonian function.

In considering an *assembly* of such dynamical systems, let the *frequency function* $f(q_1, q_2, \ldots, q_n, p_1, p_2, \ldots, p_n, t)$ represent the density of representative points at any element of phase space at the time t. The assembly evolves in time as the representative points move in phase space. Liouville's theorem, which expresses the conservation of these points, may be written

$$\frac{df}{dt} = 0. \qquad (1.2)$$

This equation shows that the density of any element of phase space consisting of a group of neighbouring points moving similarly in phase space, is constant during its motion.

We have

$$\frac{d}{dt} = \frac{\partial}{\partial t} + \sum_{i=1}^{n} \left(\dot{p}_i \frac{\partial}{\partial p_i} + \dot{q}_i \frac{\partial}{\partial q_i} \right). \qquad (1.3)$$

Using the canonical equations (1.1), Liouville's equation takes the well-known form

$$\frac{\partial f}{\partial t} + \sum_{i=1}^{n} \left(\frac{\partial H}{\partial p_i} \frac{\partial f}{\partial q_i} - \frac{\partial H}{\partial q_i} \frac{\partial f}{\partial p_i} \right) = 0. \qquad (1.4)$$

Consider at a time t the stars in an element of space in the galactic system, moving in approximately the same direction with approximately the same velocities. Under circumstances where stellar encounters can be ignored, each star moving in the general gravitational field of force of the galactic system may be considered as a conservative dynamical system with three degrees of freedom. The field of force will be supposed to be due to the smoothed-out distribution of mass and is derived from a gravitational *potential function* Φ. The number of stars in the space element is given by the *velocity-distribution function*, which we define (following JEANS) as the number of stars in a space element which have velocities in a given velocity element; by this definition the velocity-distribution function is identical to the frequency function—i.e. the number density of the representative points of the stars in the 6-dimensional phase space.

The theorem of Liouville can be applied directly to this case.

Introducing cylindrical coordinates ϖ, ϑ and z as the generalised coordinates and $p_\varpi = \dot{\varpi}$, $p_\vartheta = \varpi^2 \dot{\vartheta}$ and $p_z = \dot{z}$ as the conjugate momenta, the Hamiltonian per unit of mass, which governs the motion of individual stars, is

$$H = \tfrac{1}{2} \left(p_\varpi^2 + \frac{p_\vartheta^2}{\varpi^2} + p_z^2 \right) + \Phi(\varpi, \vartheta, z, t). \qquad (1.5)$$

Liouville's equation (1.4) now takes the form

$$\frac{\partial f}{\partial t} + \left(\frac{p_\vartheta^2}{\varpi^3} - \frac{\partial \Phi}{\partial \varpi} \right) \frac{\partial f}{\partial p_\varpi} - \frac{\partial \Phi}{\partial z} \frac{\partial f}{\partial p_z} - \frac{\partial \Phi}{\partial \vartheta} \frac{\partial f}{\partial p_\vartheta} + p_\varpi \frac{\partial f}{\partial \varpi} + p_z \frac{\partial f}{\partial z} + \frac{p_\vartheta}{\varpi^2} \frac{\partial f}{\partial \vartheta} = 0, \qquad (1.6)$$

which is the fundamental equation of stellar dynamics. It is also referred to as the *equation of continuity*, and sometimes as the equation of Boltzmann by analogy with that equation in the kinetic theory of gases (in equation (1.6) the terms due to the interaction of the particles during close encounters are absent).

The fundamental problem of stellar dynamics is to find a solution of the equation of continuity. It appears in two forms: either it is supposed that the function Φ is known or that the function f is known, the problem being the solution of the equation of continuity for f or Φ respectively. The latter problem is discussed briefly in section 3, but in the main in this work the former point of view is taken.

It was pointed out by JEANS (1916) that because (1.6) is a linear *homogeneous* partial differential equation if Φ is supposed to be given, f must be a function of the independent integrals of the Lagrangian subsidiary equations

$$dt = \frac{dp_\varpi}{\frac{p_\vartheta^2}{\varpi^3} - \frac{\partial \Phi}{\partial \varpi}} = \frac{dp_z}{-\frac{\partial \Phi}{\partial z}} = \frac{dp_\vartheta}{-\frac{\partial \Phi}{\partial \vartheta}} = \frac{d\varpi}{p_\varpi} = \frac{dz}{p_z} = \frac{d\vartheta}{\frac{p_\vartheta}{\varpi^2}}. \qquad (1.7)$$

The latter are equivalent to the equations of motion for individual particle orbits in the canonical form (1.1) with the Hamiltonian (1.5), viz.

$$\begin{aligned} \frac{dp_\varpi}{dt} &= \frac{p_\vartheta^2}{\varpi^3} - \frac{\partial \Phi}{\partial \varpi} & \frac{d\varpi}{dt} &= p_\varpi \\ \frac{dp_\vartheta}{dt} &= -\frac{\partial \Phi}{\partial \vartheta} & \frac{d\vartheta}{dt} &= \frac{p_\vartheta}{\varpi^2} \\ \frac{dp_z}{dt} &= -\frac{\partial \Phi}{\partial z} & \frac{dz}{dt} &= p_z \,. \end{aligned} \qquad (1.8)$$

Thus the fundamental problem of stellar dynamics in the form discussed here is equivalent to the problem of determining the integrals of the equations of motion (1.8).

We shall now make, and use throughout this thesis, the simplifying postulate that the mass distribution of the galactic system (and hence the potential function) is independent of time, and that it has an axis and a plane of symmetry (the galactic plane). The intersection of axis and plane (the centre of the Galaxy) will be taken as the origin of the coordinate system, and z will be measured along the axis.

Under these conditions the equations of motion (1.8) admit of at least two time-independent integrals of motion:

(1) The Hamiltonian itself is constant in time as it does not contain the time explicitly:

$$\tfrac{1}{2}\left(p_\varpi^2 + \frac{p_\vartheta^2}{\varpi^2} + p_z^2\right) + \Phi(\varpi, z) = E, \qquad (1.9)$$

in which E is the *total energy*; sometimes this integral is denoted by I_1.

(2) The *integral of angular momentum* is found by integrating the second of the equations of motion (1.8). This gives

$$p_\vartheta = \varpi^2 \dot{\vartheta} = h, \qquad (1.10)$$

in which h is the *area constant*, equal to twice the rate at which the radius vector $(\varpi, \vartheta, 0)$ sweeps out area in the galactic plane; sometimes this integral is denoted by I_2.

Without further specification of the potential function, no other integrals of motion are known.

For any given Φ, let the (non-constant) function $I(p_\varpi, p_\vartheta, p_z, \varpi, \vartheta, z, t)$ be such that the derivative of I with respect to the time is zero along any *solution path* of equations (1.8). Such a function, by definition an integral of the dynamical system of differential equations (1.8), satisfies the equation

$$I = \alpha, \qquad (1.11)$$

where α is an *integration constant*.

The complete solution of the system of equations (1.8) is furnished by 6 mutually independent integrals, which satisfy the equations

$$I_i = \alpha_i \,(i = 1, 2, \ldots, 6). \qquad (1.12)$$

For a given set of integration constants α_i, the solution path is determined by solving (1.12) for $p_\varpi, p_\vartheta, p_z, \varpi, \vartheta$ and z. By these solutions the α's are related to the initial conditions $(p_\varpi^\circ, p_\vartheta^\circ, p_z^\circ, \varpi^\circ, \vartheta^\circ, z^\circ)$.

An integral is called *conservative* if it does not contain the time explicitly; thus I_1 and I_2 are conservative integrals of motion. The adjective conservative may be omitted when no confusion is possible. A conservative integral defines by the relation (1.11) an *integral hypersurface* in phase space which contains the initial conditions as a point and the entire solution path through that point. There are as many integral hypersurfaces as there are independent conservative integrals and the solution path is contained in the intersection of the integral hypersurfaces.

There are at most 5 independent conservative integrals (excluding the trivial case that each point in phase space is a point of equilibrium). But there are also not less than 5 independent conservative integrals in the local sense, i.e. if the initial conditions are restricted to some closed and bounded domain of phase space and the time interval is supposed to be less than a constant depending on this domain (WINTNER 1947). These integrals, which are obtained by elimination of the time t from the equations (1.12), are single-valued functions in the local sense.

From the non-local point of view, however, i.e. if the initial conditions are no longer restricted to a given domain and if the solution paths of the system (1.8) are considered for $-\infty < t < +\infty$, the situation is different. In general it will not be possible to describe the system of solution paths completely by equations (1.12) without encountering singularities: some of the conservative integrals may be infinitely many-valued and other divergencies from the local situation may occur (LEVI-CIVITA 1927). Conservative integrals which do not give rise to singularities will be called *isolating*. Such integrals have the property of isolating points on the solution path from neighbouring points in phase space. For a rigorous general definition of an isolating integral, involving the structure of the corresponding integral hypersurface, we refer to WINTNER (*op. cit.*). The energy integral I_1 and the angular-momentum integral I_2 are single-valued and isolating.

If all 5 conservative integrals are isolating, the system of solution paths can be described completely by the equations (1.12), and then the system (1.8) is called *imprimitive*. In general, however, the total number of isolating integrals will be less than 5; if the system (1.8) has a total of l isolating integrals, it is called $(5-l)$-*fold primitive*.

Besides the integral of energy and the integral of angular momentum, there cannot be more than one additional independent isolating integral of motion containing the velocities $\dot{\varpi}$ and $\dot{z}$. This integral (if it exists) is called *the third integral of motion* I_3. In the case of a galactic stellar orbit which oscillates with small amplitudes around a stable circular orbit in the galactic plane, the third integral of motion can be found analytically. The treatment is given in section 9, where also the isolating property of the third integral of motion is exemplified.

Formally the fundamental problem of the determination of the frequency function is solved by setting f equal to any function of the 6 integrals of motion

$$f = g\,(I_1, I_2, \ldots, I_6)\,. \qquad (1.13)$$

Throughout this thesis another simplifying postulate will be used. It will be assumed that the galactic stellar system is in a state of statistical equilibrium. This is expressed by the fact that f does not contain the time explicitly; this postulate is referred to as the *steady-state* hypothesis. Then f can be a function only of the conservative integrals of motion; however, because the non-isolating integrals can have no influence on the density distribution owing to their singular character, they are of no use as arguments of f. Hence the density distribution is a function only of the isolating integrals of motion.

2. *A theorem of* JEANS

With the *ad hoc* assumption that the potential function of the galactic system admits, besides the integrals of energy and angular momentum, no other isolating integrals of motion, the velocity-distribution function f is, for the steady state considered, an arbitrary function of two integrals only

$$f = g\,(E, h)\,. \qquad (2.1)$$

In this case the velocity-components $\dot{\varpi}$ and $\dot{z}$ (for which we write Π and Z respectively) occur only in the quadratic form $\Pi^2 + Z^2$. This means that the meridional components of the velocities of stars in a volume element at any point in the galactic system are distributed with circular symmetry in the meridional plane. This property, which should be valid for any steady stellar system with symmetry around the z-axis, was first expressed by JEANS (1916) and it will be referred to as JEANS' theorem. In particular the meridional *velocity dispersions* σ_Π and σ_Z must be equal, where σ_Π (and similarly σ_Z) is defined as

$$\sigma_\Pi^2 = \frac{1}{n}\int_{-}^{+\infty}\int\int\int \Pi^2\, g\,(E, h)\; d\Pi\; dZ\; d\Theta\,, \qquad (2.2)$$

in which n represents the particle density at the point considered and $\Theta = h/\varpi$.

In section 4 the observations of velocity dispersions for various groups of stars in the solar neighbourhood are reviewed briefly and the well-known divergence between JEANS' theorem and observation is illustrated.

3. *The ellipsoidal distribution of velocities*

In the previous sections (and in the main body of this work) the potential function Φ is considered to be known, and a solution of the equation of continuity (1.6) for the frequency function f is sought.

Alternatively the equation (1.6) can be regarded as a linear *non-homogeneous* partial differential equation for Φ, supposing the function f to be known, e.g. from data on stellar kinematics. This approach to the fundamental problem of stellar dynamics has been pursued in considerable mathematical detail, amongst others by JEANS (1916), EDDINGTON (1916), OORT (1928) and CHANDRASEKHAR (1942).

In OORT's analysis it is supposed by analogy with the maxwellian velocity distribution in the kinetic theory of gases, that f has an exponential form and that, in a coordinate system following the mean rotational motion Θ_0 at the point considered, the exponent is a homogeneous function of the second degree in the velocities. Thus

$$f = f_0 \exp\left[-h^2\Pi^2 - k^2(\Theta-\Theta_0)^2 - l^2 Z^2 - m\,\Pi\,(\Theta-\Theta_0) - n\,\Pi\,Z - p\,(\Theta-\Theta_0)\,Z\right], \qquad (3.1)$$

in which $\Theta = \varpi\dot{\vartheta}$, and the coefficients h, k, l, m, n, p are functions of ϖ and z. The exponent of (3.1) defines the *velocity ellipsoid*.

This function is inserted in the equation of continuity, and the general solution for the coefficients is found to be

$$\left.\begin{aligned} h^2 &= c_1 + \tfrac{1}{2}c_5 z^2 + c_6 z \\ l^2 &= c_4 + \tfrac{1}{2}c_5 \varpi^2 \\ m = p &= 0 \end{aligned}\right\} \qquad (3.2a)$$

$$\left.\begin{aligned} k^2 &= c_1 + c_2\varpi^2 + \tfrac{1}{2}c_5 z^2 + c_6 z \\ n &= -c_5\,\varpi\, z - c_6\,\varpi \\ \Theta_0 &= \frac{c_3}{k^2}\,\varpi\,, \end{aligned}\right\} \qquad (3.2b)$$

in which $c_1, \ldots, c_6$ are constants and $c_6 = 0$ since the plane $z = 0$ is a plane of symmetry. Furthermore the potential Φ and the function f_0 must satisfy the relations

$$\left.\begin{aligned} \frac{1}{f_0}\frac{\partial f_0}{\partial \varpi} - \frac{\partial(k^2\Theta_0^2)}{\partial \varpi} - n\frac{\partial \Phi}{\partial z} - 2h^2\frac{\partial \Phi}{\partial \varpi} &= 0 \\ \frac{1}{f_0}\frac{\partial f_0}{\partial z} - \frac{\partial(k^2\Theta_0^2)}{\partial z} - n\frac{\partial \Phi}{\partial \varpi} - 2l^2\frac{\partial \Phi}{\partial z} &= 0\,. \end{aligned}\right\} \quad (3.3)$$

From the latter two equations we infer the integrability condition for f_0

$$\left.\begin{aligned} c_5\Big[3\left(z\frac{\partial \Phi}{\partial \varpi} - \varpi\frac{\partial \Phi}{\partial z}\right) + (z^2-\varpi^2)\frac{\partial^2 \Phi}{\partial \varpi\,\partial z} + \\ + \varpi z\left(\frac{\partial^2 \Phi}{\partial \varpi^2} - \frac{\partial^2 \Phi}{\partial z^2}\right)\Big] + 2(c_1-c_4)\frac{\partial^2 \Phi}{\partial \varpi\,\partial z} = 0\,. \end{aligned}\right\} \quad (3.4)$$

The last equation can be satisfied in several ways. FRICKE (1951) discussed all four possible cases:

$$\begin{aligned} c_5 &= 0 \qquad c_1 = c_4 \qquad \text{(i)} \\ c_5 &= 0 \qquad c_1 \neq c_4 \qquad \text{(ii)} \\ c_5 &\neq 0 \qquad c_1 = c_4 \qquad \text{(iii)} \\ c_5 &\neq 0 \qquad c_1 \neq c_4 \qquad \text{(iv)} \end{aligned}$$

If we put no other restriction on Φ than that it is rotationally symmetrical, we have case (i), treated by OORT (*op. cit.*) and reviewed recently by LINDBLAD (1959); in this case $h^2 = l^2$, which is JEANS' theorem.

For all other cases the velocity ellipsoid is tri-axial ($h^2 \neq l^2$) and Φ is restricted to special forms. Thus case (ii) leads to the form (11.14) of Φ mentioned in section 11, case (iii) is the case treated in section 11a, and case (iv) is the case of the quadratic third integral of motion, treated in section 7.

There are no further restrictions to the potential function as long as the velocity distribution of a certain class of stars, selected for instance by physical characteristics of its members, is considered. Such a class of stars may be regarded as a sub-system which moves under the general attraction of the galactic system as a whole.

However, when considering the dynamics of the Galaxy as a whole, the potential function Φ must be related to the mass-density ρ which produces it, by Poisson's equation

$$\Delta\Phi = -4\pi G\rho\,, \quad (3.5)$$

i.e. the stellar system must be *self gravitating*.

Let f now refer to the *total mass* of matter (including interstellar gas and dust) in unit volume of phase space, and assume an ellipsoidal form for f; by substitution of f into the equation of continuity, the same four cases mentioned above are obtained. Now, however, the potential function must also satisfy the equation (3.5), for which we can write

$$\Delta\Phi = -4\pi G\int_{-\infty}^{+\infty}\int\int f\,d\Pi\,dZ\,d\Theta\,. \quad (3.6)$$

CAMM (1941) and FRICKE (*op. cit.*) discussed this equation for the special forms of Φ which follow from the four cases mentioned above. Their conclusion is that a steady-state self-gravitating star system of finite mass with an ellipsoidal velocity distribution cannot exist.

On the observational side the ellipsoidal form of the function f represents remarkably well the distribution of space velocities of the low-velocity stars, as was first pointed out by K. SCHWARZSCHILD (1907). It does not however, represent the observational fact, pointed out by OORT (1928), of the asymmetry of the high-velocity stars. The velocity distribution of the stars in the solar neighbourhood with peculiar velocities higher than 63 km/sec is asymmetrical in the sense that there are no stars moving in the direction of the solar motion with velocities higher than this value. FRICKE (*op. cit.*), discussing this criticism of the ellipsoidal hypothesis, has shown that the asymmetry in the high velocities can be represented to a degree by assuming that the distribution function is of the form of a finite double series of the two integrals E and h. Of course in this case JEANS' theorem must be valid too.

It would seem that the study of the equation of continuity starting from the ellipsoidal form of f, as outlined in this section, far from solving all problems, introduces new ones. We shall therefore adopt the initial way of treating the equation of continuity, and consider Φ known. Thus we do not impose an *a priori* restriction on f. After specifying Φ, the function f may be determined, but it will be possible to find an analytical expression for f only in exceptional cases because it involves the explicit expressions of all the integrals of motion (see chapter II). When the dynamics of a stellar system as a whole are considered, Φ should be based on a model of the mass distribution so that Poisson's equation is satisfied. Also the function f should be specified in such a way that it is consistent with this mass distribution; these questions fall beyond the scope of the present investigation, which is mainly concerned with individual trajectories of particles of mass in a stellar system, rather than with the statistics of such trajectories.

4. *The observed inequality of the meridional velocity dispersions*

A short review of the observational material on space velocities of groups of stars of various spectral classes in the vicinity of the sun has recently been given by WOOLLEY (1960). From Table 1 in his article we find for the ratio of the meridional velocity dispersions the values given in the upper part of the following Table 1.

Not only for these classes but also for high-velocity objects, such as the RR Lyrae stars, the ratio of meri-

TABLE 1

Spectral type	No. of stars	σ_Π (km/sec)	σ_Z (km/sec)	σ_Z/σ_Π
A	475	18	8	0.44
F	84	29	13	0.45
G	136	38	19	0.50
K	190	37	16	0.43
M	292	40	18	0.45
RR Lyrae var. per $\leqq 0^d.4$ $\varepsilon > 0^p.25$ [1])	34	89	46	0.52
RR Lyrae var. per $> 0^d.4$	98	136	70	0.52

[1]) ε is the duration of the increase of brightness divided by the period (KUKARKIN 1948).

dional dispersions is much smaller than unity. From the work of PAVLOVSKAYA (1953) we cite the ratios for two groups of RR Lyrae variables, also given in Table 1. The uncertainty in these values is larger than in the groups of low-velocity stars, since a mean absolute magnitude is used to determine individual distances of RR Lyrae variables.

For the long-period variables, which, judging from their concentration towards the galactic plane, form an intermediate population of stars, the data are more scanty. But the velocity dispersion in the radial direction is certainly larger than the velocity dispersion perpendicular to the galactic plane (cf. OORT 1928, Table 1).

The conclusion may be drawn that for groups of stars in the vicinity of the sun ranging from extreme population I to extreme population II, the ratio of the meridional velocity dispersions has an approximate value of 0.5 instead of unity as predicted by JEANS' theorem for any dynamically steady stellar system with an axis of symmetry. Amongst many other investigations supporting this conclusion, we may mention the work by NORDSTRÖM (1936) and VYSSOTSKY (1957).

5. *Suggested explanations of the inequality of meridional velocity dispersions*

In the first three sections of this chapter some properties of the velocity-distribution function for a stellar system in statistical equilibrium were derived on the basis of the equation of continuity. In the course of the argument applied to the galactic system, two important postulates have been made, which can be summarised as follows:

(1) The mass distribution is stationary and has an axis and a plane of symmetry,

(2) The velocity-distribution function is stationary.

In addition it has been assumed in section 2 that besides the integrals of energy and angular momentum no third integral of motion exists. However, it was immediately noted that JEANS' theorem, which follows from the latter assumption and postulates (1) and (2), is not satisfied by the velocity distribution of actual classes of stars in the solar neighbourhood (section 4). It is the purpose of the present section to review some of the suggested explanations for this discrepancy.

It is a matter of some importance to state first the two points of view which can be taken concerning the initial state of stellar motions: either one can make the assumption that there was an excess of high Π-velocities when the stars were formed—and then one must inquire what could have prevented the velocity-distribution function from settling to a situation in which the meridional dispersions are equal, or one can make the assumption that initially there was a uniform distribution over Π- and Z-velocities—and then the question arises whether the Π-dispersion could possibly have increased at the expense of the Z-dispersion.

For the high-velocity stars, the former point of view may be taken. The present distribution of velocities of these objects should closely resemble the initial one as they move in orbits of high ellipticity and so have spent a considerable part of their life-times in the outer regions of the galactic system. However, for the study of the kinematical evolution of *old* stars of high velocity, an extra complication is the fact that the steady-state hypothesis may not have held in the early history of the Galaxy.

For the low-velocity stars there is not much indication as to which point of view should be taken. The rather poor statistics of motion of B stars (NORDSTRÖM, *op. cit.*) suggest that stars of population I have no preferential motion in the (ϖ,z)-plane after formation from the interstellar gas.

Returning now to the review of explanations for the discrepancy between observed and predicted meridional velocity dispersions, we can divide these into three categories:

(a) the postulate that the velocity-distribution function is stationary does not hold,

(b) there is indeed no third integral of motion, but certain conservative functions may be used as *quasi-integrals*, i.e. the functions may be nearly constant along individual orbits for considerable time intervals.

(c) there is a third isolating integral of motion after all.

The influence of none of these categories can be excluded *a priori*. For, (a) over long periods of time the distribution of mass in the Galaxy must have changed, (b) possibly the galactic potential function may be approximated in limited regions of space by specific forms which admit more than two integrals of motion,

and (c) even though the third integral of motion has not yet been found for the galactic potential function, it may exist.

On the other hand, none of the explanations proposed in the literature indicate which effect is likely to have had the greatest influence on the statistics of stellar velocities since the stars were formed. In order to see this we examine these explanations briefly. They fall in line with above mentioned categories (a) and (b).

(a) The possible influence of interstellar clouds

In two articles SPITZER and SCHWARZSCHILD (1951, 1953) investigate the influence of encounters between interstellar clouds and stars on the velocity distribution of the latter, and they show that this effect tends to increase the velocity dispersion in the galactic plane in the course of time.

Assuming first the masses of individual clouds with radii of some 5 parsecs to be of the order of 10^2 solar masses, and assuming for the solar neighbourhood the same average density for clouds and stars, they find that the *time of relaxation*—i.e. the time in which the accumulated velocity differences for encounters between stars and clouds reach the order of magnitude of the original velocities—is of the order of 10^{11} years for the low-velocity stars with an average peculiar velocity of 20 km/sec. Encounters are idealized as two-body problems.

Rather than regarding clouds as being individual entities, OSTERBROCK (1952) considers the changes in motion of a star moving in the fluctuating density field of interstellar matter, proposed by CHANDRASEKHAR and MÜNCH (1950) in their study of the fluctuating brightness in the Milky Way. The time of relaxation of a star moving in this field with a velocity of 20 km/sec comes out to be of the same order of magnitude, which is long compared to the estimated age of the Galaxy.

Consequently these small clouds cannot have been an effective agency in speeding up the stars. However, observational data on the interstellar gas show that much more massive cloud complexes also occur, e.g. the Orion nebula, with a mass probably greater than 10^4 solar masses. Under the *ad hoc* assumption that most of the interstellar matter is gathered into cloud complexes with masses of 10^5 or 10^6 solar masses, the estimate of the time of relaxation for low-velocity stars in star-cloud encounters goes down with a factor 10^3 or 10^4, and it becomes shorter than the probable age of the Galaxy. Original velocities of population I stars may consequently have undergone a considerable re-shuffling. Complete equipartion of energy between clouds and stars is not to be expected and observational evidence shows it is certainly not reached; this is indicated by statistical studies of the Ca^+ and Na absorption lines and of the H emission line at 21 cm which give 5 to 8 km/sec for the root mean square velocity component in the line of sight, for the smaller cloud complexes (masses up to 10^4 solar masses).

In the second article, SPITZER and SCHWARZSCHILD give a quantitative two-dimensional analysis of the speeding up of stars in the galactic plane due to encounters with massive cloud complexes. In this picture the stars moving in the fluctuating field of force of massive cloud complexes rotating with differential galactic rotation, gain momentum at the expense of angular momentum of the clouds. Apart from the rotational motion around the galactic centre, the clouds are supposed to have a negligible random motion. A complete three-dimensional analysis has not been given, but in a qualitative way it is clear that for the case of the low-velocity stars, where the amplitudes of the oscillatory motions perpendicular to the galactic plane are small, there can be no gain in kinetic energy from clouds which have no random velocities perpendicular to the galactic plane. Hence, since the stars are speeded up in the velocity components in the galactic plane, a qualitative explanation for the observed inequality of dispersions in the meridional plane for the older stars is given.

The SPITZER-SCHWARZSCHILD mechanism works in the right direction, but it is doubtful whether

1) there actually occur enough large cloud complexes with masses of the order of 10^6 solar masses,

2) there has been enough time to increase the dispersion in the Π-component roughly by a factor 2,

3) the clouds actually have no random Z-velocities, cf. the case of the Orion nebula, which lies outside the galactic plane.

Encounters with interstellar clouds produce a time of relaxation for high-velocity stars up to 100 times longer than for low-velocity stars. Therefore, the SPITZER-SCHWARZSCHILD effect cannot account for the inequality in velocity dispersions for high-velocity stars. Conversely the statement by these authors: "Velocity dispersions for population II stars have not been altered essentially by any encounters and must represent the initial average velocities of these stars at their formation", is in line with the point of view suggested at the beginning of this section, namely that population II stars have had excess Π-velocities at their formation. Thus we are led to consider especially categories (b) and (c) of explanations of unequal meridional velocity-dispersions for this population of stars.

(b) The possible influence of a quasi third integral of motion

A different explanation was suggested by VAN

ALBADA (1952), in connection with the theory of the third *quadratic* integral of motion. In section 7 we shall review this theory briefly with regard to its consequences for the galactic potential function. It is pointed out in section 7 that the actual galactic potential function cannot be represented exactly by the form of the potential function which follows from the theory of the third quadratic integral of motion. Therefore this integral is not an *exact* integral of motion, i.e. the quadratic function of the velocities and the position coordinates is not exactly constant along individual three-dimensional orbits of stars in the Galaxy.

VAN ALBADA has suggested that the quadratic function of the theory of the third quadratic integral may figure as a *quasi-integral* for stellar orbits in a galactic system in which the potential function is not exactly described by the form of Φ belonging to the theory of the third quadratic integral of motion.

A quasi-integral of motion is defined as a function of the velocities and the position coordinates which is not exactly constant but exhibits secular small variations along an individual orbit.

If there exists in addition to the integrals I_1 and I_2 (see section 1) a quasi-integral of motion, an initial *equality* of the meridional components of the velocity-dispersion function may evolve in one direction. The rate of change in time of the original velocity-dispersion function will depend on the character and magnitude of the mentioned secular variations of the quasi-integral.

The actual galactic gravitational field of force, which deviates from the field of force derived from the potential function described in section 7, can be examined for this effect in two different ways:

1) Direct method. The actual galactic gravitational force function is compared with the field of force derived from the specific form of the potential function (see sections 7 and 11b) which follows from the theory of the third quadratic integral. This has been done by KUZMIN (1953). Some remarks on this comparison are made in section 7 of the present work.

2) Indirect method. A number of individual test orbits of mass particles with various energies and momenta in a model of the distribution of mass in the Galaxy are computed numerically; for each orbit the third quadratic integral could be computed along the orbit and the changes of this function will give some idea of the mentioned effect.

This method is not followed up in the present investigation as we shall be concerned with orbits of mass particles with higher energy, which do not stay in limited regions of space. For such orbits it is doubtful whether the computation of the quadratic quasi-integral of motion is of any use.

The explanation of a triaxial distribution of velocities on the basis of the quasi third (quadratic) integral of motion may be adequate for low-velocity stars since they stay within a limited region of space where the galactic potential function could possibly be approximated by the specific function which admits of the existence of the third quadratic integral. However, for the high-velocity objects it seems hardly plausible. In the first place because such objects reach widely separated parts of the galactic field of force, so that the orbits are formed by forces showing considerable deviation from those corresponding to the theoretical case of the third quadratic integral of motion. And secondly because in this case we have seen that an agency must be sought which is effective in keeping up an initial inequality of meridional velocities.

Thus we are led to the consideration of the last explanation, the investigation of which is best undertaken by the numerical computation of a number of three-dimensional stellar orbits in the actual field of force of the Galaxy. The results of such numerical computations, which are discussed in chapter III, give an empirical proof of the existence of a third isolating integral of motion in the galactic field of force. This leads quite naturally to the explanation of the triaxial distribution of velocities mentioned in section 23.

6. *Summary of reasons for the numerical computation of three-dimensional stellar orbits*

The discrepancy between theory and observations on the statistics of stellar motions in the neighbourhood of the Sun, formulated in the preceding sections, and the inadequacy of the suggested explanations in accounting for it in terms of either star-cloud encounters or the possible effect of a third quasi-integral of motion, form a sufficient motive for the numerical computation of individual three-dimensional orbits of test stars in the Galaxy. For we may hope that the study of the relation between the Π- and the Z-velocity components for individual orbits of high-velocity stars will give us some insight into the questions whether and how conversion of energy from one component into the other takes place. Cases of large amplitudes in the meridional plane and thus of relatively large energies must be selected in order to obtain (ϖ, z)-coupled motions; for small oscillations in the meridional plane the mutually perpendicular ϖ- and z-oscillations are independent and there is no conversion of energy of motion from one component into the other.

Another motive for numerical orbit computations is furnished by the possibility of finding in this way the place of origin of certain stars from their observed space velocities and estimates of their age. Thus backward orbit computations can be used to determine

the association in which suspected run-away stars might have originated (BLAAUW 1961). A model of the distribution of mass not too much different from reality is evidently needed. Even then, however, due to the uncertainties in the determinations of the space velocity, such computations cannot be expected to yield a precise value of the place of origin, if carried out over a long time interval.

Finally, numerical computations of orbits in a given galactic force function (which should be based upon a model of the distribution of mass in the galactic system), provides knowledge of the length of time spent by stars with different orbital parameters in different parts of the (ϖ, z)-plane. This knowledge, combined with observational knowledge on the velocity- and density-distribution of selected classes of stars, such as the RR Lyrae stars, is a means for further study of the actual distribution of mass in the Galaxy.

Not all of these applications are considered in this investigation, but the orbit computations have been arranged so as to give all necessary data for a complete specification of the path in phase space as a function of time.

II. Analytical Solutions

7. *The third quadratic integral*

The theory has been outlined independently by VAN ALBADA (1952) and KUZMIN (1953). It is assumed that the integral

$$I_3 = (\varpi Z - z\Pi)^2 + z^2\Theta^2 - \alpha^2(Z^2 - 2\Omega), \quad (7.1)$$

quadratic in the three velocity components, exists; α is a parameter with a real or imaginary value which may be chosen in accordance with the characteristics of the field of force in the region of space considered; α^2 has the dimension of the square of a length; Ω is a rotationally symmetrical function of the space coordinates, satisfying the partial differential equations

$$\left.\begin{aligned} \frac{\partial\Omega}{\partial\varpi} &= \frac{z^2}{\alpha^2}\frac{\partial\Phi}{\partial\varpi} - \frac{\varpi z}{\alpha^2}\frac{\partial\Phi}{\partial z} \\ \frac{\partial\Omega}{\partial z} &= -\frac{\varpi z}{\alpha^2}\frac{\partial\Phi}{\partial\varpi} + \left(\frac{\varpi^2}{\alpha^2} - 1\right)\frac{\partial\Phi}{\partial z}, \end{aligned}\right\} \quad (7.2)$$

which follow from the condition that $\frac{dI_3}{dt} = 0$ along any trajectory. The assumption that (7.1) is an integral of motion implies a condition for the gravitational potential Φ; it is obtained by elimination of Ω from equations (7.2) and takes the form

$$\left.\begin{aligned} \varpi z\left(\frac{\partial^2\Phi}{\partial\varpi^2} - \frac{\partial^2\Phi}{\partial z^2}\right) + (\alpha^2 - \varpi^2 + z^2)\frac{\partial^2\Phi}{\partial\varpi\,\partial z} + \\ + 3\left(z\frac{\partial\Phi}{\partial\varpi} - \varpi\frac{\partial\Phi}{\partial z}\right) = 0. \end{aligned}\right\} \quad (7.3)$$

In order to solve the equations (7.2) and (7.3), we introduce ellipsoidal coordinates ξ and η defined by

$$\eta + i\xi = \arcsin\frac{\varpi + iz}{\alpha} \quad (7.4)$$

(see also section 11b). The surfaces $\xi = $ const. and $\eta = $ const. are confocal orthogonal ellipsoids and hyperboloids of revolution, centred at the centre of the galactic system. For α real, the circle in the galactic plane with radius α is the focal circle of the two sets of surfaces. For α imaginary, there are two focal points on the z-axis at distances $+i\alpha$ and $-i\alpha$ from the galactic centre.

The equations (7.2) become

$$\left.\begin{aligned} \frac{\partial\Omega}{\partial\xi} &= -\cos^2\eta\,\frac{\partial\Phi}{\partial\xi} \\ \frac{\partial\Omega}{\partial\eta} &= \sinh^2\xi\,\frac{\partial\Phi}{\partial\eta}, \end{aligned}\right\} \quad (7.5)$$

and the condition (7.3) becomes

$$\begin{aligned} (\cosh^2\xi - \sin^2\eta)\frac{\partial^2\Phi}{\partial\xi\,\partial\eta} = \\ = -2\sinh\xi\cosh\xi\frac{\partial\Phi}{\partial\eta} + 2\sin\eta\cos\eta\frac{\partial\Phi}{\partial\xi}. \end{aligned} \quad (7.6)$$

The solution of (7.6) is

$$\Phi = \frac{F(\xi) + G(\eta)}{\cosh^2\xi - \sin^2\eta}, \quad (7.7)$$

in which F and G are arbitrary functions of ξ and η respectively, and the solution of (7.5) is then

$$\Omega = \frac{\sinh^2\xi\,.\,G(\eta) - \cos^2\eta\,.\,F(\xi)}{\cosh^2\xi - \sin^2\eta}. \quad (7.8)$$

The expression (7.1) for the third integral of motion becomes in ellipsoidal coordinates

$$I_3 = \alpha^4\left\{\left(\frac{d\eta}{dt}\right)^2\sinh^2\xi - \left(\frac{d\xi}{dt}\right)^2\cos^2\eta\right\}(\cosh^2\xi - \sin^2\eta) + h^2\frac{\mathrm{tgh}^2\xi}{\mathrm{tg}^2\eta} + 2\alpha^2\Omega(\xi,\eta). \quad (7.9)$$

The form (7.7) of the potential function had been given already by EDDINGTON (*op. cit.* p. 46, formula (18)) although the assumptions were different, namely that the principal velocity surfaces generated by the

mutually orthogonal axes of the assumed ellipsoidal distribution of velocities should be ellipsoids and hyperboloids of revolution. The form was rediscovered by CAMM (1941) in his discussion of the ellipsoidal distribution of velocities. In section 11 we will show how the form (7.7) for Φ and the form (7.9) for I_3 can be found as a result of the assumption that the equations of motion can be integrated by the method of separation of variables. The ellipsoidal distribution of velocities with three unequal axes in the field of force derived from Φ of the form (7.7), is given in section 3 (see formulas (3.1) and (3.2) with case iv).

In the classical theory of two-dimensional dynamical systems—to which the case of three-dimensional motion in an axially symmetric field of force can be reduced, cf. section 8—possessing a quadratic integral other than the energy integral, the equivalent form of the potential is known (WHITTAKER 1904, p. 323). The potential of the Newtonian field of force of two fixed centres of mass is also described by (7.7). Finally we remark that VINTI (1959 a, b) has shown that the potential outside an oblate spheroid can be approximated by (7.7); his investigations were concerned with the description of the drag-free motion of an artificial satellite under influence of the gravitational attraction of the earth.

It was remarked in section 3 that the form (7.7) of the potential function cannot be an exact solution for the potential function of a self-gravitating galactic system, since the Poisson equation cannot be satisfied; this was first shown by EDDINGTON.

By imposing on Φ the condition that for large distances r from the galactic centre

$$\Phi \to -\frac{M}{r}, \tag{7.10}$$

where M is the total mass of the Galaxy, VAN ALBADA showed that $G(\eta) = 0$; he takes α real and then Φ is singular in the galactic plane on the focal circle. By taking α imaginary, KUZMIN finds that Φ is only singular in the two focal points on the z-axis, but in this case $\Phi \not\to -M/r$ for large r.

These considerations show that the form (7.7) of Φ is certainly not exactly satisfied for an actual stellar system. But in limited, not too large regions of the galactic field of force, (7.7) may be an approximation of the actual potential function, and then the quadratic third integral of motion I_3 may be used as a quasi-integral: instead of being constant along an orbit it varies slowly with time.

KUZMIN (*op. cit.*) has considered the question of approximating the galactic potential function over large regions in and near the system, by the form (7.7). He proposed for the functions F and G the expressions

$$\left.\begin{aligned} F(\xi) &= -\frac{\Phi^\circ}{z_0}\sqrt{x_0^2 - \sinh^2\xi} \\ G(\eta) &= \frac{\Phi^\circ}{z_0}\sqrt{x_0^2 + \cos^2\eta} \end{aligned}\right\} \tag{7.11}$$

in which Φ° and x_0 are constants and z_0 is equal to $i\alpha$ in our notation.

In this case the form (7.7) of Φ rewritten in the coordinates ϖ and z becomes

$$\Phi = \frac{\Phi^\circ z_0}{\sqrt{2}}\left\{\frac{(2x_0^2 + 2zz_0 + r_1^2 + r_1 r_2)^{\frac{1}{2}} - (2x_0^2 - 2zz_0 + r_2^2 - r_1 r_2)^{\frac{1}{2}}}{r_1 r_2}\right\}, \tag{7.12}$$

in which r_1 and r_2 are the distances of the point considered from the focal points $(z = \pm z_0, \varpi = 0)$. From this expression the following partial derivatives in the plane $z = 0$ are obtained

$$\left.\begin{aligned} \left(\frac{\partial\Phi}{\partial\varpi}\right)_{z=0} &= \frac{\Phi^\circ z_0}{v^2}\left(-2\varpi\frac{w - x_0}{v^2} + \frac{\varpi}{w}\right) \\ \left(\frac{\partial^2\Phi}{\partial z^2}\right)_{z=0} &= \frac{\Phi^\circ z_0}{v^3}\left(\frac{2v^2 - 4\varpi^2}{v^3}(w - x_0) - \right. \\ &\qquad \left. - \frac{v^2 - \varpi^2}{vx_0} - \frac{\varpi^2}{vw}\right) \\ \left(\frac{\partial^2\Phi}{\partial\varpi^2}\right)_{z=0} &= \frac{\Phi^\circ z_0}{v^3}\left(\frac{-2v^2 + 8\varpi^2}{v^3}(w - x_0) - \right. \\ &\qquad \left. - \frac{4\varpi^2}{vw} + \frac{v}{w} - \frac{\varpi^2 v}{w^3}\right) \end{aligned}\right\} \tag{7.13}$$

in which $v^2 = \varpi^2 + z_0^2$, and $w^2 = \varpi^2 + z_0^2 + x_0^2$.

For $z = 0$, (7.12) becomes

$$\Phi = \frac{\Phi^\circ z_0}{v}\,\frac{w - x_0}{v}. \tag{7.14}$$

The left-hand sides of equations (7.13) are known in terms of OORT's dynamical constants A and B and the third dynamical constant C:

$$\left.\begin{aligned} \left(\frac{\partial\Phi}{\partial\varpi}\right)_{z=0} &= \varpi(A - B)^2 \\ \left(\frac{\partial^2\Phi}{\partial\varpi^2}\right)_{z=0} &= -(A - B)(3A + B) \\ \left(\frac{\partial^2\Phi}{\partial z^2}\right)_{z=0} &= C^2. \end{aligned}\right\} \tag{7.15}$$

KUZMIN (*op. cit.*) has suggested the following values

of the constants Φ°, z_0 and x_0 in expression (7.12) for the galactic potential function:

$$\left.\begin{aligned} \sqrt{-\Phi^\circ} &= 425 \quad \text{km/sec} \\ z_0 &= \ 3.6 \text{ kpc} \\ x_0 &= \ 0.6 \text{ kpc} \end{aligned}\right\} \quad (7.16)$$

Substituting these values in equations (7.13) and taking $\varpi = 8.2$ kpc and $z = 0$ for the solar neighbourhood, we obtain the results shown in Table 2. For comparison the values given by the model of the distribution of mass by SCHMIDT (1956) are given.

TABLE 2

Comparison of some quantities following from KUZMIN's formula (7.12) with SCHMIDT's values, at $\varpi = 8.2$ kpc, $z = 0$ (units as in section 14).

	KUZMIN	SCHMIDT
$\left(\frac{\partial\Phi}{\partial\varpi}\right)_{z=0}$	64.79	57.15
$\left(\frac{\partial^2\Phi}{\partial\varpi^2}\right)_{z=0}$	−11.06	−13.6
$\left(\frac{\partial^2\Phi}{\partial z^2}\right)_{z=0}$	25.72	52.50
A	1.68	1.95
B	−1.13	−0.69
C	5.07	7.25
$V_\infty = \sqrt{-2\Phi}_{\substack{\varpi=8.2 \\ z=0}}$	36.9	28.6
M = total mass	6503	3012

In Table 3 the same comparison is made for the rotational curve, defined as

$$\Theta_c = \sqrt{\varpi \left(\frac{\partial\Phi}{\partial\varpi}\right)} \quad (7.17)$$

for $z = 0$. The table shows that the KUZMIN formula (7.12) yields a rotational curve which shows approximately the same run as SCHMIDT's curve for ϖ from about 2 to about 7 kpc although it is systematically too high for the adopted values of Φ°, z_0 and x_0. For larger ϖ the similarity between the two curves breaks down, and the sharp descent of the SCHMIDT curve is not followed by KUZMIN's. This is partly a consequence of the fact that the total mass M in KUZMIN's model, which is equal to $-\Phi^\circ z_0$, is about twice as large as the total mass in SCHMIDT's model. For large ϖ both rotational curves tend asymptotically to $\sqrt{M/\varpi}$, and therefore KUZMIN's rotational velocities will tend to be about $\sqrt{2}$ times as large as SCHMIDT's.

TABLE 3

Comparison of KUZMIN's rotational curve with the curve given by SCHMIDT (units as in section 14).

ϖ	Θ_c (KUZMIN)	Θ_c (SCHMIDT)	ϖ	Θ_c (KUZMIN)	Θ_c (SCHMIDT)
2.050	16.9	17.8	9.225	22.5	20.2
3.075	21.1	19.9	10.250	21.8	19.2
4.100	23.2	21.1	11.275	21.2	18.1
5.125	23.9	22.0	12.300	20.6	17.1
6.150	23.9	22.5	14.350	19.5	15.4
7.175	23.6	22.4	16.400	18.5	14.2
8.200	23.1	21.6			

It can be concluded that KUZMIN's formula (7.12) gives a good approximation of the galactic potential function as given by SCHMIDT's model over large regions within the orbit of the sun around the galactic centre. However at larger distances the agreement is not so good. Also it does not give a good approximation for the potential function outside the plane, since the constant C is somewhat too small. Some adaptation may be possible by variation of the numerical values of the constants Φ°, z_0 and x_0, but this question will not be pursued here.

The physical meaning of the third quadratic integral is not obvious. The function

$$I_3 + I_2^2 + 2\alpha^2 (I_1 - \Phi) \quad (7.18)$$

has been investigated by VAN ALBADA and termed the *integral of combined angular momentum;* for real values of α, the expression

$$I_3 + I_2^2 + 2\alpha^2 (I_1 - \Phi - \Omega) \quad (7.19)$$

corresponds to the mean of the squares of the angular momenta with respect to the points $z = \alpha$ and $z = -\alpha$, $\varpi = 0$.

For the limiting case $\alpha = 0$, the expression (7.19) is equal to the square of the angular momentum vector with respect to the centre of the system, and Φ is spherically symmetrical.

For the limiting case $\alpha \to \infty$, the restriction on the potential which follows from (7.3) is

$$\frac{\partial^2 \Phi}{\partial\varpi\, \partial z} = 0, \quad (7.20)$$

which is the case considered by LINDBLAD (1933, 1959) for a highly flattened stellar system. The potential then has the form

$$\Phi = F(\varpi) + G(z) \quad (7.21)$$

and LINDBLAD's integral is the following limit:

$$\lim_{\alpha\to\infty} \frac{I_3}{\alpha^2} = -Z^2 - 2\Phi(\varpi, z) + 2\Phi(\varpi, 0). \quad (7.22)$$

Returning to the general case, we write equation (7.1) as follows

$$(\varpi Z - z\Pi)^2 - \alpha^2 Z^2 = I_3 - z^2\frac{h^2}{\varpi^2} - 2\alpha^2\Omega\,. \quad (7.23)$$

We note that the right-hand side of this equation is independent of the velocity components, and therefore the expression

$$(\varpi Z - z\Pi)^2 - \alpha^2 Z^2 \quad (7.24)$$

is the same at the beginning and end points of a "loop" in the (ϖ, z)-plane, i.e. at those points where the projection of an orbit on the (ϖ, z)-plane intersects itself. Therefore in each such point only *four* velocity vectors are possible (two of these are realised when the orbit is traversed in one sense, and the two opposite vectors are realised when the orbit is traversed in the opposite sense). These properties of meridional motion hold both for periodic and non-periodic orbits. They have also been found in a number of the numerical computations (see section 18a); these, however, were carried out in a field of force which does not admit of the third quadratic integral of motion.

8. *Reduction of the three-dimensional problem by one dimension*

A particular solution of the equations of motion (1.8) is circular motion in the galactic plane

$$\begin{aligned} \varpi &= \varpi_c \qquad \Pi = 0 \\ z &= 0 \qquad Z = 0\,, \end{aligned} \quad (8.1)$$

with the condition (derived from the first of the six simultaneous equations)

$$\frac{h^2}{\varpi_c^3} = \left(\frac{\partial\Phi}{\partial\varpi}\right)_{\varpi=\varpi_c,\, z=0}\,. \quad (8.2)$$

Physically this is the condition of equality of the centrifugal and centripetal forces in circular motion. The relation between h^2 and ϖ_c for the model of the distribution of mass in the Galaxy according to SCHMIDT (1956), is illustrated in Figure 1.

By introducing the *reduced potential function* defined as

$$U = \tfrac{1}{2}\frac{h^2}{\varpi^2} + \Phi\,, \quad (8.3)$$

the equations of motion become

$$\left.\begin{aligned} \frac{d^2\varpi}{dt^2} &= -\frac{\partial U}{\partial\varpi} \\ \frac{d^2 z}{dt^2} &= -\frac{\partial U}{\partial z}\,. \end{aligned}\right\} \quad (8.4)$$

FIGURE 1

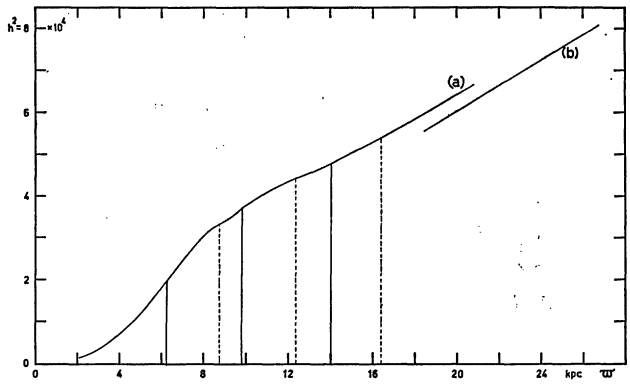

(a) Square of the area constant for SCHMIDT's model (unit 100 km².kpc²/sec²). Inflection points at $\varpi = 6.2$, 9.7 and 14.0; discontinuities in the second derivative at $\varpi = 8.68$, 12.3 and 16.4 (coincident with the boundaries of the Schmidt spheroids).
(b) Asymptotic approximation with total mass concentrated at centre.

In this way the problem of the computation of three-dimensional orbits in the gravitational field of force described by the potential function Φ is reduced to the computation of two-dimensional orbits in the field of force derived from the reduced potential U. The orbit in the (ϖ, z)-plane will be called the *meridional orbit*. It can be regarded either as the path of a particle in the moving meridional plane (angular velocity $\dot{\vartheta} = \frac{h}{\varpi^2}$), or as the cylindrical projection of the three-dimensional orbit in a fixed plane. The third velocity and position coordinates of the space orbit are found from

$$\left.\begin{aligned} \vartheta &= \int_{t_0}^{t}\frac{h}{\varpi^2}\,dt + \alpha_6 \\ \Theta &= \frac{h}{\varpi}\,. \end{aligned}\right\} \quad (8.5)$$

Without further specification of U, the equations of motion (8.4) admit only of the energy integral

$$\tfrac{1}{2}(\Pi^2 + Z^2) + U = E\,, \quad (8.6)$$

in which E is the total energy as before.

The function U contains h explicitly (or ϖ_c implicitly) as a parameter. For the galactic system some equipotential curves $U = \text{const.}$, for $\varpi_c = 5.2$ and 8.2 kpc, are drawn in Figures 2 and 3. They were derived from the interpolation formula for the potential of the Galaxy discussed in section 15. The corresponding values of h are given in Table 4. The function U for $z = 0$ is illustrated in Figure 4 for the values of ϖ_c in Table 4.

FIGURE 2

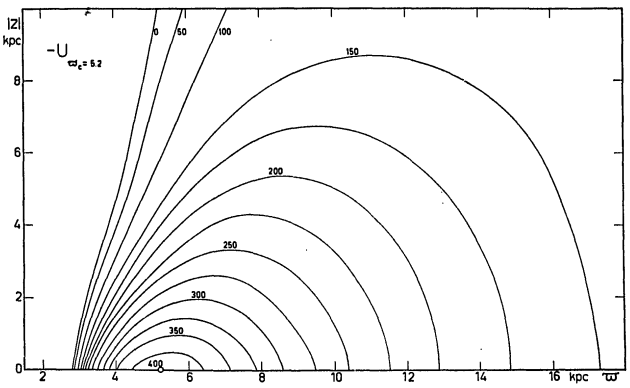

FIGURE 3

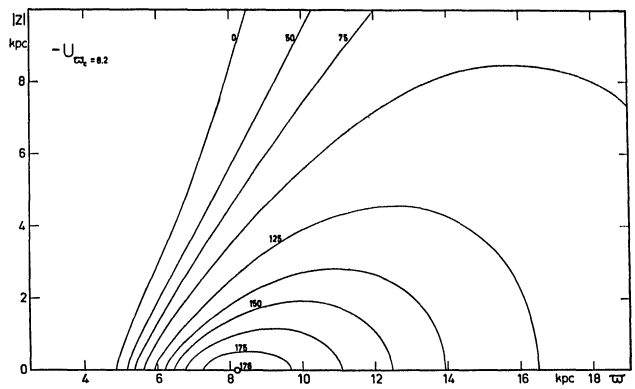

Equipotential curves for various values of the reduced potential U (unit 100 km²/sec²) in the meridional plane for $\varpi_c = 5.2$ ($h = 114$) and $\varpi_c = 8.2$ ($h = 177$) based on the interpolation formula IF.

FIGURE 4

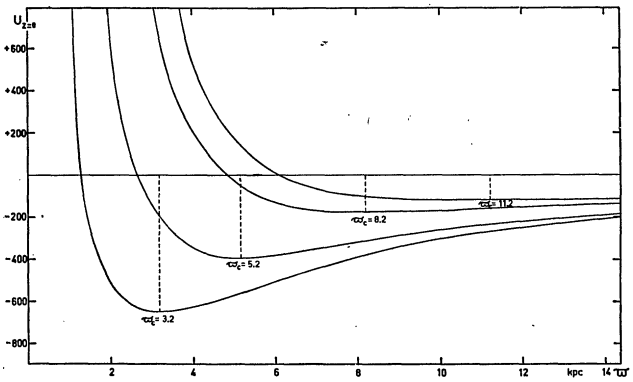

Reduced potential function U in the galactic plane for various ϖ_c, based on the interpolation formula IF (unit 100 km²/sec²).

TABLE 4

Values of the area constant h, and, for small amplitudes around the point of equilibrium ($\varpi = \varpi_c$, $z = 0$), values of the periods of oscillation in the radial direction and perpendicular to the galactic plane, derived from the interpolation formula (section 15).

ϖ_c (kpc)	h (10 km. kpc/sec)	P_a° (10^8 years)	P_c° (10^8 years)
3.2	63.49	0.6528	0.2816
5.2	114.45	0.9245	0.4007
8.2	177.12	2.1002	0.8229
11.2	203.58	4.3797	1.7959

The reduction of the three-dimensional problem by one dimension is known in classical mechanics as the *ignoration* of the coordinate ϑ. This is possible because the Hamiltonian function does not contain ϑ explicitly (for the three-dimensional dynamical system of the star moving in the galactic field of force the angular momentum integral exists).

For unspecified U, the system (8.4) contains no further ignorable coordinates, and further reduction by another dimension is not possible. However, by elimination of the time t from the *two* equations of motion (8.4), a *single* (non-linear) second-order *differential equation for the meridional orbit* is obtained, which relates z to ϖ.

In order to obtain this equation consider z as a function of ϖ, and write the derivatives of z with respect to ϖ as z' and z''. Differentiating the equation $z = z\{\varpi(t)\}$ twice with respect to t we have

$$\left.\begin{aligned} Z &= z'\,\Pi \\ \frac{d^2z}{dt^2} &= z'\,\frac{d^2\varpi}{dt^2} + z''\,\Pi^2 . \end{aligned}\right\} \quad (8.7)$$

Elimination of the variables Π, Z, $\frac{d^2\varpi}{dt^2}$ and $\frac{d^2z}{dt^2}$ from (8.4), (8.6) and (8.7) gives

$$2(E-U)\,z'' = (1+z'^2)\left(z'\frac{\partial U}{\partial \varpi} - \frac{\partial U}{\partial z}\right) . \quad (8.8)$$

This differential equation for the orbit in the (ϖ,z)-plane cannot, in general, be integrated by quadratures. As the original equations of motion did not contain any further ignorable coordinates, there are no integrals of motion without further specification of the function U. For numerical integration the form of this second-order equation is inconvenient, the system (8.4) is to be preferred.

However, some properties of the meridional orbit can be found from this equation. For instance, let us assume, near the point ($\varpi = \varpi_c$, $z = 0$), the expansion (9.1) of the U function (see next section), retain only the terms up to the third degree, and substitute the expression into the differential equation. The solution near this point may be written as

$$z = \sum_{n=0}^{\infty} h_n (\varpi - \varpi_c)^n . \quad (8.9)$$

By substitution in the equation and comparing equal powers of $(\varpi - \varpi_c)$, the following relation is obtained

$$h_2 = \frac{(1 + h_1^2)\,(-c_0 h_0 + a_1 h_1 h_0^2)}{4\,(E - U_c - \frac{1}{2} c_0 h_0^2)} \qquad (8.10)$$

and a recurrence relation for successive coefficients h_n. On including more terms of the expansion (9.1) the form of the above equation for h_2 remains the same, except for higher powers of h_0 which appear in the second factor of the numerator and in the denominator. The quantities h_0 and h_1 may be chosen as integration constants and then all h_n are fixed. In particular if h_0 is chosen equal to zero, that is to say that the integral curve (the orbit) passes through $(\varpi = \varpi_c, z = 0)$, it follows that h_2 is equal to zero and hence the orbit can have an *inflection point* at this point.

9. *Linearisation for small oscillations*

Near the *point of equilibrium* for two-dimensional motion (corresponding to circular motion in the galactic plane with the area constant derived from (8.2)), we may develop the function U in a double power-series in $(\varpi - \varpi_c)$ and z

$$U = U_c + \tfrac{1}{2} a_0 (\varpi - \varpi_c)^2 + \tfrac{1}{2} c_0 z^2 + a_1 (\varpi - \varpi_c) z^2 + c_1 (\varpi - \varpi_c)^3 + \ldots \qquad (9.1)$$

For the coefficients of the terms of the second degree we have

$$a_0 = 3\frac{h^2}{\varpi_c^4} + \left(\frac{\partial^2 \Phi}{\partial \varpi^2}\right)_{\varpi = \varpi_c,\, z = 0} = -4B(A - B) \qquad (9.2)$$

$$c_0 = \left(\frac{\partial^2 \Phi}{\partial z^2}\right)_{\varpi = \varpi_c,\, z = 0} = C^2 \,, \qquad (9.3)$$

in which A and B are OORT's constants of differential rotation, and C is the third dynamical constant.

For infinitesimal oscillations around the point of equilibrium we retain in expression (9.1) only the quadratic terms. In this approximation the equations of motion become

$$\left.\begin{aligned} \frac{d^2\varpi}{dt^2} &= -a_0 (\varpi - \varpi_c) \\ \frac{d^2 z}{dt^2} &= -c_0 z \,. \end{aligned}\right\} \qquad (9.4)$$

These are the equations of motion of a two-dimensional harmonic oscillator around the point of equilibrium. The solution of (9.4) is

$$\left.\begin{aligned} \varpi - \varpi_c &= M \sin (\sqrt{a_0}\, t + \varphi_1) \\ z &= N \sin (\sqrt{c_0}\, t + \varphi_2) \,, \end{aligned}\right\} \qquad (9.5)$$

and the velocities are given by

$$\left.\begin{aligned} \Pi &= M\sqrt{a_0} \cos (\sqrt{a_0}\, t + \varphi_1) \\ Z &= N\sqrt{c_0} \cos (\sqrt{c_0}\, t + \varphi_2) \,, \end{aligned}\right\} \qquad (9.6)$$

in which M, N, φ_1 and φ_2 are the independent integration constants. In the approximation treated here, the equipotential curves $U = \text{const.}$ are ellipses with the constant axial ratio of $\sqrt{a_0/c_0}$, centred on the point of equilibrium. The periods P_a° and P_c° of the two (independent) oscillations are equal to $2\pi/\sqrt{a_0}$ and $2\pi/\sqrt{c_0}$, and are given for the galactic system in Table 4, for various ϖ_c.

The meridional orbit is a Lissajous figure. Depending on whether or not $\sqrt{a_0/c_0}$ is rational, it is either a closed curve or it fills a rectangular region the four corners of which lie on the curve $U = E$ (E is again the total energy of the orbit).

The phase space for meridional motion is four-dimensional, so there are at most 3 isolating integrals of motion (see section 1). The first two of these are

$$\left.\begin{aligned} E_1 &= \tfrac{1}{2}\Pi^2 + \tfrac{1}{2} a_0 (\varpi - \varpi_c)^2 \\ E_2 &= \tfrac{1}{2} Z^2 + \tfrac{1}{2} c_0 z^2 \end{aligned}\right\} \qquad (9.7)$$

and the total energy is the sum of U_c, E_1 and E_2. These two integrals are isolating, because for any given set of initial conditions (or for any set of integration constants) the meridional orbit is confined to a sub-region of the region bounded by the ellipse $U = E$. Either integral can be used as the third integral of motion for the three-dimensional orbit.

From (9.7) we find with (9.5) and (9.6) the dependence of E_1 and E_2 on the integration constants

$$\left.\begin{aligned} E_1 &= \tfrac{1}{2} a_0 M^2 \\ E_2 &= \tfrac{1}{2} c_0 N^2 \,. \end{aligned}\right\} \qquad (9.8)$$

The remaining independent integral of motion, which contains the position coordinates ϖ and z and no velocity components, is obtained by elimination of t from the equations (9.5). It takes the following form

$$F = \frac{1}{\sqrt{a_0}} \arcsin \frac{\varpi - \varpi_c}{M} - \frac{1}{\sqrt{c_0}} \arcsin \frac{z}{N} \qquad (9.9)$$

and the dependence of the integral on the integration constants is

$$F = \frac{\varphi_1}{\sqrt{a_0}} - \frac{\varphi_2}{\sqrt{c_0}} \,. \qquad (9.10)$$

Whether or not the integral F is isolating depends upon whether or not the ratio $\sqrt{a_0/c_0}$ is rational. If the ratio is rational, (9.5) describes a closed Lissajous figure which does not fill the whole of the rectangular

FIGURE 5

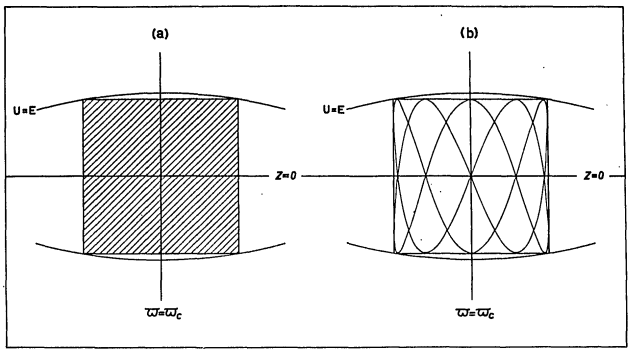

Meridional oscillation for small amplitudes; E_1 and E_2 isolating.
(a) ratio of frequencies irrational: non-periodic orbit, E_3 non-isolating.
(b) ratio of frequencies rational: periodic orbit, E_3 isolating.

region specified by the values of E_1 and E_2. In this case the integral F is isolating, and the system (9.4) is 0-fold primitive.

However, if $\sqrt{a_0/c_0}$ is not rational, the whole of the rectangle is filled eventually by the meridional orbit; then the integral is not isolating and the system (9.4) is 1-fold primitive. The two cases are illustrated in Figure 5.

10. *Contopoulos' third integral*

The theory of the formal third integral of motion, proposed by Contopoulos (1960), is based upon the expansion (9.1) of the reduced potential function U. It may be summarized as follows.

Consider first the special case in which the function U can be written as

$$U = U_c + \tfrac{1}{2}a_0(\varpi - \varpi_c)^2 + \tfrac{1}{2}c_0 z^2 + a_1(\varpi - \varpi_c) z^2. \quad (10.1)$$

For this case the energy integral of the equations of motion (8.4) can be written

$$E = U_c + E_1 + E_2 + a_1(\varpi - \varpi_c) z^2, \quad (10.2)$$

in which E_1 and E_2 are given by the expressions (9.7).

After introducing F_0 and F_1 defined by

$$\begin{aligned} F_0 &= U_c + E_1 + E_2 \\ F_1 &= (\varpi - \varpi_c) z^2 \end{aligned} \quad (10.3)$$

the equation (10.2) can be written

$$E = F_0 + a_1 F_1. \quad (10.4)$$

In the expansion (10.1) the last term can be treated as a *perturbation term* if a_1 is sufficiently small. Contopoulos has sought for a time independent integral, other than the energy integral E, of the form

$$K = K_0 + a_1 K_1 + a_1^2 K_2 + \ldots \quad (10.5)$$

in which $K_0, K_1, K_2, \ldots$ are polynomials in $(\varpi - \varpi_c)$, z, Π and Z.

A necessary and sufficient condition for K to be an integral of the equations of motion (1.8) is, that the Poisson bracket of K and E is equal to zero, viz.:

$$(K, E) = \frac{\partial K}{\partial(\varpi - \varpi_c)}\frac{\partial E}{\partial \Pi} + \frac{\partial K}{\partial z}\frac{\partial E}{\partial Z} - \frac{\partial K}{\partial \Pi}\frac{\partial E}{\partial(\varpi - \varpi_c)} - \frac{\partial K}{\partial Z}\frac{\partial E}{\partial z} = 0. \quad (10.6)$$

Making use of the relation (10.4), this condition can be written

$$(K_0, F_0) + a_1\{(K_0, F_1) + (K_1, F_0)\} + \ldots + a_1^{n+1}\{(K_n, F_1) + (K_{n+1}, F_0)\} + \ldots = 0. \quad (10.7)$$

The equation (10.7) must be satisfied for a range of values of a_1. Therefore each of the terms must vanish separately and we have the equations

$$\begin{aligned} (K_0, F_0) &= 0 && (10.8) \\ (K_0, F_1) + (K_1, F_0) &= 0 && (10.8.0) \\ &\vdots \\ (K_n, F_1) + (K_{n+1}, F_0) &= 0 && (10.8.n) \end{aligned}$$

From (10.8) it is seen that K_0 must be an integral of the unperturbed system (i.e. $a_1 = 0$) treated in section 9, and so it can be put equal to E_1 or E_2. For known K_0, (10.8.0) is a partial differential equation for the unknown polynomial K_1. Contopoulos gave the general solution of this equation and for the polynomial K_1 he found

$$K_1 = -\frac{1}{a_0 - 4c_0}\left\{(a_0 - 2c_0)(\varpi - \varpi_c) z^2 - 2(\varpi - \varpi_c) Z^2 + 2\Pi z Z\right\}. \quad (10.9)$$

When the function K_n is known, the function K_{n+1} can be found from the general solution of (10.8.n). Contopoulos proved that if K_n is a polynomial, K_{n+1} is also a polynomial. Besides the expression (10.9) for K_1, he also derived the explicit expression for K_2.

The convergence of the series (10.5) has not been established. A method of studying the properties of K defined by (10.5), would be to write it as a quintuple power series and to substitute the series in Poisson's condition (10.6). The resulting difference equation

for the coefficients is a linear homogeneous partial difference equation of the third order; the analytical solution of this equation has not been found.

CONTOPOULOS has also discussed the general case, in which U has the expanded form (9.1). He assumed that a third integral K exists and can be expanded into a series, each term of which is a polynomial in $(\varpi - \varpi_c)$, z, Π and Z, and the coefficients of which are the coefficients of (9.1) and their cross products. The series for K is substituted into Poisson's condition (10.6) and the discussion of the resulting equation is similar to that of the case discussed above.

For each value of α_1 the equation $E = \alpha_1$ defines a three-dimensional integral hypersurface in the four-dimensional phase space. The intersection of such an energy surface with the meridional plane is a curve of the form shown in Figures 2 and 3. If the series (10.5) is convergent, the equation $K = \alpha_3$ defines likewise a three-dimensional surface in phase space. The intersection of this surface with an energy surface is a two-dimensional surface containing all paths in phase space which have the integration constants α_1 and α_3 in common.

The boundary in the meridional plane of all meridional orbits which have α_1 and α_3 in common, can be shown to be defined by

$$E = \alpha_1 \quad K = \alpha_3 \quad J = 0, \qquad (10.10)$$

in which J is the Jacobian of K and E with respect to Π and Z.

CONTOPOULOS and P. O. LINDBLAD (1958) have computed two orbits numerically using the electronic computer BESK. For comparison with the numerical computations reported in the present investigation, we give some data on these two orbits.

In the expansion (9.1) for U, CONTOPOULOS and P. O. LINDBLAD have retained only the terms up to the third degree in the variables $(\varpi - \varpi_c)$ and z. The following numerical values of the coefficients in (9.1) were used:

$a_0 = 729$ km^2/sec^2.kpc^2 $\quad a_1 = -1970$ km^2/sec^2.kpc^3
$c_0 = 5250$ km^2/sec^2.kpc^2 $\quad c_1 = -170$ km^2/sec^2.kpc^3.

Both orbits have the same area constant (corresponding to $\varpi_c = 8.2$ kpc), and both orbits have small ϖ- and z-amplitudes. The initial position (for $t = 0$) is for both orbits $\varpi_0 = 8.2$ kpc and $z = 0$; the initial velocities are the following:

	Orbit A (Sun's orbit)	Orbit B
Π_0	− 9.6 km/sec	+ 5.0 km/sec
Z_0	+ 7.3 km/sec	+ 11.0 km/sec

Orbit A was computed over 5.10^9 years and orbit B over 1.10^9 years.

The motion in the meridional plane is best described as a slightly distorted two-dimensional harmonic motion. CONTOPOULOS indicated that each of the orbits may be enclosed accurately by an equilaterial trapezium defined by the straight lines (the unit of length is 1 kpc):

$$\text{Orbit } A \quad \left.\begin{array}{l} (1)\ \varpi - \varpi_c = -0.322 \\ (2)\ z = +0.022\,(\varpi - \varpi_c) + 0.102 \\ (3)\ \varpi - \varpi_c = +0.416 \\ (4)\ z = -0.022\,(\varpi - \varpi_c) - 0.102, \end{array}\right\} \quad (10.11)$$

$$\text{Orbit } B \quad \left.\begin{array}{l} (1)\ \varpi - \varpi_c = -0.154 \\ (2)\ z = +0.031\,(\varpi - \varpi_c) + 0.152 \\ (3)\ \varpi - \varpi_c = +0.238 \\ (4)\ z = -0.031\,(\varpi - \varpi_c) - 0.152. \end{array}\right\} \quad (10.12)$$

The trapezia are only approximations for the actual envelopes of the orbits (provided they exist, which is qualitatively indicated by these computations) because the four corners of an envelope must be rectangular (cf. section 18c).

CONTOPOULOS has found that the empirically obtained envelopes (10.11) and (10.12) agree very well with the envelopes defined by (10.10) on the basis of the formal third integral of motion. The latter gives, instead of the straight lines (1), (2), (3) and (4), quadratic curves which fit even better to the graphs of the meridional trajectories. The quadratic curves replacing (2) and (4) are both slightly convex to the ϖ-axis. This phenomenon appears magnified in the computations reported in the present investigation.

Summarizing, it can be stated that the good fit between the predicted and empirically obtained envelopes of the orbits computed by CONTOPOULOS and P. O. LINDBLAD gives strong support to the conjecture that the third integral of motion K exists[1]). Its usefulness is limited to motions which are confined to the vicinity of the point of equilibrium ($\varpi = \varpi_c$, $z = 0$).

When we are, however, concerned with orbits of higher energy, the reduced potential function U can no longer be approximated by a few terms of the expansion (9.1), and consequently the formal third integral of motion loses its usefulness. The region of the meridional plane to which an orbit of higher energy is confined cannot then be found from the series (10.5) for K. Since the radius of convergence of the series is not known, the formal third integral of motion in these cases also fails to give an answer to the question whether or not a given orbit is confined to a certain region within the curve $E = \alpha_1$ in the meridional plane.

[1]) Because the integral has the form of an infinite series, the convergence of which has not been established, CONTOPOULOS has called the function K a *formal third integral.*

11. *Application of the Hamilton-Jacobi theory*

In this section we investigate the possibilities of solving the equations of motion (8.4) by the method of separation of variables in the Hamilton-Jacobi equation. We begin by writing the equations of motion (8.4) in the canonical form

$$\left.\begin{aligned} \frac{d\varpi}{dt} &= \frac{\partial H}{\partial p_\varpi} & \frac{dp_\varpi}{dt} &= -\frac{\partial H}{\partial \varpi} \\ \frac{dz}{dt} &= \frac{\partial H}{\partial p_z} & \frac{dp_z}{dt} &= -\frac{\partial H}{\partial z}, \end{aligned}\right\} \quad (11.1)$$

in which the Hamiltonian is given by

$$H = \tfrac{1}{2}(p_\varpi{}^2 + p_z{}^2) + U(\varpi, z) . \quad (11.2)$$

The momenta p_ϖ and p_z are equal to $\dot{\varpi}$ and $\dot{z}$ respectively. The value of H, which is constant in time, is equal to the total energy E.

We introduce new orthogonal curvilinear coordinates (λ, μ) by considering the conformal representation of the plane (ϖ, z) on the plane (λ, μ), by means of the analytical function $g = F(\varpi, z) + i\,G(\varpi, z)$, viz.

$$\lambda + i\mu = g(\varpi + iz) . \quad (11.3)$$

We have by definition

$$\frac{\partial F}{\partial \varpi} = \frac{\partial G}{\partial z}, \qquad \frac{\partial F}{\partial z} = -\frac{\partial G}{\partial \varpi} . \quad (11.4)$$

For the functional determinant, defined as

$$J = \frac{\partial(\lambda, \mu)}{\partial(\varpi, z)}$$

we have

$$J = \left(\frac{\partial F}{\partial \varpi}\right)^2 + \left(\frac{\partial F}{\partial z}\right)^2 = \left(\frac{\partial G}{\partial \varpi}\right)^2 + \left(\frac{\partial G}{\partial z}\right)^2 . \quad (11.5)$$

Finally, orthogonality given by

$$\frac{\partial F}{\partial \varpi}\frac{\partial G}{\partial \varpi} + \frac{\partial F}{\partial z}\frac{\partial G}{\partial z} = 0 , \quad (11.6)$$

follows from (11.4).

From the coordinates ϖ and z and the conjugate momenta p_ϖ and p_z we transform to new variables λ, μ, p_λ and p_μ by means of the transformation generated by the function (Goldstein 1957)

$$P(\varpi, z, p_\lambda, p_\mu) = F \cdot p_\lambda + G \cdot p_\mu . \quad (11.7)$$

The transformation equations are then

$$\left.\begin{aligned} p_\varpi &= \frac{\partial P}{\partial \varpi} = \frac{\partial F}{\partial \varpi} p_\lambda + \frac{\partial G}{\partial \varpi} p_\mu \\ p_z &= \frac{\partial P}{\partial z} = \frac{\partial F}{\partial z} p_\lambda + \frac{\partial G}{\partial z} p_\mu \\ \lambda &= \frac{\partial P}{\partial p_\lambda} = F \\ \mu &= \frac{\partial P}{\partial p_\mu} = G . \end{aligned}\right\} \quad (11.8)$$

This is a point transformation and therefore it is canonical, whence the new Hamiltonian becomes

$$\begin{aligned} K &= \tfrac{1}{2}\left(\frac{\partial F}{\partial \varpi} p_\lambda + \frac{\partial G}{\partial \varpi} p_\mu\right)^2 + \tfrac{1}{2}\left(\frac{\partial F}{\partial z} p_\lambda + \frac{\partial G}{\partial z} p_\mu\right)^2 + U(\lambda, \mu) \\ &= \tfrac{1}{2} J (p_\lambda{}^2 + p_\mu{}^2) + U(\lambda, \mu) , \end{aligned} \quad (11.9)$$

making use of relations (11.5) and (11.6).

The new equations of motion—which may be more complicated than the original ones—are

$$\frac{d\lambda}{dt} = J \cdot p_\lambda \quad \frac{dp_\lambda}{dt} = -\tfrac{1}{2}\frac{\partial J}{\partial \lambda}(p_\lambda{}^2 + p_\mu{}^2) - \frac{\partial U}{\partial \lambda} \quad \frac{d\mu}{dt} = J \cdot p_\mu \quad \frac{dp_\mu}{dt} = -\tfrac{1}{2}\frac{\partial J}{\partial \mu}(p_\lambda{}^2 + p_\mu{}^2) - \frac{\partial U}{\partial \mu} . \quad (11.10)$$

The Hamilton-Jacobi method of solving these equations of motion consists of searching for a solution for the *characteristic function* W from the *Hamilton-Jacobi equation*; this equation is obtained by replacing the momenta p_λ and p_μ in the Hamiltonian K by $\frac{\partial W}{\partial \lambda}$ and $\frac{\partial W}{\partial \mu}$ respectively and equating the resulting function to E, viz.:

$$\tfrac{1}{2} J \left\{ \left(\frac{\partial W}{\partial \lambda}\right)^2 + \left(\frac{\partial W}{\partial \mu}\right)^2 \right\} + U(\lambda . \mu) = E . \quad (11.11)$$

We write the solution, which is a function of λ, μ, and, apart from the constant E, of an additional constant α_3, as $W \equiv W(\lambda, \mu, E, \alpha_3)$. This function solves the equations of motion as it generates a canonical transformation in which all the new coordinates are cyclic (cf. e.g. Goldstein 1957); the solution of the equations of motion is

$$\left.\begin{aligned} t + \alpha_4 &= \frac{\partial W}{\partial E} & p_\lambda &= \frac{\partial W}{\partial \lambda} \\ \alpha_5 &= \frac{\partial W}{\partial \alpha_3} & p_\mu &= \frac{\partial W}{\partial \mu} . \end{aligned}\right\} \quad (11.12)$$

Of course the complete three-dimensional problem is solved too, with the 5 integration constants E, h, α_3, α_4, α_5, the 6th integration constant α_6 being the additional constant which determines the zero point in azimuth for the third space component (see the first of equations (8.5)).

The solution of the Hamilton-Jacobi equation (11.11) is feasible only if the occurring variables are *separable*. This is the case if a function of the form

$$W = W_1(\lambda, E, \alpha_3) + W_2(\mu, E, \alpha_3) \quad (11.13)$$

splits the equation (11.11) into two separate equations. In general this is not the case, unless some restriction is imposed upon the function U and hence on the potential function Φ. The form to which Φ is restricted when (11.11) is demanded to be separable, depends upon the choice of coordinates (λ,μ). For instance if we take λ and μ to be ϖ and z themselves it is easily found that Φ must be of the form

$$\Phi = F(\varpi) + G(z), \qquad (11.14)$$

if the corresponding Hamilton-Jacobi equation is to be separable. For this case the equations of motion can be integrated completely by quadratures, by methods much simpler than the present one. The case of small oscillations treated in section 9 is a special case of this. The conditions under which the solution of the Hamilton-Jacobi equation (11.11) is possible can be formulated as follows (we do not give the rather lengthy but straightforward derivation, see HAMEL 1949):

There exists a point (λ_0, μ_0) for which the following relations hold

$$\frac{1}{J(\lambda,\mu_0)} + \frac{1}{J(\lambda_0,\mu)} - \frac{1}{J(\lambda_0,\mu_0)} = \frac{1}{J}, \qquad (11.15)$$

$$\frac{U(\lambda,\mu)}{J} = \frac{U(\lambda,\mu_0)}{J(\lambda,\mu_0)} + \frac{U(\lambda_0,\mu)}{J(\lambda_0,\mu)}. \qquad (11.16)$$

We shall examine three coordinate systems which are of interest for the problem of stellar orbits in the Galaxy and we shall find the form of the potential function Φ to which condition (11.16) leads for each of these cases. Also the form of the third integral of motion is obtained.

(a) Polar coordinates

The coordinate transformation

$$r + i\varphi = \ln(\varpi + iz) \qquad (11.17)$$

gives

$$\begin{aligned} \varpi &= e^r \cos\varphi \qquad & 0 \le r < +\infty \\ z &= e^r \sin\varphi \qquad & 0 \le \varphi \le 2\pi \end{aligned} \qquad (11.18)$$

with the Jacobian $J = e^{-2r}$. (11.19)

The condition (11.15) is satisfied for all (r_0, φ_0); the condition (11.16) is satisfied if Φ is a function of r only, with a suitable zero point depending upon the choice of r_0 and φ_0.

The Hamiltonian becomes

$$\tfrac{1}{2}e^{-2r}(p_r^2 + p_\varphi^2) + \frac{h^2}{2e^{2r}\cos^2\varphi} + \Phi(r) \qquad (11.20)$$

and the equations of motion

$$\frac{dr}{dt} = e^{-2r}p_r \qquad \frac{dp_r}{dt} = e^{-2r}(p_r^2 + p_\varphi^2) + \frac{h^2}{e^{2r}\cos^2\varphi} - \frac{\partial\Phi(r)}{\partial r} \qquad \frac{d\varphi}{dt} = e^{-2r}p_\varphi \qquad \frac{dp_\varphi}{dt} = -\frac{h^2\sin\varphi}{e^{2r}\cos^3\varphi}. \qquad (11.21)$$

We have here the case of the *spherical galaxy* and in this case three-dimensional motion can of course be treated in a much simpler way. It is, however, interesting to note that the Hamilton-Jacobi equation is separable for the case of the Spherical Galaxy, and that a simple solution for the velocities of the meridional motion is obtained from this equation, in the following way:

The Hamilton-Jacobi equation is

$$\tfrac{1}{2}\left(\frac{dW_1}{dr}\right)^2 + \tfrac{1}{2}\left(\frac{dW_2}{d\varphi}\right)^2 + \frac{h^2}{2\cos^2\varphi} + e^{2r}\Phi(r) = e^{2r}\cdot E \qquad (11.22)$$

and the dependence of this equation upon φ is involved in two terms only so that if the equation is to hold identically it must be true that

$$\tfrac{1}{2}\left(\frac{dW_2}{d\varphi}\right)^2 + \frac{h^2}{2\cos^2\varphi} = \text{const} = \alpha_3, \qquad (11.23)$$

from which

$$W_2 = \int \sqrt{2\alpha_3 - h^2/\cos^2\varphi}\, d\varphi. \qquad (11.24)$$

The Hamilton-Jacobi equation can now be solved for W_1, from which the characteristic function is obtained

$$W = \int \sqrt{2(E-\Phi(r))e^{2r} - 2\alpha_3}\, dr + \int \sqrt{2\alpha_3 - h^2/\cos^2\varphi}\, d\varphi. \qquad (11.25)$$

Finally from (11.12) we find the momenta

$$\left.\begin{aligned} p_r &= \frac{\partial W}{\partial r} = \sqrt{2(E-\Phi(r))e^{2r} - 2\alpha_3} \\ p_\varphi &= \frac{\partial W}{\partial \varphi} = \sqrt{2\alpha_3 - h^2/\cos^2\varphi}, \end{aligned}\right\} \qquad (11.26)$$

from which the velocities follow:

$$\left.\begin{aligned} \frac{dr}{dt} &= e^{-2r}\sqrt{2(E-\Phi(r))e^{2r} - 2\alpha_3} \\ \frac{d\varphi}{dt} &= e^{-2r}\sqrt{2\alpha_3 - h^2/\cos^2\varphi}. \end{aligned}\right\} \qquad (11.27)$$

Also the coordinates r and φ are implicitly determined as functions of E, α_3, α_4, α_5 and t, but owing to the elliptic integral occurring in (11.25), they cannot be evaluated explicitly. Along similar lines as discussed in the next case (of elliptic coordinates) we can see that the meridional orbit is bounded by two arcs of

circles and two line sections determined by two angles $\varphi_{min} = \varphi_{max}$ (cf. Figure 6); a non-periodic orbit fills the whole of this region, which has the shape of a distorted rectangle in this case. As in section 7, only four velocities are possible in each point because the expressions for the velocities are two-valued.

By squaring equations (11.27) and adding, we obtain the energy integral

$$E = \tfrac{1}{2}\left\{\left(\frac{dr}{dt}\right)^2 + \left(\frac{d\varphi}{dt}\right)^2\right\} e^{2r} + \frac{h^2}{2\,e^{2r}\cos^2\varphi} + \Phi(r). \quad (11.28)$$

The third integral of motion is obtained by solving one of the equations (11.27) for α_3. As a function of r only it can be written

$$I_3 = \left\{\tfrac{1}{2}\left(\frac{dr}{dt}\right)^2 e^{2r} + \Phi(r) - E\right\} e^{2r} = -\alpha_3 . \quad (11.29)$$

(*b*) Elliptic coordinates

The coordinate transformation [1])

$$\eta + i\xi = \arcsin\frac{\varpi + iz}{\alpha} \quad (11.30)$$

gives

$$\begin{aligned} \varpi &= \alpha\cosh\xi\sin\eta & 0 \le \xi < +\infty \\ z &= \pm\alpha\sinh\xi\cos\eta & -\pi \le \eta \le +\pi \end{aligned} \quad (11.31)$$

where $(\varpi = \pm\alpha,\ z = 0)$ or $\left(\xi = 0,\ \eta = \pm\frac{\pi}{2}\right)$ are the focal points of the confocal ellipses ξ = constant, and hyperbolas η = constant; the Jacobian is

$$J = \frac{1}{\alpha^2(\cosh^2\xi - \sin^2\eta)} . \quad (11.32)$$

For any ξ_0 and η_0 the relation (11.15) is satisfied; from (11.16) it is found that

$$\Phi = \frac{F(\xi) + G(\eta)}{\cosh^2\xi - \sin^2\eta} , \quad (11.33)$$

in which F and G are arbitrary functions of ξ and η respectively, with suitable zero points depending upon the choice of ξ_0 and η_0.

Thus, the assumption that the Hamilton-Jacobi equation is separable in elliptic coordinates leads to the form of the potential function (7.7) obtained in section 7 in connection with the theory of the third quadratic integral.

The Hamiltonian becomes

$$\left.\begin{aligned} &\frac{p_\xi^2 + p_\eta^2}{2\alpha^2(\cosh^2\xi - \sin^2\eta)} + \frac{h^2}{2\alpha^2\cosh^2\xi\sin^2\eta} + \\ &+ \frac{F(\xi) + G(\eta)}{\cosh^2\xi - \sin^2\eta} \end{aligned}\right\} \quad (11.34)$$

and the equations of motion can be written

$$\left.\begin{aligned} \frac{d\xi}{dt} &= \frac{p_\xi}{\alpha^2(\cosh^2\xi - \sin^2\eta)} & \frac{dp_\xi}{dt} &= -\tfrac{1}{2}\frac{\partial J}{\partial\xi}(p_\xi^2 + p_\eta^2) - \frac{\partial U}{\partial\xi} \\ \frac{d\eta}{dt} &= \frac{p_\eta}{\alpha^2(\cosh^2\xi - \sin^2\eta)} & \frac{dp_\eta}{dt} &= -\tfrac{1}{2}\frac{\partial J}{\partial\eta}(p_\xi^2 + p_\eta^2) - \frac{\partial U}{\partial\eta} \end{aligned}\right\} \quad (11.35)$$

The complete solution for the meridional motion is now obtained through the solution of the Hamilton-Jacobi equation, which can be brought into the form

$$\tfrac{1}{2}\left(\frac{dW_1}{d\xi}\right)^2 + \tfrac{1}{2}\left(\frac{dW_2}{d\eta}\right)^2 - \frac{h^2}{2\cosh^2\xi} + \frac{h^2}{2\sin^2\eta} + \alpha^2 F(\xi) + \alpha^2 G(\eta) = E\alpha^2(\cosh^2\xi - \sin^2\eta) . \quad (11.36)$$

The solution of this equation is

$$\left.\begin{aligned} W_1 &= \int\sqrt{V_1(E, h, \alpha, \alpha_3, \xi)}\,d\xi \\ W_2 &= \int\sqrt{V_2(E, h, \alpha, \alpha_3, \eta)}\,d\eta \end{aligned}\right\} \quad (11.37)$$

with

$$\begin{aligned} V_1 &= 2E\alpha^2\cosh^2\xi - 2\alpha^2 F(\xi) + \frac{h^2}{\cosh^2\xi} + 2\alpha_3 \\ V_2 &= -2E\alpha^2\sin^2\eta - 2\alpha^2 G(\eta) - \frac{h^2}{\sin^2\eta} - 2\alpha_3 . \end{aligned} \quad (11.38)$$

From (11.12) the complete solution is obtained; the momenta are

$$p_\xi = \frac{\partial W}{\partial\xi} = \sqrt{V_1} \qquad p_\eta = \frac{\partial W}{\partial\eta} = \sqrt{V_2} \quad (11.39)$$

from which, with the first two equations of motion, the velocities are found

$$\left.\begin{aligned} \frac{d\xi}{dt} &= \frac{\sqrt{V_1}}{\alpha^2(\cosh^2\xi - \sin^2\eta)} \\ \frac{d\eta}{dt} &= \frac{\sqrt{V_2}}{\alpha^2(\cosh^2\xi - \sin^2\eta)} . \end{aligned}\right\} \quad (11.40)$$

Also the coordinates ξ and η are implicitly determined as functions of E, α_3, α_4, α_5 and t, but not explicitly for general functions F and G. Nor can the *orbital equation* (the solution of (8.8)), which should be found by elimination of the time t, be written out explicitly. The interest of the Hamilton-Jacobi method lies in the explicit evaluation of the velocity components (11.40).

[1]) It is assumed here, as in section 7, that the two axes of symmetry of the elliptic coordinate system are the ϖ- and the z-axis. However, the assumption that the vertical axis of symmetry of the coordinate system in the meridional plane coincides with the rotation axis, is an unnecessary restriction (VAN DE HULST 1962a). This restriction can be removed by replacing ϖ in (11.30) by ϖ + a constant. The derivation in this section then remains precisely the same, but the results are more general.

For an attractive force which decreases with distance from the centre of the Galaxy, the orbit will be limited and therefore quasi-periodic in the limited region where the galactic potential function can be approximated by the form derived above. For chosen values of h, E and α_3 the equations (11.40) determine the limits of ξ and η between which the orbit is confined: the expressions V_1 and V_2 must be non-negative for real velocities. Consequently a non-periodic meridional orbit fills a region which has the shape of a distorted rectangle (cf. Figure 6). In this case of separability of the Hamilton-Jacobi equation in elliptic coordinates the region is bounded by sections of ellipses and hyperbolas. Again only four velocities are possible at each point (ξ, η) within the region. For chosen h and E, the integration constants α_4 and α_5 determine the shape of the orbit, the integration constant α_3 the *permissible rectangular region* and the magnitude of the velocity components. Meridional motion which fills a region as sketched in Figure 5, is termed *librational* (see also CONTOPOULOS 1957, p. 31 and KUZMIN 1953, p. 379); *rotational* meridional motion, in which the orbit fills the whole of the space between two ellipses, can also occur (GOLDSTEIN *op. cit.* p. 290). Such motion is only possible if $h = 0$. Whether the whole of the permissible regions are filled or not in these cases, depends upon the commensurability of the frequencies in the ξ and η oscillations.

In order to obtain an expression for the third integral of motion, which is obtained by solving one of the equations (11.40) for α_3, we write for these equations

$$\left.\begin{aligned} V_1 &= \alpha^4 \left(\frac{d\xi}{dt}\right)^2 (\cosh^2\xi - \sin^2\eta)^2 \\ V_2 &= \alpha^4 \left(\frac{d\eta}{dt}\right)^2 (\cosh^2\xi - \sin^2\eta)^2. \end{aligned}\right\} \quad (11.41)$$

Addition of these equations gives the energy integral

$$E = \tfrac{1}{2}\alpha^2 \left\{ \left(\frac{d\xi}{dt}\right)^2 + \left(\frac{d\eta}{dt}\right)^2 \right\} (\cosh^2\xi - \sin^2\eta) + \frac{h^2}{2\alpha^2 \cosh^2\xi \sin^2\eta} + \Phi(\xi, \eta). \quad (11.42)$$

Subtraction of the two equations gives the relation

$$I_3 = -2\alpha_3 - h^2 - 2\alpha^2 E, \quad (11.43)$$

in which I_3 is the third quadratic integral of motion in the form given by expression (7.9).

As there are 3 integration constants for given h and E, there are ∞^3 meridional orbits. Of these only ∞^2 are geometrically different, since there are ∞^1 orbits which are geometrically identical but have a different zero point in time. From the fact that for a given α_3 the permissible region is fixed, we find that there are ∞^1 different orbits which fill this region. Non-periodic orbits are of course asymptotically the same, as each will come arbitrarily close to each point within the permissible region. We shall return to these questions in section 18, where the phenomenology of the numerically computed orbits is briefly reviewed.

If we assume, near the point of equilibrium $(\varpi = \varpi_c, z = 0)$ or $\left(\xi = \xi_c, \eta = \frac{\pi}{2}\right)$ the expansion

$$\left.\begin{aligned} F(\xi) &= \beta_0 + \beta_1(\xi - \xi_c) + \beta_2(\xi - \xi_c)^2 + \dots \\ G(\eta) &= \gamma_2(\eta - \pi/2)^2 + \gamma_4(\eta - \pi/2)^4 + \dots, \end{aligned}\right\} \quad (11.44)$$

in which β_0 is determined by the value of U_c, we find that the second partial derivative of U with respect to ϖ in the point of equilibrium is a linear combination of the coefficients β_0, β_1, β_2 and γ_2; we designate it by a_0 in view of the expansion (9.1) of U:

$$\left(\frac{\partial^2 U}{\partial \varpi^2}\right)_{\varpi = \varpi_c, z = 0} = L_{20}(\beta_0, \beta_1, \beta_2, \gamma_2) = a_0. \quad (11.45)$$

For the other partial derivatives of the 2nd and 3rd order which are not equal to zero, we have in the same way

$$\left.\begin{aligned} \left(\frac{\partial^2 U}{\partial z^2}\right)_{\varpi = \varpi_c, z = 0} &= L_{02}(\beta_0, \beta_1, \beta_2, \gamma_2) = c_0 \\ \left(\frac{\partial^3 U}{\partial \varpi\, \partial z^2}\right)_{\varpi = \varpi_c, z = 0} &= L_{12}(\beta_0, \beta_1, \beta_2, \beta_3, \gamma_2) = 2a_1 \\ \left(\frac{\partial^3 U}{\partial \varpi^3}\right)_{\varpi = \varpi_c, z = 0} &= L_{30}(\beta_0, \beta_1, \beta_2, \beta_3, \gamma_2) = 6c_1. \end{aligned}\right\} \quad (11.46)$$

Suppose that we can solve these 4 linear equations for $\beta_1, \beta_2, \beta_3$ and γ_2. In considering the three 4th-order derivatives which are not equal to zero, only two new coefficients β_4 and γ_4 appear in the linear expressions L_{04}, L_{22}, L_{40}. In order that they may be solved as functions of the expansion coefficients of (9.1), there must exist a relation between the coefficients of the terms of the 4th degree in this expansion.

In general: only if specific relations exist between the coefficients of the terms of the nth degree in the expansion (9.1) of U, the quadratic integral holds exactly in the field of force belonging to it.

The relations are not simple and we have made no attempt to derive them [1]).

(c) Parabolic coordinates

The above-mentioned relations between the coefficients of the expansion (9.1) of U take a simple form if we assume the Hamilton-Jacobi equation to be separable in *parabolic coordinates*.

The coordinate transformation

$$\frac{u+iv}{\sqrt{2}} = \sqrt{\varpi + iz} \tag{11.47}$$

gives

$$\left.\begin{aligned} \varpi &= \frac{u^2-v^2}{2} \qquad 0 \leq u < +\infty \\ z &= \pm uv \qquad\quad 0 \leq v < +\infty . \end{aligned}\right\} \tag{11.48}$$

The ϖ-axis is the axis of u and v parabolas. The Jacobian is

$$J = \frac{1}{u^2+v^2} . \tag{11.49}$$

For any (u_0, v_0) the relation (11.15) is satisfied; (11.16) gives

$$\left.\begin{aligned} &(u^2+v^2) \,.\, U(u,v) = \\ &= (u^2+v_0^2) \,.\, U(u,v_0) + (u_0^2+v^2) \,.\, U(u_0,v) \\ &\text{or } (u^2+v^2) \,.\, U(u,v) = F(u) + G(v) \end{aligned}\right\} \tag{11.50}$$

with $F(u_0) = 0$, $G(v_0) = 0$.

Similarly as in the previous case the Hamiltonian and the equations of motion can be written down, and the Hamilton-Jacobi equation can be integrated. Of the result we write only the velocities

$$\left.\begin{aligned} \frac{du}{dt} &= \frac{\sqrt{2(Eu^2 - F(u) + \alpha_3)}}{u^2+v^2} \\ \frac{dv}{dt} &= \frac{\sqrt{2(Ev^2 - G(v) - \alpha_3)}}{u^2+v^2} . \end{aligned}\right\} \tag{11.51}$$

By taking the square of equations (11.51) and adding, the energy integral is obtained

$$E = \tfrac{1}{2}\left\{\left(\frac{du}{dt}\right)^2 + \left(\frac{dv}{dt}\right)^2\right\}(u^2+v^2) + U(u.v) . \tag{11.52}$$

The third integral of motion is obtained in two forms by solving equations (11.51) for α_3. These two forms are linearly dependent upon each other.

The permissible region to which the orbit is constrained is now bounded by sections of parabolas, see Figure 6. Note that the horizontal sections are concave to the ϖ-axis, as they are in case (b) too, and contrary to the sense of curvature of the envelopes of numerically computed orbits (section 18). In the case treated by KUZMIN (cf. section 7), where the horizontal sections are formed by confocal hyperbolas with the focal points on the z-axis, they are convex to the ϖ-axis.

We shall assume now the expansion (9.1) for U and retain all terms up to the fourth degree. In order that the function U may be of the form (11.50), we have the condition

$$\begin{aligned} (u^2+v^2)\{U_c + \tfrac{1}{8}a_0(u^2-v^2-2\varpi_c)^2 + \tfrac{1}{2}c_0u^2v^2 + \tfrac{1}{2}a_1(u^2-v^2-2\varpi_c)u^2v^2 + \tfrac{1}{8}c_1(u^2-v^2-2\varpi_c)^3 + \\ + \tfrac{1}{16}a_2(u^2-v^2-2\varpi_c)^4 + \tfrac{1}{4}b_2(u^2-v^2-2\varpi_c)^2u^2v^2 + c_2u^4v^4\} = F(u) + G(v) . \end{aligned} \tag{11.53}$$

From this condition we find the relations

$$\left.\begin{aligned} a_0 - 4c_0 + \varpi_c(8a_1 - 6c_1) &= 0 \\ 2a_1 &= c_1 \\ a_2 = b_2 &= c_2 = 0 \end{aligned}\right\} \tag{11.54}$$

and for the function U we find

$$\left.\begin{aligned} U = (u^2+v^2)^{-1}\{&(U_c + \tfrac{1}{2}a_0\varpi_c^2 - c_1\varpi_c^3)(u^2+v^2) + \frac{\varpi_c}{2}(3c_1\varpi_c - a_0)(u^4-v^4) - \\ &- \tfrac{1}{4}(3c_1\varpi_c - a_0)(u^6+v^6) + \tfrac{1}{2}c_1(u^8-v^8)\} . \end{aligned}\right\} \tag{11.55}$$

This case clearly cannot represent the force field of an actual Galaxy. The relations are so simple, however, and the equations for the orbit so lucid, that they may be of use for the study of stellar motions near the point $(\varpi = \varpi_c, z = 0)$ in a higher approximation than that of the small oscillations treated in section 9. For the vicinity of the local centroid CONTOPOULOS (1958) estimates $c_1 \approx \frac{1}{12}a_1$, which means that this approximation is of no use there.

[1]) After this thesis was written, this has been done by VAN DE HULST (1962a) in an investigation concerned with the applicability of ellipsoidal coordinates for the description of the motion of low-velocity stars.

12. *General separation variables*

By specifying a coordinate system and requiring that the Hamilton-Jacobi equation (11.11) be separable in that system, we have found in section 11 the corresponding forms of the potential function U and the solutions of the differential equations of motion. Conversely, in case the function $U(\varpi, z)$ is given (based for instance on a model of the distribution of

FIGURE 6

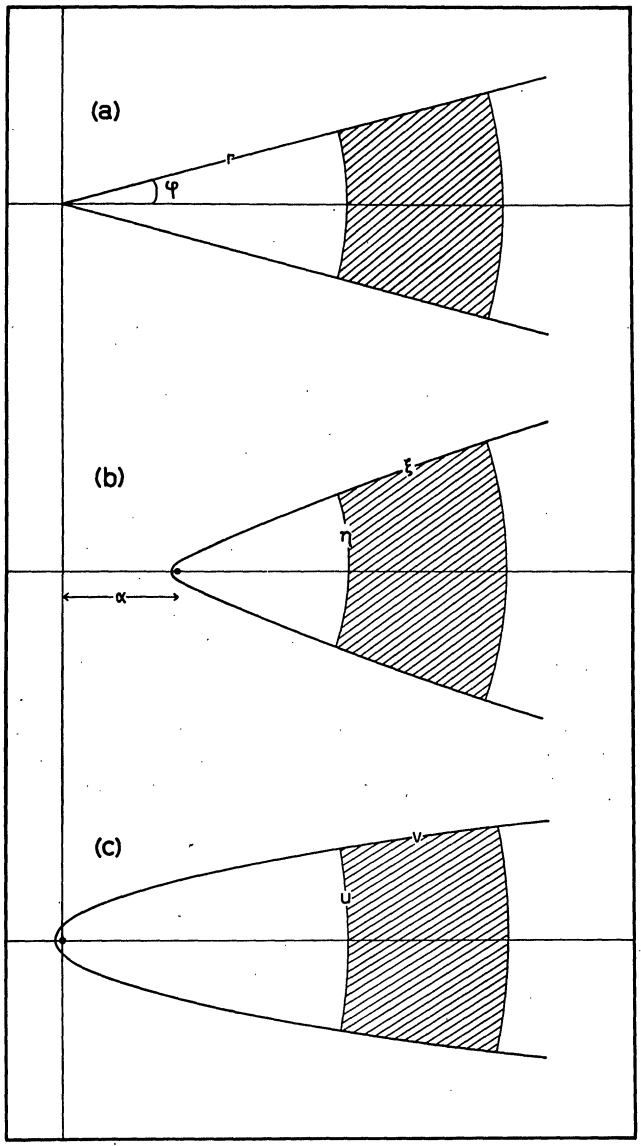

Schematic drawing of the region in the meridional plane filled by the orbit when the Hamilton-Jacobi equation is separable in (a) polar coordinates, (b) elliptic coordinates, (c) parabolic coordinates.

mass in the Galaxy), we may ask whether the corresponding Hamilton-Jacobi equation can be made separable in some coordinate system by choosing appropriate curvilinear coordinates (λ, μ).

In order to bring this problem into the form in which it has been discussed by STÄCKEL (1891) and WEINACHT (1923), we start as in section 11 from the equations of motion (11.1) with the Hamiltonian (11.2), and we introduce new curvilinear coordinates (λ, μ) by (11.3). Since now general separation variables are sought, we do not suppose the function $g = F(\varpi, z) + i\,G(\varpi, z)$ to be analytical. For the line element in the new coordinate system we have

$$ds^2 = g_{11}\,d\lambda^2 + 2\,g_{12}\,d\lambda\,d\mu + g_{22}\,d\mu^2 \qquad (12.1)$$

in which

$$\left.\begin{aligned} g_{11} &= \frac{1}{J^2}\left\{\left(\frac{\partial G}{\partial \varpi}\right)^2 + \left(\frac{\partial G}{\partial z}\right)^2\right\} \\ g_{12} &= -\frac{1}{J^2}\left\{\left(\frac{\partial F}{\partial \varpi}\right)\left(\frac{\partial G}{\partial \varpi}\right) + \left(\frac{\partial F}{\partial z}\right)\left(\frac{\partial G}{\partial z}\right)\right\} \\ g_{22} &= \frac{1}{J^2}\left\{\left(\frac{\partial F}{\partial \varpi}\right)^2 + \left(\frac{\partial G}{\partial z}\right)^2\right\} \end{aligned}\right\} \qquad (12.2)$$

with

$$J = \frac{\partial F}{\partial \varpi}\,\frac{\partial G}{\partial z} - \frac{\partial F}{\partial z}\,\frac{\partial G}{\partial \varpi}\,. \qquad (12.3)$$

We apply now the point transformation (11.7), (11.8) to the Hamiltonian (11.2) and obtain for the new Hamiltonian (see also (11.9)):

$$K = J^2\left(\tfrac{1}{2}\,g_{22}\,p_\lambda^2 - g_{12}\,p_\lambda\,p_\mu + \tfrac{1}{2}\,g_{22}\,p_\mu^2\right) + U(\lambda, \mu)\,. \qquad (12.4)$$

By replacing p_λ by $\frac{\partial W}{\partial \lambda}$ and p_μ by $\frac{\partial W}{\partial \mu}$ in this expression for K, and equating K to E, we obtain the Hamilton-Jacobi equation.

STÄCKEL (*op. cit.*) has shown that the Hamilton-Jacobi equation $K = E$ in which the occurring potential function is not constant and not dependent on one variable only, is separable if and only if it has the following form

$$\frac{1}{2}\,\frac{\left(\frac{\partial W}{\partial \lambda}\right)^2 + \left(\frac{\partial W}{\partial \mu}\right)^2}{A(\lambda) + B(\mu)} - \frac{M(\lambda) + N(\mu)}{A(\lambda) + B(\mu)} = E. \qquad (12.5)$$

In this equation A, B, M and N are arbitrary functions of λ or μ. The line element is then given by

$$ds^2 = \left\{A(\lambda) + B(\mu)\right\}\left(d\lambda^2 + d\mu^2\right). \qquad (12.6)$$

WEINACHT (*op. cit.*) has shown that the most general coordinate system (λ, μ) with this line element, satisfying the condition of Euclidean geometry in the (λ, μ)-plane, is the elliptic coordinate system. It can be defined by (11.30) with the generalization specified in the footnote on page 27.

This result shows that the variables of the elliptic coordinate system are the most general separation variables for the meridional motion of a star in a Galaxy. In section 11 the case of these coordinates was treated; it is the case in which the three-dimensional motion admits of the third quadratic integral of motion. In section 7 we have seen that the field of force of the galactic system in general does not admit of the third quadratic integral of motion.

TABLE 5

Reduced potential function	Integrals besides energy integral	Usefulness of integral and comparisons
SERIES EXPANSION:		
(1) $U=U_c+\frac{1}{2}a_0(\varpi-\varpi_c)^2+\frac{1}{2}c_0z^2$ (9.1)	$E_1=\frac{1}{2}\Pi^2+\frac{1}{2}a_0(\varpi-\varpi_c)^2$ $E_2=\frac{1}{2}Z^2+\frac{1}{2}c_0z^2$ (9.7) $F=\frac{\varphi_1}{\sqrt{a_0}}-\frac{\varphi_2}{\sqrt{c_0}}$ (9.10)	Approximation only valid for small oscillations. E_1 or E_2 can be regarded as the third integral of motion. Only isolating if $\sqrt{a_0/c_0}$ is rational.
(2) as (1) $+a_1(\varpi-\varpi_c)z^2$ (10.1)	$K=K_0+a_1K_1+a_1^2K_2+\ldots.$ (10.5)	Formal third integral of motion; explicit expressions for K_1 (10.9) and K_2 (CONTOPOULOS 1960).
(3) as (2) $+c_1(\varpi-\varpi_c)^3$	Formal third integral in the form of a polynomial expansion	Numerical results of CONTOPOULOS (cf. section 10) indicate validity of assumption of existence of third integral of motion.
(4) as (3), but with all terms of higher degree included		Formal integral of limited use for orbits of higher energy.
POLAR COORDINATES:		
(5) $U=\frac{1}{2}\frac{h^2}{r^2}+\Phi(r)$	I_3 given by (11.29)	Spherical galaxy.
ELLIPTIC COORDINATES:		
(6) $U=\frac{F(\xi)+G(\eta)}{\cosh^2\xi-\sin^2\eta}$ ~ (7.7) ~ (11.33)	Third quadratic integral of motion (7.1) or (7.9); Ω defined by (7.8).	Physical meaning given by (7.19). Comparison with (1) at end of section 7.
(7) as (6) with special forms (7.11) of F and G (KUZMIN).	I_3 as in (7.1)	Comparison of potential function in the galactic plane with the SCHMIDT model made in Tables 2 and 3.
PARABOLIC COORDINATES:		
(8) $U=\frac{F(u)+G(v)}{u^2+v^2}$ (11.50)	Two forms of third integral obtained from (11.51)	Horizontal sections of permitted region concave to ϖ-axis; only useful in limited regions of space where U can be approximated by (11.50).
(9) as (8) with relations (11.54) and (11.55)	I_3 as in (8) with F and G given by (11.55)	Not valid in vicinity of sun.
OFF-CENTRE ELLIPTIC COORDINATES: (see footnote page 25)		
(10) as (6), with F and G in form of series expansion (11.44) near point of equilibrium.	I_3 as in (7.9)	Relation to (4) derived by VAN DE HULST (1962a).

The conclusion is that if the potential function of the Galaxy does not admit of the third quadratic integral of motion (or one of the limiting forms mentioned in section 7) the Hamilton-Jacobi equation cannot be integrated, in any coordinate system obtained from the cartesian coordinates ϖ and z by a point transformation, by the method of separation of variables.

13. *Summary of analytical solutions*

We summarise in Table 5 the various forms which have been proposed as suitable approximations to the galactic potential function in a limited region of space. We mention also the integrals which have been derived for each of these forms. These integrals could be used as quasi-integrals of the actual motion in the Galaxy.

III. Numerical computations

14. *Units*

Throughout this chapter a unit of length of 1 kpc and a unit of time of 0.1 kpc. sec/km will be used. The resulting units of some quantities together with the most frequently occurring symbols of that quantity are listed in Table 6, in which G is the constant of gravitation, with the dimension of (force) (length)^2 (mass)$^{-2}$.

TABLE 6

Units

time	t	0.1 kpc. sec/km $= 0.97749 \cdot 10^8$ years
length	ϖ, z	kpc
velocity	Π, Z, Θ	10 km/sec
energy per unit mass	E	100 km^2/sec^2
potential energy per unit mass	Φ, U	100 km^2/sec^2
OORT's constants	A, B	10 km/sec.kpc
third dynamical constant	C	10 km/sec.kpc
acceleration	K_ϖ, K_z	100 km^2/sec^2.kpc $= 0.324 \cdot 10^{-9}$ cm/sec^2
area constant	h	10 km.kpc/sec
mass density	ρ	$\frac{1}{G}$ (100 km^2/sec^2.kpc^2) $= 1.578 \cdot 10^{-24}$ gr/cm^3 $= 2.32 \cdot 10^{-2} \odot$ /pc^3
mass	M	$= \frac{1}{G}$ kpc (100 km^2/sec^2) $= 4.63 \cdot 10^{40}$ gr $= 2.32 \cdot 10^7 \odot$

Some numerical values for the local centroid, based on the well-known model of the mass distribution in the galactic system developed by M. SCHMIDT (1956), are given in Table 7. Potential and kinetic energies are per unit mass.

TABLE 7

Some numerical data for the local centroid. Units are as specified in Table 6.

distance from gal. centre	8.2
potential energy	−410.2
kinetic energy of circular motion	234.4
circular velocity	21.65
area constant	177.5
period in circular motion	2.38
centripetal force	−57.2
OORT's constant A	1.95
OORT's constant B	−0.69
third dynamical constant C	7.25

15. *Representation of the galactic potential function by an interpolation formula*

(a) Introduction

As a basis for the computation of three-dimensional orbits of particles of mass in the Galaxy, the model of the distribution of mass in the galactic system developed by SCHMIDT (1956) will be used. The "SCHMIDT Model", hereafter referred to as SM, consists of 4 inhomogeneous and 9 homogeneous ellipsoids of revolution with various ellipticities and density laws as specified in Table 4 of SCHMIDT's publication.

Numerical computation of the force components parallel and perpendicular to the galactic plane

$$\left.\begin{aligned} K_\varpi &= -\frac{\partial \Phi}{\partial \varpi} \\ K_z &= -\frac{\partial \Phi}{\partial z}, \end{aligned}\right\} \qquad (15.1)$$

from the formulae given by SCHMIDT presents some difficulties to an automatic computer. These may be summarized as follows:

(i) For each inhomogeneous spheroid, the expressions for K_ϖ and K_z contain an arcsin function if (ϖ, z) is an external point (the solution for γ of the last of the definition equations (15.3)); the expression for K_z contains a logarithmic function.

(ii) Computation of K_ϖ and K_z in the model must be preceded by an administrative programme to determine for which spheroids the point (ϖ, z) is an external point, and for which an internal point.

In order to circumvent the last difficulty, it would be possible to use a simplified model of the mass distribution consisting merely of one inhomogeneous spheroid (SCHMIDT's first model, *ibid.*). That introduces however, a region in the plane of symmetry of the force field where the criterion for stability of circular orbits is not fulfilled. We give a short discussion of this matter as follows:

The criterion for stability of circular orbits is:

$$\frac{d(\varpi^3 K_\varpi)}{d\varpi} = -\frac{dh^2}{d\varpi} < 0. \qquad (15.2)$$

For one inhomogeneous spheroid, in SCHMIDT's notation, we have the definitions

$a_r = -\frac{q}{p}$, semi-major axis;

c_r , semi-minor axis;

$\rho = p + \frac{q}{\varpi}$, density in plane of symmetry, where p and q are constants; $\rho = 0$ for $\varpi \geq a_r$;

$e = \sqrt{1 - \frac{c_r^2}{a_r^2}}$, eccentricity;

$\sin\gamma = e$, for internal points, $a(\varpi, z) \leq a_r$;

$\varpi^2 \sin^2\gamma + z^2 \operatorname{tg}^2\gamma = a_r^2 e^2$, for external points,

$a(\varpi, z) > a_r$. (15.3)

From condition (15.2) the region of instability can be derived by simple analysis. The result is

$$\frac{3 a_r e (1 - \sqrt{1-e^2})}{2(\arcsin e - e\sqrt{1-e^2})} < \varpi < \frac{a_r e}{0.9816}, \qquad (15.4)$$

in which the constant 0.9816 is the value of $\sin\gamma$ satisfying the equation

$$2\gamma + \sin\gamma(\cos\gamma - 3) = 0, \qquad (15.5)$$

FIGURE 7

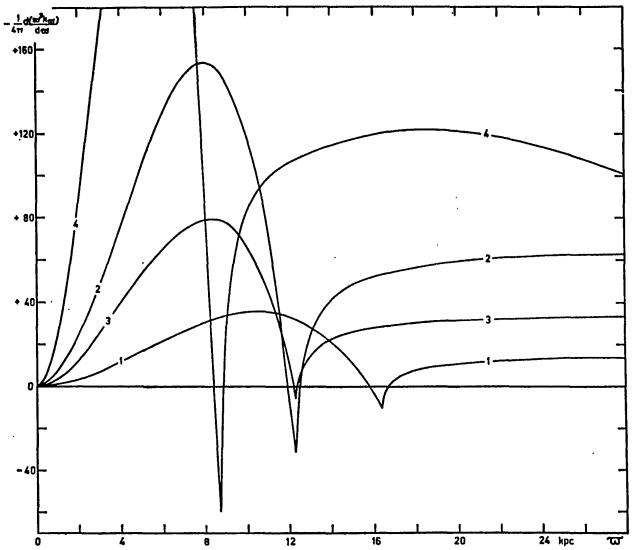

Curves demonstrating regions of instability of circular orbits in the galactic plane for each of the four inhomogeneous spheroids separately. Numbers of the curves refer to spheroids in SCHMIDT's designation. Unit in ordinate: 100 km².kpc/sec².

while at $\varpi = a_r$, the function $d(\varpi^3 K_\varpi)/d\varpi$ has a turning point, with a two-valued derivative[1]).

The formulae in (15.4) give for SCHMIDT's first model the region of instability $9.32 < \varpi < 9.74$. For each of the four individual inhomogeneous spheroids of the final model SM, the (narrow) regions are illustrated in Figure 7. In the final model obtained by superposition of the spheroids and the addition of correcting homogeneous spheroids, all circular orbits are stable, corresponding to the absence of extrema in the function $h^2(\varpi)$ (cf. Figure 1); this is illustrated by the behaviour of the derivative of h^2. In Figure 8 the left-hand side of (15.2) for the SM is compared with the same quantity derived from the "Interpolation Formula" to be described in this section (and referred to in the sequel as IF). Also for the IF all circular orbits are stable.

FIGURE 8

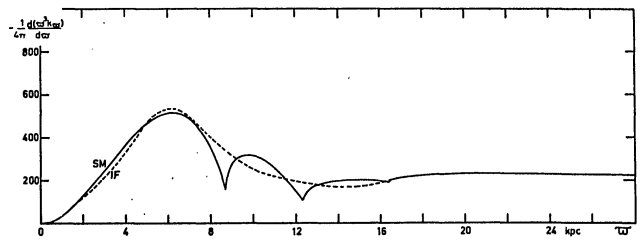

Curve demonstrating the absence of unstable circular orbits in the final SCHMIDT model and in the force function K_ϖ of the interpolation formula. Unit in ordinate: 100 km².kpc/sec².

[1]) From (15.4) we find that instability of circular motions at the periphery of an inhomogeneous ellipsoid occurs when the ratio of the axes is smaller than 0.191.

The absence of a region of instability implies that the envelope of the *characteristic lines* in the (E, h^2)-diagram satisfying for each ϖ

$$E = \Phi(\varpi, 0) + \frac{h^2}{2\varpi^2}, \qquad (15.6)$$

and drawn for SM in Figure 9, for $\varpi > 2$ kpc, has no singular points.

From the energy equation (1.9) it is clear that not every combination (E, h^2) is possible for actual orbits with a positive kinetic energy. This means that in the characteristic diagram of Figure 9 a possible point must lie to the *right and below* the characteristic envelope. Points on the envelope correspond to circular orbits.

FIGURE 9

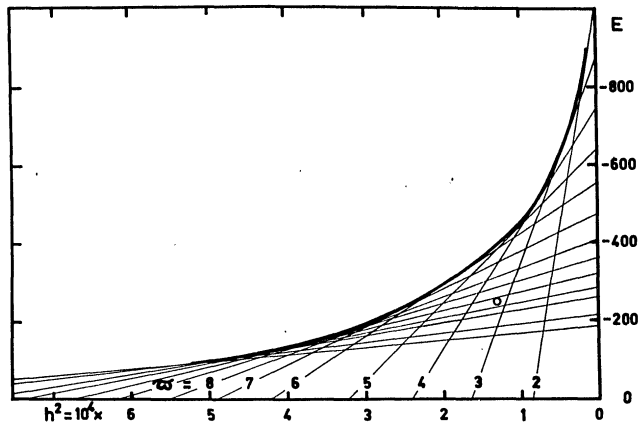

Characteristic diagram for the SCHMIDT model. The open circle represents the family of orbits for which numerical computations were performed. Unit in the abscissa: 100 km².kpc²/sec². Unit in the ordinate: 100 km²/sec².

We return now to the discussion of the problem how the numerical computations of K_ϖ and K_z by the automatic computer should be arranged. The imperative demand for the evaluation of these quantities in a relatively short computation time, which is brought about by the necessity of computing orbits for a long period of time in the Galaxy, suggests that we discard a method which would require computations on all 13 spheroids of the SM.

As we have seen, it is not possible to use the simplified model consisting of merely one inhomogeneous spheroid, due to the occurrence of the region of instability for circular orbits. Using a model consisting only of the 4 inhomogeneous spheroids of the SM, and thus discarding the 9 correcting homogeneous spheroids, would avoid this difficulty. This method has been considered but was not used for the following reasons: (1) the SM would not have been used any longer and that might have reduced the usefulness of the orbit computations for astronomical purposes, (2) the evaluation of the arcsin and logarithmic

functions and the extraction of 5 square roots per spheroid would have caused the computation time to remain high.

(b) Curve fitting

Two alternative means of computing the force components in the SM by an automatic computer seemed acceptable in principle.

(1) The storage in the memory of a sufficiently large two-dimensional table of SCHMIDT's Φ_{SM}, from which K_ϖ and K_z would have to be computed by two-dimensional numerical partial differentiation.

(2) The development of an interpolation formula for Φ, of which the analytical partial derivatives are suitable for computation (preferably no transcendental functions), and which approximates Φ_{SM} rather closely.

Neither of the two methods seemed to be evidently better, and a decision as to which method to follow was made with a view to the possibilities of the computers to be used, first the ARMAC of the Mathematisch Centrum, Amsterdam, and later the BESK of Matematikmaskin Nämnden, Stockholm. Some disadvantages of both methods may be mentioned:

Method (1): the table of Φ given by SCHMIDT is not extensive enough for simple interpolation so that either it would have to be enlarged to (say) 5 points per kpc, or an elaborate interpolation method would have to be used, which takes us in the direction of method (2). In the former case this would mean, for the family of orbits later to be described, the storage of about 600 values of Φ; this is more than half of BESK's fast memory (the ARMAC has no fast memory), thus necessitating storage in the slow (drum) memory plus an administrative programme for periodic transport, during the orbit computation, of the relevant part of the table from slow to fast memory. Also, the numerical partial differentiation in two variables is a complicated matter.

Method (2): even if it is possible to find a simple formula, suitable for use in an automatic computer, which represents Φ_{SM} to a high degree of accuracy, it must be expected that the force components are represented less well, and the density distribution still less or not with any accuracy at all. This disadvantage however, was considered to carry no great weight, for it is the potential function which forms the orbit. Variations in the potential function (i.e. systematic differences between Φ_{SM} and Φ_{IF}) will have a pronounced effect on the shape of the orbits in one or the other force field; variations in the force function will show up less in the orbits, and variations in the density function still less.

It was decided to use method (2) and to represent the potential function Φ_{SM} by an interpolation formula of the type

$$\Phi_{IF} = -\frac{1000}{\sqrt[4]{Q_{IF}}}, \tag{15.7}$$

in which Q_{IF} is an algebraic function of the variables ϖ and z. The rest of this section is devoted to a brief description of the considerations leading to the form:

$$Q_{IF} = P_n + \frac{P_a}{P} - \frac{P_c}{P_k} + \frac{P_c}{P_k + z^2} + P_m = R + \frac{P_c}{P_k + z^2} + P_m, \tag{15.8}$$

in which
$$\left.\begin{aligned} P_n &= n_4 \varpi^4 + n_2 \varpi^2 + n_0 \\ P_a &= a_8 \varpi^8 \\ P_b &= \varpi^4 + b_2 \varpi^2 + b_0 \\ P_c &= c_6 \varpi^6 + c_4 \varpi^4 + c_0 \\ P_k &= k_{10} \varpi^{10} + k_2 \varpi^2 + k_0 \\ P_m &= m_4 z^4 + 2 m_4 \varpi^2 z^2 + m_2 z^2, \end{aligned}\right\} \tag{15.9}$$

and
$$R = P_n + \frac{P_a}{P_b} - \frac{P_c}{P_k}, \tag{15.9a}$$

which depends on ϖ only.

The adopted values of the 14 constants are listed in Table 8.

For $\varpi \to \infty$, $z \to \infty$ we have

$$\begin{aligned} Q_{IF} &= (n_4 + a_8)\, \varpi^4 + 2 m_4 \varpi^2 z^2 + m_4 z^4 \\ &= m_4 (\varpi^2 + z^2)^2 . \end{aligned} \tag{15.10}$$

Thus for large ϖ and z the potential function is that of a mass point with mass

$$M = \frac{1000}{\sqrt[4]{m_4}} . \tag{15.11}$$

TABLE 8

The numerical values of the 14 constants occurring in the interpolation formula IF.

n_0	$+ 0.34178$	c_4	$- 0.6607 \cdot 10^{-3}$
n_2	$+ 0.14023$	c_6	$- 0.9516 \cdot 10^{-5}$
n_4	$+ 0.1184 \cdot 10^{-2}$	k_0	$+ 0.2$
a_8	$+ 0.139 \cdot 10^{-1}$	k_2	$+ 0.1045 \cdot 10^{-1}$
b_0	$+ 4.21937 \cdot 10^{3}$	k_{10}	$+ 0.12464 \cdot 10^{-10}$
b_2	$+ 0.7857 \cdot 10^{2}$	m_2	$+ 0.59$
c_0	$- 0.4 \cdot 10^{-1}$	m_4	$+ 0.15084 \cdot 10^{-1}$

$n_4 + a_8 = m_4$; $M = 1000/\sqrt[4]{m_4} = 2852$ units $= 66.5 \cdot 10^9\, m_\odot$.

Two features of the SM which rest on considerable observational material must be represented well by the IF:

(1) the rotational curve $\Theta_c(\varpi)$,

(2) K_z $(\varpi = 8.2)$ for small z.

Examination of the function $\Phi_{SM}^{-4}(z = 0)$ sug-

gested the form $Q_{IF}(z=0) = P_n$. It was, however, impossible to represent the SM curve

$$\Theta_c^2 = -\varpi K_\varpi \qquad (15.12)$$

using this simple expression, and therefore the correction term P_a/P_b was added. The latter behaves as $\frac{a_8}{b_0}\varpi^8$ for small ϖ and as $a_8\,\varpi^4$ for large ϖ [1]).

The best values of the 6 constants $n_0, n_2, n_4, a_8, b_0, b_2$ on which $Q_{IF}(z=0)$ depends, were found by fitting Φ_{IF}^{-4} to Φ_{SM}^{-4}, and $\Theta^2_{c,IF}$ to $\Theta^2_{c,SM}$. Table 9 shows these comparisons. The value of m_4 was obtained as the sum of n_4 and a_8. Substitution of the value of m_4 in (13.11) gives for M_{IF} 95% of M_{SM}. Therefore the value of Φ_{IF} will tend to be 5% higher than Φ_{SM} for large values of ϖ and/or z. Table 9 shows that this effect is unimportant in the plane for $\varpi < 16$ kpc.

TABLE 9

Comparison of Q (unit 10^4 sec^8/km^8), Φ and Θ_c^2 (unit 100 km^2/sec^2) for SM and IF, for $z=0$.

ϖ (kpc)	Q_{SM}	Q_{IF}	Φ_{SM}	Φ_{IF}	$\Theta_{c,SM}^2$	$\Theta_{c,IF}^2$
0	0.235	0.342	−1436	−1308	0	0
2.050	0.953	0.953	−1012	−1012	318	337
3.075	1.754	1.796	− 869	− 864	394	390
4.100	3.195	3.225	− 748	− 746	447	431
5.125	5.814	5.792	− 644	− 645	482	482
6.150	10.616	10.639	− 554	− 554	504	510
7.175	19.643	19.644	− 475	− 475	502	503
8.200	35.386	35.385	− 410	− 410	467	467
9.225	60.864	61.025	− 358	− 358	406	419
10.250	97.752	100.174	− 318	− 315	369	371
11.275	151.56	156.846	− 285	− 283	327	331
12.300	225.68	235.405	− 258	− 255	293	295
14.350	451.06	477.37	− 217	− 214	237	243
16.400	800.60	868.27	− 188	− 184	202	203

FIGURE 10

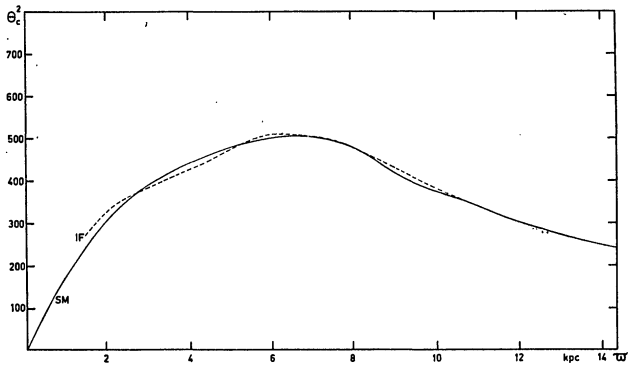

Rotation curve for SCHMIDT's model and for the interpolation formula. Unit in ordinate: 100 km^2/sec^2.

FIGURE 11

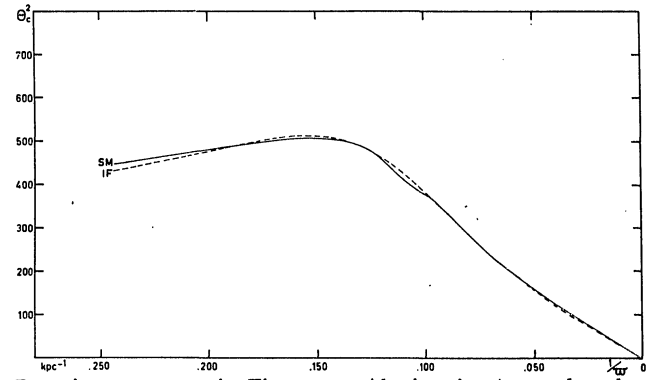

Rotation curves as in Figure 10. Abscissa is $1/\varpi$ to show behaviour at large ϖ.

In Figures 10 and 11 the comparison of the circular velocities is illustrated in a linear scale ($\varpi = 0$ to 14.35) and in a reciprocal scale ($\varpi = 4$ to ∞). Around $\varpi \approx 9$ the steep gradient of $\Theta^2_{c,SM}$ is not reproduced by the IF. This shows up in the comparison between $K_{\varpi,SM}$ and $K_{\varpi,IF}$ for $z=0$ (cf. Figure 14).

[1]) There is of course no reason to restrict oneself to even powers of ϖ only, as long as this behaviour is complied with. However, more terms besides $b_2\varpi^2$ were not needed in P_b. Also in P_c and P_k, odd powers of ϖ might have been added, but the dependences $P_c \sim \varpi^6$ and $P_k \sim \varpi^{10}$ for large ϖ, are peremptory, and from there on we have searched for a representation with as few terms as possible.

Next we consider $z \neq 0$, and, in order to find the form of Q_{IF} outside the galactic plane, we examine Figure 12, in which Q_{SM} (ϖ = const.) is drawn as a function of z^2. In the next schematic Figure 13, some formulae have been written to show how the form (15.8) was arrived at. The curve $Q_{SM}(z^2)$ for a fixed ϖ has an inflection point at $z = z_0$, which was found by graphical determination of the minimum of

$$\frac{\partial Q_{SM}}{\partial z^2} = \frac{2}{z}\,10^{12}\,K_{z,SM}\,\Phi_{SM}^{-5} \qquad (15.13)$$

as a function of z. Table 10 gives the values of z_0 found in this way.

FIGURE 12

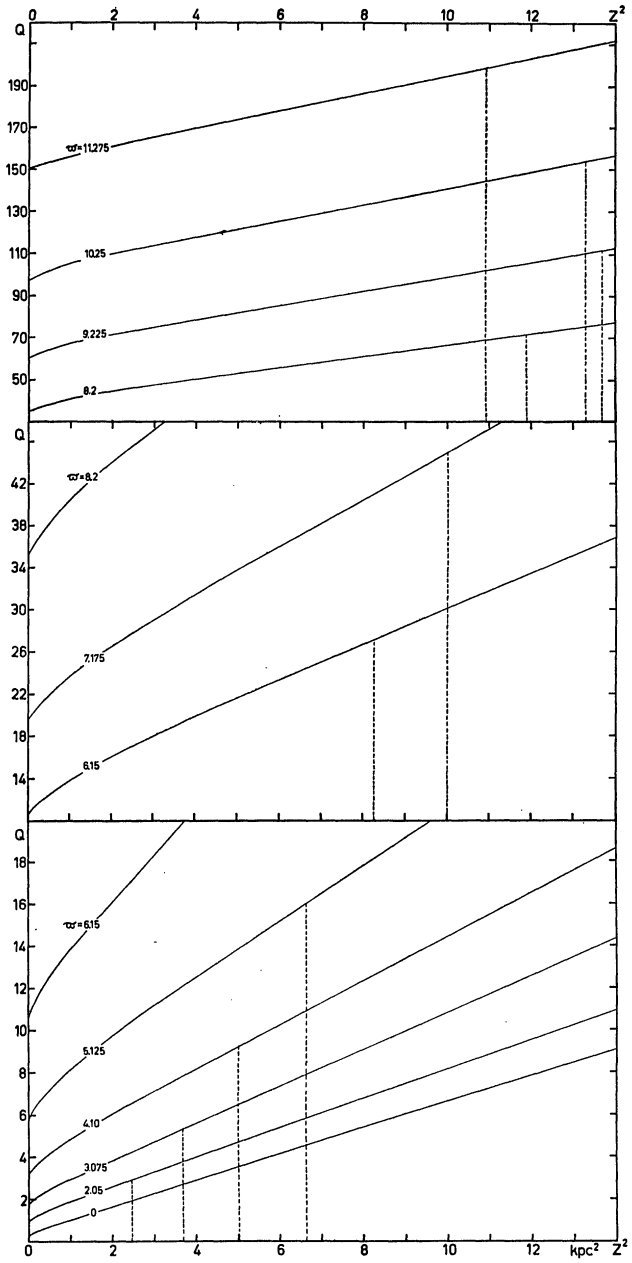

Function used in finding the interpolation formula for the potential outside the galactic plane.
Inflection points at z_0^2. Unit in ordinate: $10^4 \mathrm{sec}^8/\mathrm{km}^8$.

TABLE 10

The inflection points (ϖ, z_0) of the curves Φ_{SM}^{-4} (ϖ = const.) as found by graphical determination.

ϖ (kpc)	z_0 (kpc)	ϖ (kpc)	z_0 (kpc)
2.05	1.575	8.20	3.45
3.075	1.92	9.225	3.70
4.10	2.24	10.25	3.65
5.125	2.575	11.275	3.30
6.15	2.875	12.30	2.95
7.175	3.16	14.35	2.275

Through the inflection point of each curve $Q_{SM}(z^2)$ the tangential line was drawn.

The dependence of the gradient of this line on ϖ,

$$\left(\frac{\partial Q_{IF}}{\partial z^2}\right)_{z_0} = -\frac{P_c}{(P_k + z_0^2)^2} + 2m_4\varpi^2 + m_2 + 2m_4 z_0^2 \approx$$
$$\approx 2m_4\varpi^2 + m_2 , \qquad (15.14)$$

gives a straightforward determination of m_2. The intersection of the tangential line with the Q-axis gives, for each ϖ, a preliminary determination of R (see Figure 13), which we designate by R_{SM}.

Remains to be found the form of $P_c(\varpi)$ and $P_k(\varpi)$.

We approximate (15.8) for small z by leaving out the term $m_4 z^4$

$$Q_{IF} \approx R + \frac{P_c}{P_k + z^2} + (2m_4\varpi^2 + m_2) z^2 . \qquad (15.15)$$

Then

$$(Q_{IF} - R - (2m_4\varpi^2 + m_2) z^2)^{-1} \qquad (15.16)$$

should be a linear function of z^2 for each ϖ. From graphs of (15.16) using Q_{SM}, the already determined function R_{SM} and the constants m_2 and m_4, it was found that

$$P_c = c_6\varpi^6 + c_4\varpi^4 + c_0 \qquad (15.17)$$

of which the coefficients were readily determined.

FIGURE 13

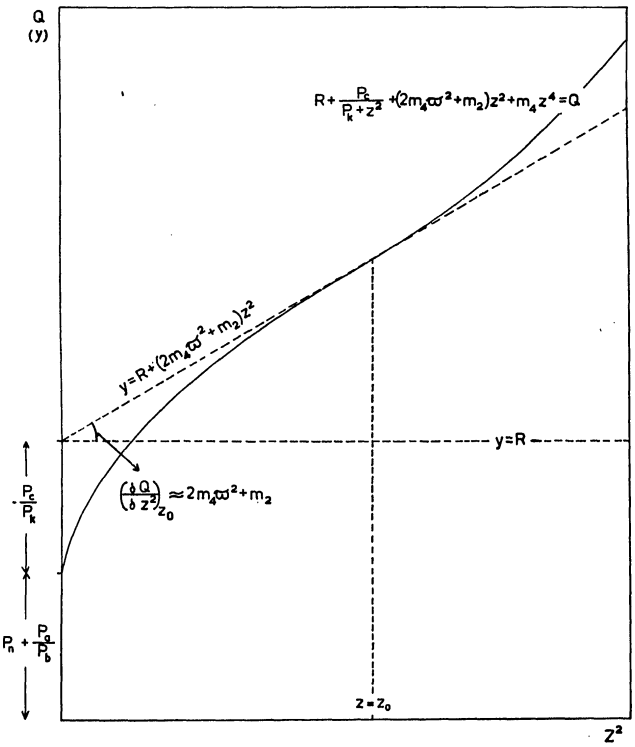

Schematic illustration of the derivation of the form of the interpolation formula outside the galactic plane. Tangent is drawn through the inflection point.

The quantity P_k/P_c could also have been determined from these graphs, and hence P_k, but it was considered better to derive P_k by curve fitting such that the quantity $(K_z/z)_{z=0}$ in the SM is represented well. We have

$$\frac{K_z}{z} = -\frac{1000}{4.z} \cdot Q^{-5/4} \frac{\partial Q}{\partial z} \qquad (15.18)$$

from which (for $z = 0$)

$$\frac{2}{1000}\left(\frac{K_z}{z}\right)_{z=0}\left(P_n + \frac{P_a}{P_b}\right)^{5/4} + (m_2 + 2\,m_4\,\varpi^2) = \frac{P_c}{P_k^{\,2}}\,.$$

Finally, in

$$P_k = P_c^{\,\frac{1}{2}}\left\{-2\left(\frac{K_z}{z}\right)_{z=0}\frac{P_n + P_a/P_b}{\Phi_{z=0}} + (m_2 + 2\,m_4\,\varpi^2)\right\}^{-\frac{1}{2}}, \qquad (15.19)$$

SCHMIDT's values of $\Phi_{z=0}$ and $(K_z/z)_{z=0}$ were used in combination with m_2, m_4 and the coefficients in $P_n + P_a/P_b$ determined earlier; it was found that P_k can be represented by

$$P_k = k_{10}\,\varpi^{10} + k_2\,\varpi^2 + k_0 \qquad (15.20)$$

and the values of the coefficients giving best fit were determined.

(c) Comparison with SCHMIDT's model

Equations (15.8) and (15.9) imply that the potential function is represented in the galactic plane by 6 constants, and that 7 additional constants are needed for the representation outside the galactic plane.In the previous section only the *method* of deriving the values of the coefficients of the polynomials (15.9) was discussed, but not the extensive calculations which gave these values. It is now appropriate to inspect the final representation of Φ, which is after all the only thing of interest.

Table 11 gives a comparison between Φ_{SM} and Φ_{IF} — the fit is very good over the whole range of 10 × 10 kpc². In Figure 14, $K_{\varpi,SM}$ and $K_{\varpi,IF}$ are compared for various z. For $z = 0$ the high gradient of $K_{\varpi,SM}$ at $\varpi \approx 9$ is not reproduced by $K_{\varpi,IF}$. In Figure 15, $K_{z,SM}$ and $K_{z,IF}$ are compared for various ϖ, and in Figure 16 $K_{z,IF}$ is compared with the recent determinations of K_z by HILL (1960) and OORT (1960) at $\varpi = 8.2$ (cf. Table 6 in the latter paper). The occurrence, in the K_z curves for the IF, of *three* inflection points instead of only *one*, for a rather large range in ϖ, is the weakest point of the representation of the potential function by (15.8). Attempts were made to eliminate this feature by the addition of "correcting terms" of various kinds but it was not possible to find a simple term, with one or two additional constants. In view of the fact that local irregularities in K_z will not greatly affect the general properties of orbits — which are obtained by *integration* of the forces —, this point was not pursued further and the subsequent numerical orbit computations have

FIGURE 14

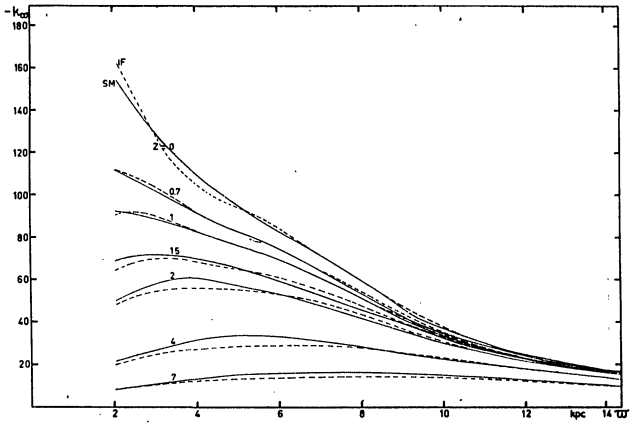

Radial force components in and outside the galactic plane (unit 100 km²/sec².kpc), in the SCHMIDT model and in the interpolation formula.

TABLE 11

Comparison of the potential function given by the interpolation formula with the potential function in SCHMIDT's model. The unit of potential is 100 km²/sec².

ϖ (kpc)	2.05		4.1		6.15		8.2		10.25		12.3	
z (kpc)	$-\Phi_{SM}$	$-\Phi_{IF}$	$-\Phi_{SM}$	$-\Phi_{IF}$	$-\Phi_{SM}$	$-\Phi_{IF}$	$-\Phi_{SM}$	$-\Phi_{IF}$	$-\Phi_{SM}$	$-\Phi_{IF}$	$-\Phi_{SM}$	$-\Phi_{IF}$
0	1012	1012	748	746	554	554	410	410	318	316	258	255
0.1	1003	1008	745	745	553	553	410	410	318	316	258	255
0.2	991	997	740	740	551	551	409	409	318	316	258	255
0.4	959	965	725	725	544	544	407	406	317	315	258	255
0.7	904	911	700	700	531	531	402	400	315	312	257	254
1.0	851	857	675	673	518	517	396	394	312	309	257	253
1.5	775	771	630	629	495	495	386	384	308	304	256	250
2.0	706	696	591	585	473	473	376	374	304	299	254	248
3.0	605	580	522	508	433	428	354	351	292	288	247	241
4.0	520	496	460	446	395	387	332	327	280	275	239	234
5.0	458	433	414	396	361	351	312	304	268	261	229	225
7.0	362	343	339	321	306	294	273	264	243	234	212	207
10.0	270	259	260	248	247	233	228	217	208	199	188	182

been carried out using the interpolation formula (15.8) with the constants of Table 8. Extensive calculations have been performed on the ARMAC in order to determine the positions of the inflection points and the magnitude of the differences between $K_{z,\mathrm{IF}}$ and $K_{z,\mathrm{SM}}$. As these differences have had no apparent effect on the orbits to be described in this thesis, these computations are not discussed here.

FIGURE 15

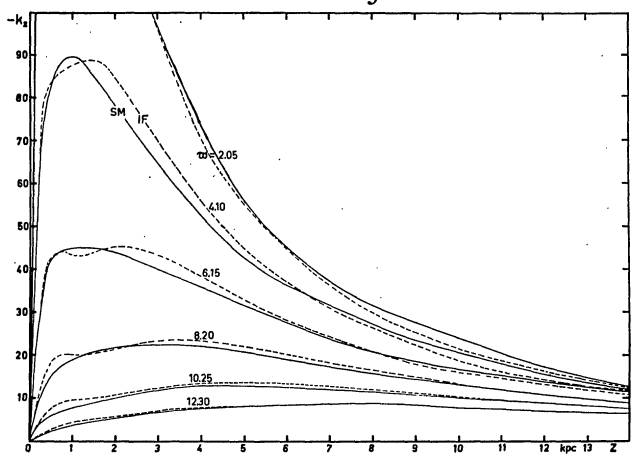

Force components perpendicular to the galactic plane at various ϖ (unit 100 km²/sec².kpc), in the SCHMIDT model and in the interpolation formula.

FIGURE 16

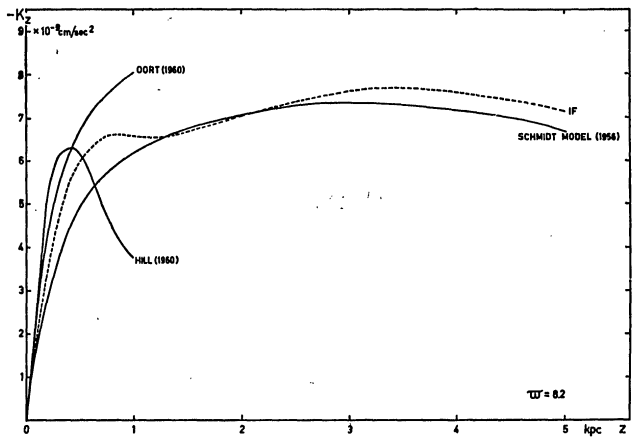

Comparison between the force components K_z at the sun given by observations (HILL and OORT), by the SCHMIDT model and by the interpolation formula.

16. *Some notes on the programme for the integration of orbits by the BESK*

Programming both for the ARMAC and for the BESK was done jointly by Dr INGRID TORGÅRD and the author of this paper. In a forthcoming paper the method will be discussed more fully. It may suffice to mention here some properties of the programme for computing orbits on the BESK, and the programme for computing the curves $U=$ const. in the (ϖ, z)-plane on the ARMAC, as these programmes are still in use for additional calculations. A programme for the computation of orbits on the ARMAC was used only a few times, after which it was decided that the ARMAC is too slow for the extensive series of orbits which was planned.

All computations in the programmes are done with floating-point arithmetic, which is necessitated by

(a) the fact that orbits with high initial Π and Z velocities are to be computed, which can travel over considerable ranges in ϖ and z, with considerable ranges in Π and Z.

(b) the occurrence of high powers of ϖ in the interpolation formula IF, described in section 15.

The programme for the BESK uses built-in floating-point orders, thus ensuring optimal computing speed; for the ARMAC use was made of existing subroutines, while new ones were developed where necessary to avoid the time-consuming interpretative floating-point programme.

The BESK programme for the computation of orbits makes use of the standard subroutine MF4 which integrates a simultaneous system of differential equations as (1.8) by the method of Runge-Kutta, including the 1/15 correction term and automatic step control. The method is described e.g. in COLLATZ (1955); the automatic step control used in the BESK is mentioned by P. O. LINDBLAD (1960). For all orbits the tolerances which govern the step size $2\varkappa$ were taken equal to 0.0002, for all variables t, ϖ, z, ϑ, Π and Z. Not only the positions but also the angle ϑ and the velocities were used for automatic control of the step size.

The mean value of the step size is for each of the orbits discussed in this thesis about equal to 0.01 time units (or about 10^6 years).

The computation time for one Runge-Kutta step is determined mainly by the time it takes to compute K_ϖ and K_z with the aid of the IF, which must be done twelve times per step. The mean computation time per accepted RK step for a particular orbit depends upon the proportion of rejected to accepted steps controlled by the set of tolerances. For the orbits discussed here values between 0.8 and 0.9 sec were found. This means that for the computation of an orbit over a time interval of 5.10^9 years, where about 5000 steps must be taken, about 70 minutes net computation time were needed. To this must be added the time needed for output of results on tape, as in the BESK the computations and the punching of tape are carried out serially. The result tapes are printed out off-line on a telex-printer[1]). The addi-

[1]) Copies of result tapes can be made available on request.

tional time needed for output varied between 10 and 20 percent depending upon the amount of results retained.

The standard sequence MF4 is left after each accepted RK step, and the programme entered then contains the *energy check*. If the difference between the energy E after an accepted step and the initial value E_0 (at $t = t_0$) is larger than a given tolerance (taken always as 5.10^{-4} units), a stop occurs. Thus derangement of the programme is detected by this mathematical check. Recently, *energy control*, in which the size of the step is also controlled by the change in energy, was programmed by Dr TORGÅRD, but it will not be reported upon here.

The standard sequence MF4 is also left at regular intervals $t_0 + n \,.\, \varkappa_s (n = 1, 2, \ldots)$ where $\varkappa_s$ must be specified beforehand. In the programme entered then, the computed quantities

$$t, \varpi, z, \vartheta, \Pi, Z, \Theta \text{ and } \Phi, E, S^{-1} = (\Pi^2 + Z^2)^{-1/2} \quad (16.1)$$

are transported to result registers. When S^2 is less than a certain limit, E and S^{-1} are replaced by Π^2 and Z^2. For most computations $\varkappa_s = 0.04$ was used, sometimes $\varkappa_s = 0.08$. As soon as the reserved result registers in the slow memory are filled, their contents are punched out in teleprinter code by means of a standard subroutine, so that the result registers can be used again. At the end of a computation all data necessary for a possible continuation later are punched out on tape. Most orbits were computed in several parts in this way.

The ARMAC programme for the computation of curves $U = E$ in the (ϖ, z)-plane is based on the Newton-Raphson iterative process, in which for a given ϖ the value of z is found as the limit of a series, between the successive terms of which the recurrence relation

$$z_{m+1} = z_m - \frac{U(z_m) - E}{\left(\frac{\partial U}{\partial z}\right)_m}, \quad (16.2)$$

holds.

The end of the iterations is detected by:
if abs $(U(z_m) - E) <$ tol U **then** ready. The value of tol U determines the accuracy in which z is obtained, to be estimated as follows: from the relation

$$\ddot{z} = -\frac{\partial U}{\partial z}$$

we obtain the approximation tol $U \approx |\ddot{z}| \,.\, |\delta z|$, and by estimates of $\ddot{z}$ as a function of ϖ along the part of the curve $U = E$ to be computed, tol U and δz can be found from one another. For small $|\ddot{z}|$, i.e. near the ϖ-axis, this method of computing the curve is evidently not so suitable. For the curve $U = -250.108$ $(\varpi_c = 5.2)$, Table 12 gives z as a function of ϖ, accurate to 5 decimal places, computed by the ARMAC programme. In this table the potential Φ, the accelerations $\ddot{\varpi}$ and $\ddot{z}$, and the quantity $(\ddot{\varpi}/\ddot{z})$ are also given for the same curve.

TABLE 12

The boundary in the (ϖ, z)-plane for $\varpi_c = 5.2$ kpc, $E = -250.108$ (100 km²/sec²).

ϖ (kpc)	z (kpc)	Φ (100 km²/sec²)	$\ddot{\varpi}$ (100 km²/sec².kpc)	$\ddot{z}$ (100 km²/sec².kpc)	$\ddot{\varpi}/\ddot{z}$
3.40	.19128	−816.66	217.545	− 71.541	−3.04085
3.45	.31804	−800.35	207.714	− 92.880	−2.23636
3.50	.42312	−784.74	198.291	− 99.114	−2.00063
3.55	.51997	−769.79	189.365	−100.546	−1.88338
3.60	.61204	−755.46	180.962	−100.361	−1.80310
3.65	.70050	−741.70	173.060	− 99.667	−1.73639
3.70	.78579	−728.50	165.621	− 98.813	−1.67611
3.75	.86818	−715.84	158.600	− 97.883	−1.62029
3.80	.94788	−703.66	151.953	− 96.882	−1.56844
3.85	1.02509	−691.96	145.646	− 95.799	−1.52033
3.90	1.09998	−680.70	139.646	− 94.627	−1.47574
3.95	1.17271	−669.86	133.928	− 93.371	−1.43436
4.00	1.24346	−659.44	128.470	− 92.037	−1.39586
4.05	1.31234	−649.40	123.255	− 90.637	−1.35988
4.10	1.37948	−639.72	118.267	− 89.184	−1.32610
4.15	1.44498	−630.38	113.492	− 87.692	−1.29421
4.20	1.50893	−621.38	108.918	− 86.172	−1.26396
4.25	1.57140	−612.70	104.533	− 84.635	−1.23511
4.30	1.63246	−604.32	100.329	− 83.091	−1.20746
4.35	1.69217	−596.22	96.296	− 81.548	−1.18084
4.40	1.75056	−588.40	92.425	− 80.014	−1.15511
4.45	1.80769	−580.84	88.709	− 78.494	−1.13014
4.50	1.86359	−573.53	85.139	− 76.992	−1.10582

TABLE 12 (*continued*)

ϖ (kpc)	z (kpc)	Φ (100 km^2/sec^2)	$\ddot{\varpi}$ (100 km^2/sec^2.kpc)	$\ddot{z}$ (100 km^2/sec^2.kpc)	$\ddot{\varpi}/\ddot{z}$
4.55	1.91828	−566.46	81.710	− 75.512	−1.08207
4.60	1.97180	−559.62	78.413	− 74.058	−1.05881
4.65	2.02417	−553.00	75.244	− 72.632	−1.03597
4.70	2.07540	−546.59	72.197	− 71.235	−1.01350
4.75	2.12552	−540.38	69.265	− 69.869	− .99135
4.80	2.17454	−534.36	66.443	− 68.534	− .96948
4.85	2.22248	−528.54	63.726	− 67.232	− .94787
4.90	2.26933	−522.88	61.111	− 65.961	− .92647
4.95	2.31513	−517.40	58.591	− 64.722	− .90527
5.00	2.35986	−512.08	56.163	− 63.516	− .88424
5.05	2.40355	−506.92	53.822	− 62.340	− .86336
5.10	2.44620	−501.90	51.566	− 61.196	− .84263
5.15	2.48782	−497.04	49.389	− 60.083	− .82202
5.20	2.52841	−492.32	47.288	− 58.999	− .80152
5.25	2.56797	−487.72	45.261	− 57.944	− .78112
5.30	2.60652	−483.26	43.304	− 56.917	− .76083
5.35	2.64406	−478.92	41.414	− 55.918	− .74061
5.40	2.68058	−474.70	39.588	− 54.946	− .72048
5.45	2.71611	−470.60	37.822	− 54.000	− .70042
5.50	2.75063	−466.61	36.116	− 53.078	− .68043
5.55	2.78415	−462.73	34.466	− 52.181	− .66050
5.60	2.81668	−458.95	32.869	− 51.307	− .64064
5.65	2.84821	−455.27	31.324	− 50.456	− .62082
5.70	2.87876	−451.69	29.829	− 49.627	− .60106
5.75	2.90832	−448.20	28.380	− 48.819	− .58134
5.80	2.93690	−444.80	26.978	− 48.031	− .56167
5.85	2.96449	−441.48	25.618	− 47.263	− .54203
5.90	2.99110	−438.25	24.300	− 46.513	− .52244
5.95	3.01673	−435.10	23.022	− 45.782	− .50287
6.00	3.04139	−432.03	21.783	− 45.068	− .48334
6.05	3.06507	−429.04	20.580	− 44.371	− .46383
6.10	3.08777	−426.12	19.413	− 43.690	− .44434
6.15	3.10950	−423.27	18.280	− 43.024	− .42488
6.20	3.13026	−420.48	17.179	− 42.374	− .40542
6.25	3.15004	−417.77	16.110	− 41.738	− .38599
6.30	3.16886	−415.12	15.071	− 41.115	− .36656
6.35	3.18670	−412.53	14.061	− 40.506	− .34713
6.40	3.20357	−410.00	13.078	− 39.909	− .32770
6.45	3.21947	−407.53	12.123	− 39.325	− .30828
6.50	3.23440	−405.12	11.193	− 38.753	− .28884
6.55	3.24835	−402.76	10.288	− 38.191	− .26939
6.60	3.26134	−400.46	9.407	− 37.641	− .24992
6.65	3.27334	−398.21	8.549	− 37.100	− .23043
6.70	3.28437	−396.00	7.713	− 36.570	− .21091
6.75	3.29443	−393.85	6.898	− 36.050	− .19136
6.80	3.30351	−391.74	6.104	− 35.538	− .17177
6.85	3.31161	−389.69	5.330	− 35.035	− .15214
6.90	3.31873	−387.67	4.575	− 34.540	− .13245
6.95	3.32485	−385.70	3.838	− 34.054	− .11270
7.00	3.33000	−383.77	3.119	− 33.575	− .09289
7.05	3.33414	−381.88	2.417	− 33.103	− .07301
7.10	3.33730	−380.03	1.731	− 32.638	− .05305
7.15	3.33945	−378.22	1.062	− 32.180	− .03300
7.20	3.34059	−376.44	.408	− 31.728	− .01285
7.25	3.34073	−374.71	− .231	− 31.283	+ .00740
7.30	3.33985	−373.01	− .856	− 30.843	+ .02776
7.35	3.33795	−371.34	−1.467	− 30.408	+ .04825
7.40	3.33502	−369.71	−2.065	− 29.979	+ .06888
7.45	3.33106	−368.11	−2.649	− 29.554	+ .08964
7.50	3.32606	−366.54	−3.221	− 29.134	+ .11057

TABLE 12 (*continued*)

ϖ (kpc)	z (kpc)	Φ (100 km²/sec²)	$\ddot{\varpi}$ (100 km²/sec².kpc)	$\ddot{z}$ (100 km²/sec².kpc)	$\ddot{\varpi}/\ddot{z}$
7.55	3.32000	−365.00	−3.781	− 28.719	+ .13166
7.60	3.31289	−363.50	−4.329	− 28.308	+ .15293
7.65	3.30471	−362.02	−4.866	− 27.900	+ .17440
7.70	3.29544	−360.57	−5.391	− 27.497	+ .19608
7.75	3.28509	−359.15	−5.906	− 27.096	+ .21798
7.80	3.27364	−357.76	−6.411	− 26.700	+ .24012
7.85	3.26108	−356.39	−6.905	− 26.306	+ .26251
7.90	3.24739	−355.05	−7.390	− 25.914	+ .28518
7.95	3.23256	−353.73	−7.865	− 25.525	+ .30814
8.00	3.21657	−352.44	−8.332	− 25.139	+ .33142
8.05	3.19941	−351.18	−8.789	− 24.755	+ .35503
8.10	3.18106	−349.93	−9.237	− 24.372	+ .37900
8.15	3.16151	−348.71	−9.677	− 23.992	+ .40335
8.20	3.14072	−347.51	−10.109	− 23.613	+ .42811
8.25	3.11869	−346.33	−10.533	− 23.235	+ .45330
8.30	3.09539	−345.18	−10.949	− 22.859	+ .47896
8.35	3.07078	−344.04	−11.357	− 22.483	+ .50513
8.40	3.04486	−342.93	−11.758	− 22.109	+ .53182
8.45	3.01759	−341.83	−12.152	− 21.735	+ .55909
8.50	2.98894	−340.76	−12.538	− 21.361	+ .58696
8.55	2.95888	−339.70	−12.918	− 20.988	+ .61549
8.60	2.92738	−338.66	−13.291	− 20.615	+ .64472
8.65	2.89440	−337.64	−13.657	− 20.242	+ .67469
8.70	2.85990	−336.64	−14.017	− 19.869	+ .70546
8.75	2.82384	−335.65	−14.370	− 19.496	+ .73709
8.80	2.78617	−334.68	−14.717	− 19.122	+ .76964
8.85	2.74686	−333.73	−15.058	− 18.748	+ .80316
8.90	2.70584	−332.79	−15.393	− 18.374	+ .83774
8.95	2.66306	−331.87	−15.721	− 17.999	+ .87345
9.00	2.61847	−330.96	−16.044	− 17.624	+ .91036
9.05	2.57201	−330.07	−16.361	− 17.248	+ .94856
9.10	2.52359	−329.20	−16.671	− 16.872	+ .98814
9.15	2.47317	−328.33	−16.976	− 16.495	+1.02918
9.20	2.42065	−327.49	−17.275	− 16.118	+1.07177
9.25	2.36596	−326.65	−17.568	− 15.742	+1.11601
9.30	2.30902	−325.83	−17.855	− 15.366	+1.16199
9.35	2.24973	−325.02	−18.136	− 14.991	+1.20978
9.40	2.18801	−324.23	−18.411	− 14.618	+1.25945
9.45	2.12376	−323.45	−18.680	− 14.248	+1.31106
9.50	2.05687	−322.68	−18.943	− 13.882	+1.36461
9.55	1.98726	−321.92	−19.200	− 13.520	+1.42008
9.60	1.91483	−321.18	−19.450	− 13.165	+1.47740
9.65	1.83949	−320.44	−19.694	− 12.818	+1.53641
9.70	1.76117	−319.72	−19.932	− 12.482	+1.59690
9.75	1.67979	−319.00	−20.165	− 12.158	+1.65854
9.80	1.59530	−318.30	−20.392	− 11.849	+1.72097
9.85	1.50768	−317.61	−20.613	− 11.556	+1.78381
9.90	1.41692	−316.93	−20.832	− 11.280	+1.84682
9.95	1.32300	−316.26	−21.047	− 11.019	+1.91010
10.00	1.22589	−315.60	−21.263	− 10.769	+1.97452
10.05	1.12549	−314.95	−21.481	− 10.518	+2.04232
10.10	1.02152	−314.31	−21.706	− 10.248	+2.11820
10.15	.91339	−313.68	−21.942	− 9.923	+2.21124
10.20	.79983	−313.06	−22.196	− 9.490	+2.33889
10.25	.67834	−312.45	−22.473	− 8.856	+2.53767
10.30	.54345	−311.84	−22.780	− 7.855	+2.90013

17. *Some general properties of meridional orbits*

Before reviewing the results of the numerical computations, we shall consider some of the properties of the solutions of the equations of motion which can be formulated without numerical computation.

The equations of motion of a particle of mass in the galactic field of force are (1.8). The solution of these equations is the (solution) *path* described by the particle in phase space. In the three-dimensional configuration space the particle describes a *three-dimensional trajectory* and in the meridional plane it describes a *meridional trajectory*. We use the word "trajectory" when the geometrical properties of a dynamical curve are considered (KASNER 1913). An *orbit* corresponds to a unique parametrization of the path, with the time as the parameter. We use the word "orbit" when the motion of a particle in a configuration space, whether it be the ordinary threedimensional space or the meridional plane, is considered. The adjectives "three-dimensional" and "meridional" are omitted when no confusion is possible.

As the coordinates of each point in phase space (corresponding to all points in configuration space with at each point all combinations of the three velocity components), may be taken as initial conditions, the system of all particle orbits is sextuply infinite. The system of paths in phase space forms a quintuply infinite system of curves, since the same curve is described by the particle if it is started from any of the single infinity of points on any path (this corresponds to the fact that one path is determined by each set of given values of the five integration constants figuring in the complete solution of (1.8)). This system of paths fills phase space. The corresponding system of ∞^5 three-dimensional trajectories fills the three-dimensional configuration space.

A path in phase space cannot intersect itself. If a path is closed, the corresponding orbit is periodic. A periodic orbit is *stable* if every solution path which is, at a certain time, sufficiently near to the closed path corresponding to the periodic orbit, will stay in the neighbourhood of the closed path for all time. A periodic orbit is *unstable* if every solution path, no matter how near to the closed path of the periodic orbit at a certain time, will digress from it eventually.

The system of all meridional trajectories is quadruply infinite, since in a field of force which has rotational symmetry, the same meridional curve is obtained by starting orbits in points of space which have identical cylindrical coordinates (defined as in section 1) except for the azimuth.

The system of those meridional trajectories which have the same area constant h, is obviously a triply infinite subsystem of the system of all meridional trajectories; the corresponding motion is described by the two second-order equations (8.4) or the four first-order equations (11.1). The phase space is four-dimensional and it is filled by the triply infinite system of trajectories obtained by considering each point in the meridional plane and in each point each combination of the velocity vectors, as initial conditions. In the complete solution of the equations of motion (8.4) or (11.1) there are four integration constants; one of these is the energy constant E.

If we consider meridional trajectories with the same E and h, we restrict ourselves to a doubly infinite system of trajectories. Such a system will be called a *family* of trajectories. The family can also be defined as the system of integral curves defined by the orbital equation (8.8). The corresponding triply infinite system of meridional orbits is called a family of orbits.

There are some general properties of the meridional orbit which can be proved *prior* to computation and to which the computed orbits should comply. The properties mentioned here do not form a complete list.

The conservation of energy may be written

$$U + \tfrac{1}{2}S^2 = E, \qquad (17.1)$$

where

$$S^2 = \Pi^2 + Z^2 \qquad (17.2)$$

is twice the kinetic energy. When the kinetic energy becomes zero, the potential energy U is equal to the total energy E; hence all orbits in the selected family must stay inside the egg-shaped region in the meridional plane enclosed by the boundary $U = E$. Some of the equipotential curves $U = E$ are given in Figures 2 and 3. In three-dimensional space the orbits must remain inside the torus-like volume obtained by rotation of the boundary around the z-axis.

If an orbit reaches a point on the boundary (say at $t = 0$), the velocities Π and Z become zero (but not the accelerations). Therefore, shortly before and after reaching the boundary at (ϖ_0, z_0), we can write

$$\begin{aligned} \varpi &= \varpi_0 + \tfrac{1}{2}p t^2 & \Pi &= p t \\ z &= z_0 + \tfrac{1}{2}q t^2 & Z &= q t\ ; \end{aligned} \qquad (17.3)$$

it follows that

$$\left.\begin{aligned} (\ddot{\varpi})_{t=0} &= p = -\left(\frac{\partial U}{\partial \varpi}\right)_{\varpi_0, z_0} \\ (\ddot{z})_{t=0} &= q = -\left(\frac{\partial U}{\partial z}\right)_{\varpi_0, z_0} \end{aligned}\right\} \qquad (17.4)$$

from which

$$\left(\frac{\Pi}{Z}\right)_{\varpi_0, z_0} = \frac{p}{q} = \left(\frac{\partial U}{\partial \varpi}\Big/\frac{\partial U}{\partial z}\right)_{\varpi_0, z_0}, \qquad (17.5)$$

and this proves that the motion to and from the boundary is *perpendicular* to the boundary. The boundary point is an *end point* of the trajectory.

The *radius of curvature* of the meridional orbit in an arbitrary point can be written

$$\left.\begin{aligned} \rho &= \frac{\{1+(z')^2\}^{3/2}}{z''} \\ \text{or} \qquad \rho &= \frac{(\Pi^2+Z^2)^{3/2}}{(-\ddot{\varpi}Z+\ddot{z}\,\Pi)}\,; \end{aligned}\right\} \qquad (17.6)$$

with the equations of motion in the form (8.4), and the energy equation (8.6) we find

$$\left.\begin{aligned} \rho &= \frac{(2E-2U)^{3/2}}{\left(Z\frac{\partial U}{\partial \varpi}-\Pi\frac{\partial U}{\partial z}\right)} \\ \text{and thus} \qquad \rho &= \frac{\{1+(z')^2\}^{1/2}\,2(E-U)}{\left(z'\frac{\partial U}{\partial \varpi}-\frac{\partial U}{\partial z}\right)}\,, \end{aligned}\right\} \qquad (17.7)$$

which gives, with the first of equations (17.6), the orbital equation (8.8).

For $(\varpi=\varpi_c,\ z=0)$, we have $\frac{\partial U}{\partial \varpi}=0$ and $\frac{\partial U}{\partial z}=0$, and hence $\rho=\infty$; in words:

in the point of lowest potential energy the trajectory can possess an inflection point. This property is mentioned in section 8 as a special result. In Figures 21.1 and 23 the property is illustrated for two computed orbits.

Trajectories which intersect the ϖ-axis perpendicularly are symmetrical with respect to this axis.

Generally speaking we can divide all meridional orbits of a family into two classes:

(1) periodic orbits, subdivided into

(1a) Non-symmetrical orbits with two end points on the boundary,

(1b) Symmetrical orbits with two end points on the boundary,

(1c) Symmetrical orbits with two perpendicular intersections with the ϖ-axis.

(2) non-periodic orbits.

The existence of orbits in each sub-class of periodic orbits has not been proved for the galactic field of force, but an empirical proof is given by the numerical computations by the BESK discussed in section 18. An example of classes (1a) and (1b) is the (trivial) case of an orbit with $Z=0$. An example of class (1b) is the orbit which is started on the boundary and on the first intersection crosses the ϖ-axis perpendicularly. This case is discussed later on in this section.

Which subdivision is to be made in the class of the non-periodic orbits depends on the form of the reduced potential function U. We make no attempt to divide these orbits in sub-classes prior to numerical computation.

One orbit of any of these classes cannot fill the point set (i.e. approach arbitrarily close to every point formed by the region within the curve $U=E$, as the orbit cannot come arbitrarily close to more than two points on the boundary.

All ∞^2 trajectories of the family fill the region. It is a question of some concern how to choose the initial coordinates and velocities for numerical computations such that a good representation of the members of the family is obtained. Not every orbit actually reaches the boundary—orbits of class (1c) do not. But every orbit passes the ϖ-axis (infinitely often), therefore the complete family is obtained by taking as initial conditions all ∞^1 points on the section of the ϖ-axis contained between its intersections with the boundary, and in each point all ∞^1 directions of motion. This is the reason why most orbits in our numerical computations were started with $z=0$.

The issue can be studied conveniently for the numerical computations by studying $(\Pi/Z)_{z=0}$ as a function of ϖ (see also section 20). Consider all orbits of a given family. The boundary $U=E$ in the meridional plane defines a section $\varpi_l<\varpi<\varpi_r$ of the ϖ-axis in which all intersections of the orbits are contained. Each intersection with the ϖ-axis defines one value of ϖ and one value of Π/Z. This corresponds to one point in the *inclination diagram*, which has ϖ and Π/Z as coordinate axes. All ∞^2 orbits of the family together fill a domain S in the $(\varpi,\ \Pi/Z)$-plane, bounded by the lines $\varpi=\varpi_l$ and $\varpi=\varpi_r$.

Any point P_0 in the domain S can be used as an initial point for a meridional orbit. The points of S, considered as initial conditions, together generate the ∞^2 orbits of a family. Consider an orbit defined by the coordinates of a point P_0 in S as initial conditions at $t=t_0$. When the moving particle crosses the ϖ-axis again, at time $t=t_1$, the values of ϖ and Π/Z define a point P_1 in S. By considering all orbits of the family a transformation T is set up which transforms S into itself, namely the transformation which takes uniquely any P_0 over into the corresponding P_1[1]). We shall now consider some properties of this transformation, which can be formulated prior to numerical computation.

By a (*finite*) *set of invariant points* of S is meant a number of points $P_0, P_1, \ldots, P_{k-1}$ which go over into

[1]) This reduction of the dynamical problem to a transformation problem is similar to the reduction originally suggested by POINCARÉ (1892) and studied by BIRKHOFF (1922). In these theories the existence of a "surface of section" in phase space is supposed, which is intersected by the moving point and which is taken over into itself by a (surface-preserving) transformation obtained in the same way as described above.

each other under T. This can be expressed symbolically by

$$P_1 = T(P_0) \quad P_2 = T(P_1) \quad \ldots \quad P_0 = T(P_{k-1}) .$$

It follows that each point P_i is invariant under the k-th iterate of T. To a set of invariant points in S corresponds a periodic meridional orbit of one of the subclasses (1). Each orbit of subclass (1a) gives a set of at least two invariant points, of which none lie on the ϖ-axis. Each orbit of subclass (1b) gives a set of at least three invariant points, of which one lies on the ϖ-axis, and the rest are situated in S symmetrically with respect to the ϖ-axis. Each orbit of subclass (1c) gives a set of two invariant points, both lying on the ϖ-axis.

We shall distinguish between *stable* and *unstable* invariant points. Stable will mean that a point P very close to the invariant point, will stay quite close to it under successive applications of the k-th iterate of T, unstable will mean that P departs from the invariant point. The corresponding periodic orbits will also be called stable or unstable.

A *single invariant point* of S goes over into itself under T. To each single invariant point corresponds a periodic orbit of class (1b), intersecting the ϖ-axis perpendicularly in one point. Therefore all single invariant points of S must lie on the ϖ-axis section $\varpi_l < \varpi < \varpi_r$. We can make plausible the existence of at least one single invariant point as follows. We consider the locus of points in S which are defined by the first intersection with the ϖ-axis of a particle "dropped" from the boundary $U = E$ in the meridional plane; we assume that this locus is a continuous curve. Starting the particle from $(\varpi_l, 0)$ in the meridional plane gives the point $(\varpi_l, +\infty)$ in S and starting the particle from $(\varpi_r, 0)$ in the meridional plane, gives the point $(\varpi_r, -\infty)$ in S. Since the locus is a continuous curve each value of Π/Z must be taken at least once; in particular there is at least one value ϖ_0 of ϖ for which $\Pi/Z = 0$. The point $(\varpi_0, 0)$ of S is a single invariant point. The corresponding orbit will be called a *central orbit.*

In the same way we can make plausible the existence of at least one set of two invariant points lying on the ϖ-axis. We consider the locus of points in S which are defined by the first intersection with the ϖ-axis of a particle started in the meridional plane from the ϖ-axis with $\Pi = 0$ and $Z > 0$; we assume that this locus is a continuous curve. Reasoning as before it can be seen that $(\varpi_l, +\infty)$ and $(\varpi_r, -\infty)$ must lie on the locus. Obviously the locus must pass through each single invariant point $(\varpi_0, 0)$. If it does not intersect the ϖ-axis in any other point, each single invariant point can be regarded as a degenerate set of two invariant points. If the locus intersects the ϖ-axis in points other than the single invariant points, it must be in at least two more points, and then there exists at least one set of two invariant points.

In the same way the existence of a set of k invariant points ($k \geq 3$) may be demonstrated, either by starting meridional orbits from the boundary, or by starting them from the ϖ-axis with $\Pi = 0$ and studying the appropriate intersection with the ϖ-axis. Degeneracies of various degree and complexity may be present, depending upon the function $U(\varpi, z)$. We may mention that for the case of small oscillations around $(\varpi = \varpi_c, z = 0)$ in the meridional plane, treated in section 9, all sets of invariant points in S degenerate into the point $(\varpi = \varpi_c, \Pi/Z = 0)$ if $\sqrt{a_0/c_0}$ is irrational.

A non-periodic orbit gives a set of ∞^1 different points in S. They are obtained by successive application of T to the initial point P_0. None of these points belongs to the set of ∞^1 points of any other orbit in the family. If the single infinity of points of a given orbit is arranged along a closed curve in the domain S, this curve goes over into itself under T. If two closed curves exist which transform into themselves under T, they cannot intersect one another.

We shall return in section 20 to the discussion of the properties of meridional orbits, by studying the transformation T of the inclination diagram $(\varpi, \Pi/Z)$ into itself, after having reviewed the results of the numerical computations.

18. *Phenomenology of orbits of the box type*

In this section we discuss a rather small part of all orbit computations performed so far: we restrict ourselves to orbits of the box type (to be defined presently) of one family, and the phenomenology is concerned only with the meridional orbit.

A complete analysis of the results of the computations, including other types of orbits, will be given in a forthcoming paper by Dr Ingrid Torgård and the author. All necessary data for a complete specification of the motion in three dimensions were computed by the BESK and subsequently stored on telex-tape (see section 16). Some remarks on the angular-momentum vector are made in section 21.

The selected family of orbits is characterized by

$$E = -250.108 \quad \varpi_c = 5.2 \quad (h = 114.449) \qquad (18.1)$$

It is an arbitrary family, except that the area constant has been chosen smaller than the area constant of the sun's circular motion, and that the energy value has been chosen so high that orbits passing through the solar neighbourhood correspond to orbits of high-velocity stars. This is shown by the following data for the neigh-

TABLE 13

Initial and auxiliary data for some numerically computed orbits of the box type.

Orbit no.	initial conditions ($t = 0$; $z = \vartheta = 0$)					break-off time		
	ϖ	Π	Z	$\sqrt{\lvert\Pi/Z\rvert}$	Θ	t (units)	t (10^9 years)	no. of revolutions
13	3.43	0	+ 5.2461	0	+ 33.3670	12.1	1.18	15.5
2	6.20	+ 15.2734	+ 4.9872	1.750	+ 18.4595	10.8	1.06	13
36	4.37	− 14.0041	+ 7.3803	1.3775	+ 26.1897	26.6	2.60	30
5	5.20	+ 15.2479	+ 7.6239	1.4142	+ 22.0094	72.2	7.05	76
4	5.10	− 12.5077	+ 11.5641	1.040	+ 22.4410	37.3	3.64	31.5
10	4.00	0	+ 13.9584	0	+ 28.6122	19.0	1.86	14.5
19	6.70	+ 8.1322	+ 12.7065	0.80	+ 17.0819	19.1	1.87	13.5
3	5.20	0	+ 17.0477	0	+ 22.0094	44.2	4.32	30
30	6.52	− 3.1219	+ 15.1465	0.454	+ 17.5535	39.5	3.87	27
6	5.80	0	+ 16.6563	0	+ 19.7326	54.8	5.36	37
9	6.00	0	+ 16.3875	0	+ 19.0748	19.8	1.94	13

bourhood of the sun, taken at ($\varpi = 8.2$, $z = 0$):

$$\left.\begin{aligned} \Theta = h/\varpi &= 13.96 \\ \sqrt{\Pi^2 + Z^2} = S &= 5.00 \\ \sqrt{\Pi^2 + Z^2 + \Theta^2} &= 17.88\,, \end{aligned}\right\} \qquad (18.2)$$

while the escape velocity is

$$V_{esc} = \sqrt{-2\Phi} = 28.64\,. \qquad (18.3)$$

Each orbit computed was given a serial number. Orbits 13, 2, 36, 5, 4, 10, 19, 3, 30, 6 and 9 are discussed here, in this order. Table 13 gives the initial data, the values of $\sqrt{|\Pi/Z|}$ and Θ for the starting point, and some data concerning the point where the computation was broken off.

(a) Characteristics of box-type orbits

We propose to use the following terms for motions in the meridional plane:

By a *meridional revolution* will be understood the part of the orbit contained between two successive crossings of the ϖ-axis with the same sign of Z. In general the value of the third space coordinate ϑ will not differ by 2π at the beginning and at the end of a meridional revolution, so the meridional revolution does not correspond to a revolution in three-dimensional space. Usually the adjective "meridional" is left out in the term meridional revolution, as we are concerned in this section only with revolutions in the (ϖ, z)-plane.

The rotational direction of motion in a given revolution can be clockwise, anti-clockwise, or of the figure of eight (*switching*) type, changing from clockwise to anti-clockwise motion, or vice versa.

The time difference between the beginning and the end of a revolution is called the *revolution time*. Successive revolutions of an orbit will have different revolution times. The mean revolution time, averaged over a number of revolutions, tends to a limit as the number of revolutions increases. This limit is designated by P_c.

For decreasing energy the amplitudes of the meridional oscillations decrease and we have

$$\lim_{E \to E_c} P_c = P_c^\circ \qquad (18.4)$$

in which P_c° is the period of oscillation perpendicular to the ϖ-axis introduced in section 9; E_c is defined as

$$E_c = U_c = \frac{h^2}{2\varpi_c^2} + \Phi_{\substack{\varpi=\varpi_c \\ z=0}}\,. \qquad (18.5)$$

A periodic meridional orbit is said to have a *period* of n revolutions, in which n is the number of revolutions which separates two successive identical crossings of the ϖ-axis (i.e., crossings at the same point ϖ, with the same velocities Π and Z).

The phenomenological characteristics defining the non-periodic box-type orbits, are:

1) The trajectory is topologically equivalent to a Lissajous figure. Some of the following characteristics are consequences of this equivalence.

2) The orbit has an envelope. The envelope is symmetric with respect to the axis $z = 0$, consists of four curved line sections called *sides*, and the region enclosed by it forms a simply-connected region, called the *box*. The sides meet at the boundary in the four *corners C, D, C′ and D′ of the box*, and intersect at right angles there (this property is proved under (c) of this section). The envelope and the region of a box are shown schematically in Figure 17. In Figure 31 the envelopes of the computed box-type orbits are sketched.

FIGURE 17

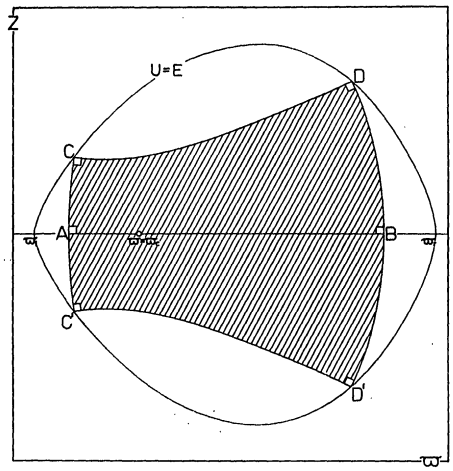

Schematic drawing of the region in the meridional plane filled by a box-type orbit, showing the fundamental points of the box.

The two sides connecting the boundary point C with C′ and D with D′ intersect the ϖ-axis perpendicularly; the intersections define the points A and B on the ϖ-axis ($\varpi_A < \varpi_B$). The orbits of Tables 13 and 14 are ordered according to increasing values of ϖ_A (the value of ϖ_A given in the corresponding column has been determined graphically). The four corners C, D, C′ and D′ of the box, and the points A and B are called the 6 *fundamental points* of the box.

The two sides connecting two boundary points situated at the same side of the ϖ-axis, may be folded (see Figure 28 for orbit 6, where the envelope is not (yet) folded, and Figures 29 and 30 for orbit 9, where folding occurs).

Both during a clockwise and during an anti-clockwise motion the orbit connects all sides of the envelope in succession. "Crossing over" from one side of the envelope to the opposite side occurs only in a revolution of the switching type. The trajectory is tangent to the sides for each of these types of revolutions.

3) The whole of the trajectory is contained in the box and the box is filled by the trajectory.

In other words, the orbit cannot come outside the envelope and each point of the region within it, including the four corner points, is approached arbitrarily closely.

4) In each point where the trajectory intersects itself two velocity vectors of equal magnitude are defined. (For periodic orbits there could be four velocity vectors, the two additional ones being opposite to the others). This property is the same as that mentioned in section 7 in connection with the theory of the third quadratic integral.

The points of self-intersection lie everywhere dense within the box. The trajectory cannot intersect itself in a point on the envelope (where it is tangent to the envelope).

Within an arbitrarily small region around any point of self-intersection, there is another point of self-intersection in which the velocity vectors are nearly opposite to the ones defined in the first point. Consider a series of such pairs of points converging to a point in the box (not necessarily one through which the trajectory passes). By taking the limit we find that in each point within the box four velocity vectors are defined, two being opposite to the other two. The permitted directions of motion can be characterised by two angles α and β, both $< \pi$, measured in the (ϖ, z)-coordinate system. For points in the box on the axis $z = 0$, $\alpha + \beta = \pi$. The trajectory can be tangent to the envelope in at most one of the two points of the envelope with $z = 0$; then $\alpha = \pi/2$. For all other points of the trajectory with $z = 0$, $\alpha \neq \pi/2$, $\beta \neq \pi/2$.

5) If the envelope is folded (i.e. intersects itself and possesses two cusps) a triangular region is formed. For points of intersection of the trajectory with itself within the triangular region more than two velocity vectors are possible.

(b) Review of computed box-type orbits

We shall now describe the individual orbits of this family in the order in which they have been arranged in Table 14. The data for these orbits which are collected in the table have been obtained as follows:

The fundamental point B has in all cases been determined graphically, as were the fundamental points C and D. If $\Pi \neq 0$ at the start, the fundamental point A was also determined graphically.

The quantity Δs is the length of arc along the boundary between the corners C and D of the box. It has been obtained by a numerical integration on the basis of the data given in Table 12.

The column labelled "switching occurs at revolution no" gives the number of the first revolution of the switching type counted from a ϖ-axis crossing close to the point A.

The quantity P_c is the mean revolution time defined earlier in this section. We may remark that the individual revolution times are not constant. The dispersion of the distribution of these around the mean value diminishes with increasing value of ϖ_A.

Finally, the quantity P_c/P_a represents the ratio of the frequencies of oscillation of the Lissajous figure to which the box-type trajectory is topologically equivalent. This ratio has been derived by comparison with this Lissajous figure, by a graphical method. The attainable accuracy is smaller for the higher ratios than for the lower ones, since the number of revolutions computed is relatively lower. In the quoted values of P_c/P_a all figures are significant.

TABLE 14

The fundamental points and some other data of the box-type orbits discussed

Orbit	ϖ_A	ϖ_B	$\varpi_B - \varpi_A$	Δs	ϖ_C	z_C	z_D	ϖ_D	Switching occurs at revolution no.	P_c (in time units)	P_c/P_a
$Z =$ 0	3.37	10.40	7.03	10.30	3.366	0	0	10.403	—	—	—
13	3.43	10.30	6.87	9.45	3.431	0.273	0.645	10.263	1	0.748	0.487
2	3.46	10.24	6.78	9.24	3.455	0.329	0.779	10.209	1	0.821	0.513
36	3.52	10.16	6.64	8.77	3.513	0.450	1.075	10.074	1	0.886	0.593
5	3.56	10.10	6.54	8.34	3.548	0.513	1.305	9.960	1	0.946	0.604
4	3.78	9.74	5.96	7.01	3.838	1.007	2.039	9.510	1	1.185	0.754
10	4.00	9.45	5.45	5.72	4.064	1.333	2.696	8.910	2	1.300	0.824
19	4.35	9.10	4.75	4.18	4.463	1.822	3.165	8.137	3	1.405	0.882
30	5.20	8.25	3.05	1.56	5.342	2.639	3.291	6.733	5	1.468	0.947
3	5.20	—	—	—	—	—	3.2911	6.7327	5	1.468	0.947[1]
6	5.80	7.60	1.80	0.45	5.798	2.935	3.127	6.195	11	1.488	0.977
9	6.00	7.40	1.40	0.18	5.911	2.997	3.077	6.073	14	1.491 :	—
limiting	6.10	7.30	1.20	0	5.992	3.037	3.037	5.992	—	—	1

[1]) This ratio is equal to 18:19 for the periodic orbit 3.

With increasing value of ϖ_A the orbits have increasing values of the z-amplitude. Arranging the orbits in order of increasing ϖ_A, it is convenient to distinguish between *low orbits* (large range in ϖ, small range in z), *intermediate orbits* (about equal ranges in ϖ and z) and *high orbits* (small range in ϖ, large range in z).

Orbits 13, 2 and 36 are examples of low orbits. For these orbits each revolution drawn in Figures 18, 19 and 20 is of the switching type. For orbit 13 only 9.5 revolutions have been drawn in Figure 18, as the trajectory almost repeats after that. For orbit 2 only 9.5 revolutions have been drawn in Figure 19 for the same reason.

In the case of orbit 36 the initial conditions have been so chosen that the fundamental point C is nearly reached: see Figure 20.1, in which the first 13.5 revolutions have been drawn. After these 13.5 revolutions the orbit has almost reached the fundamental point B; in Figure 20.2 the next 13.5 revolutions have been drawn: the fundamental point C′ is now nearly reached and the figure is approximately the former figure reflected with respect to the ϖ-axis.

Orbit 5 is also an example of a low orbit (see Figures 21.1 and 21.2, in which 10 revolutions have been drawn). The sense of rotation is clockwise in revolutions 1 and 6, anti-clockwise in revolutions 2, 5, 7 and 10, while the revolutions 3 and 8, and 4 and 9 respectively, are of the switching type of opposite sense.

The slow development of orbit 4 is illustrated in two figures. In Figure 22.1 the first 4 revolutions are drawn, and it is seen that the orbit is almost periodic with 3:4 as the ratio of the frequencies of oscillation of the corresponding Lissajous figure. In this part of the orbit the fundamental points C and D are nearly reached. Seventeen revolutions after the start the orbit has almost the shape of the periodic orbit with the frequency ratio 3:4, which goes through the fundamental points A and B. This is shown in Figure 22.2, where the revolutions 17, 18, 19 and 20 are drawn.

In orbit 10, also of the low type (see Figure 23, where 8.5 revolutions are drawn), the sense of rotation is clockwise in revolutions 1, 6, 7, anti-clockwise in revolutions 3, 4, 8, while the revolutions 2 and 5 are of the switching type of opposite sense. Here *series* of either clockwise or anti-clockwise revolutions appear. In the 5th revolution the fundamental point D is nearly reached, after which the trajectory is almost retraced. In the 10th revolution the fundamental point D′ is nearly reached. After 15 revolutions the orbit has approximately the shape of a distorted Lissajous figure with 14:17 as the frequency ratio.

In orbit 19, which is of the intermediate type (see Figure 24, where 11 revolutions are drawn), the sense of rotation is clockwise in revolutions 2, 3, 4, 10 and 11, anti-clockwise in revolutions 6, 7, 8 and 9, while revolutions 1 and 5 are of the switching type of opposite sense. The series of clockwise or anti-clockwise revolutions are longer compared to orbit 10. This is also seen from the column in Table 14 giving the number of the switching revolution, counted from a close passage to the point A. The higher the value of ϖ_A, the longer the series of revolutions of a given sense.

Orbit 3 is periodic to a high degree of approximation. It approaches the fundamental point

$$D' \ (\varpi = 6.7327, \ z = -3.2911)$$

in the 5th revolution. The period of this orbit is 19 revolutions (see the definition in part (a) of this section) and D′ is approached again in the 24th revo-

Figures 18, ..., 27 form a catalogue of meridional trajectories of the family of orbits discussed in this thesis. A filled circle marks the starting point, an open circle the point of lowest reduced potential energy at ($\varpi_c = 5.2$, $z = 0$). The numbers n written in the trajectories indicate the ascending node after n revolutions, counted from the starting point. Where necessary the direction of motion is indicated by arrows in the trajectories. The egg-shaped curve is the boundary curve.

FIGURE 18

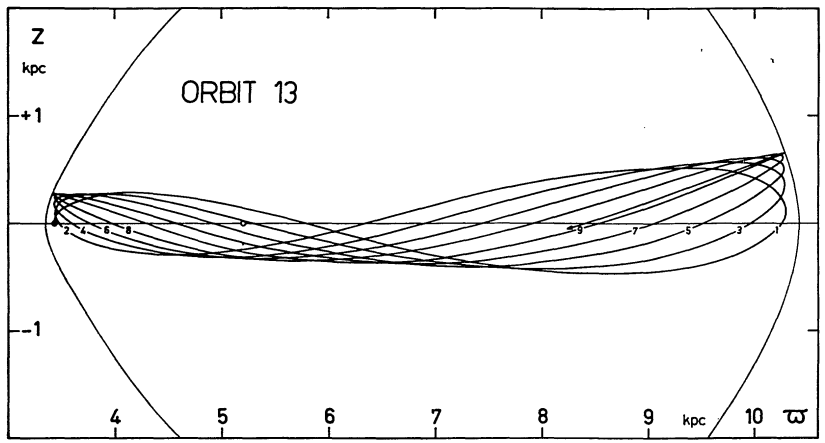

Orbit 13, *special*, the lowest orbit computed in the series reported here.

FIGURE 19

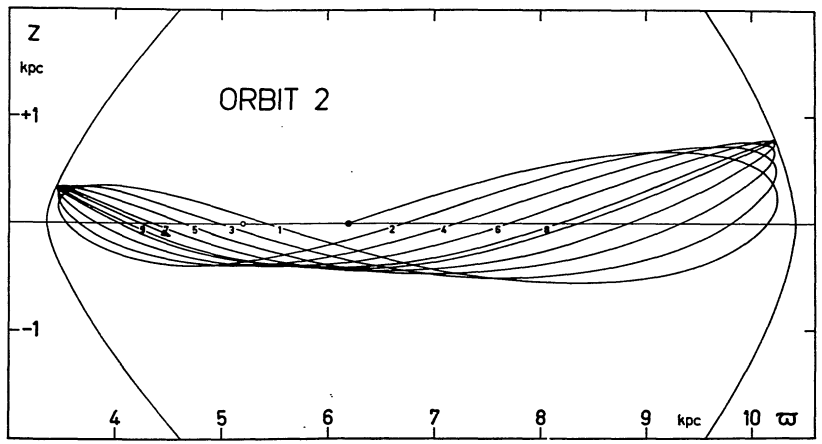

Orbit 2, *low*; each revolution is of the switching type.

FIGURE 20.1

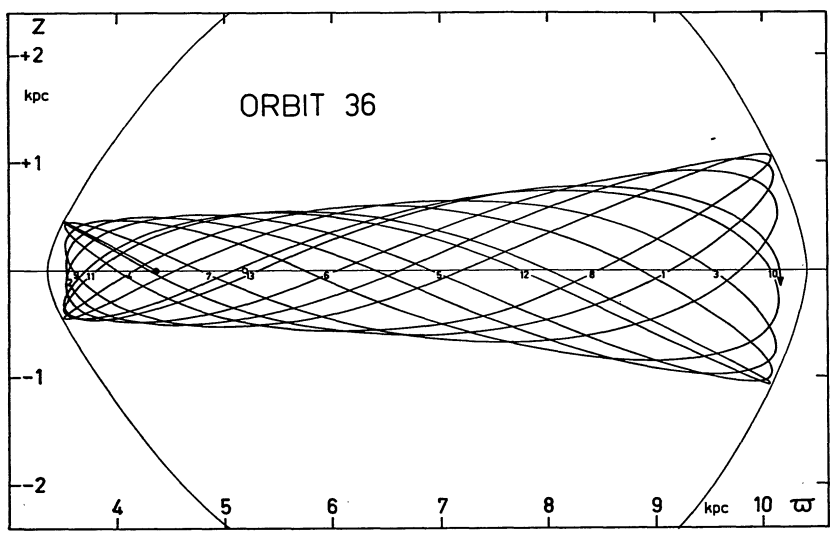

Revolutions 1 to 13 and the first half of revolution 14 for orbit 36 (*low* type). In revolution 1 the fundamental point C is approached, in revolution 14, the fundamental point B.

FIGURE 20.2

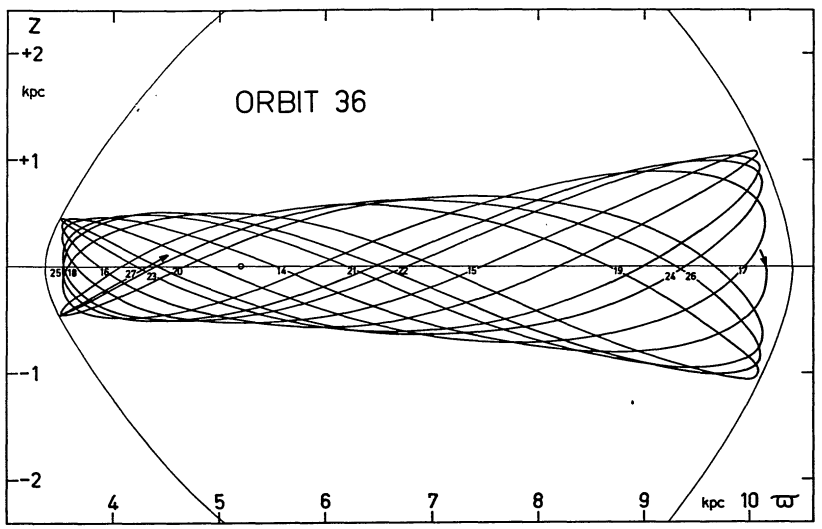

Second half of revolution 14 and revolutions 15 to 27 for orbit 36, are almost a mirror image of the first 13.5 revolutions shown in Figure 20.1. The fundamental point C′ is approached in revolution 27.

FIGURE 21.1

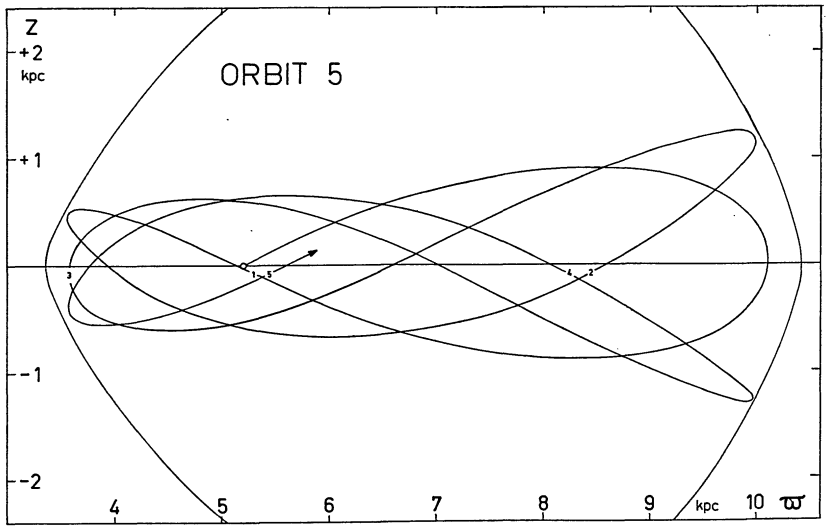

Orbit 5, *low*, frequency ratio near 3 : 5. In revolutions 1 and 4 the fundamental points B and A are approached.

FIGURE 21.2

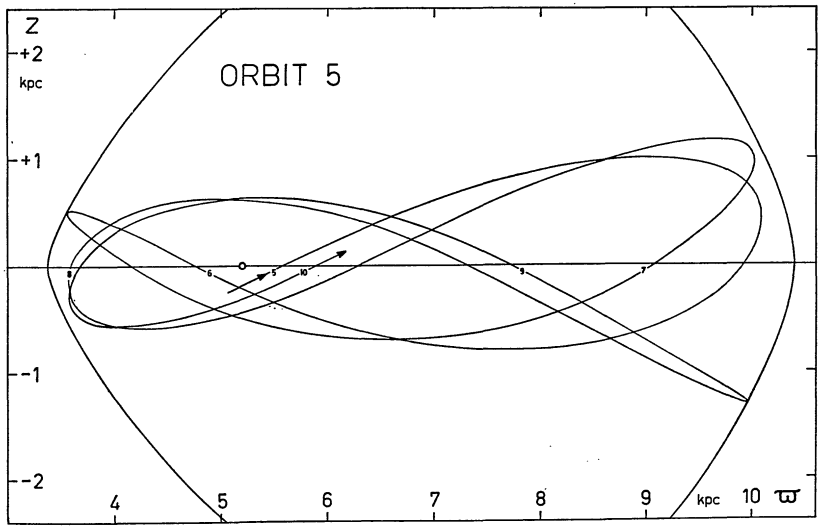

Revolutions 6 to 10 of orbit 5; the fundamental points C and D′ are approached; in revolutions 11 to 15 (not shown) the fundamental points A and B are approached again.

FIGURE 22.1

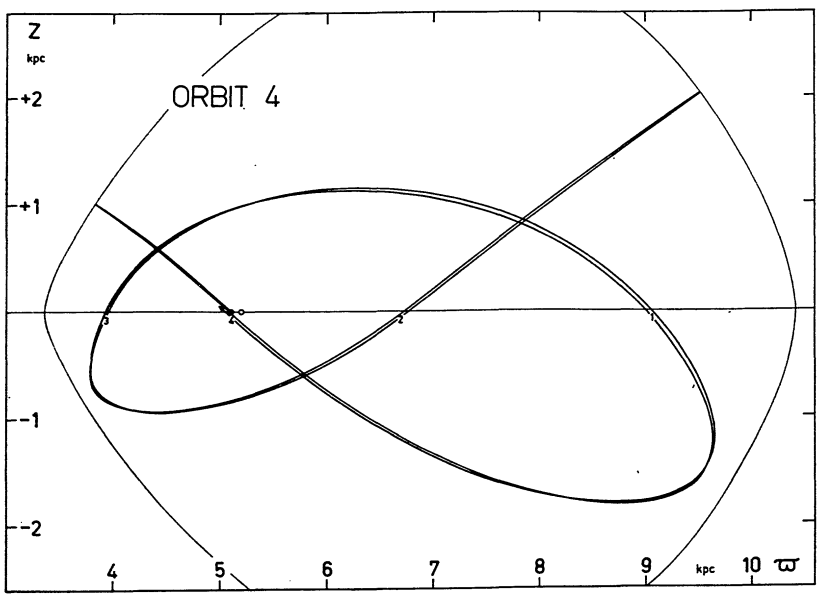

Orbit 4, *low*, frequency ratio near 3 : 4. In revolutions 1 to 4, the fundamental points C and D are approached closely.

FIGURE 22.2

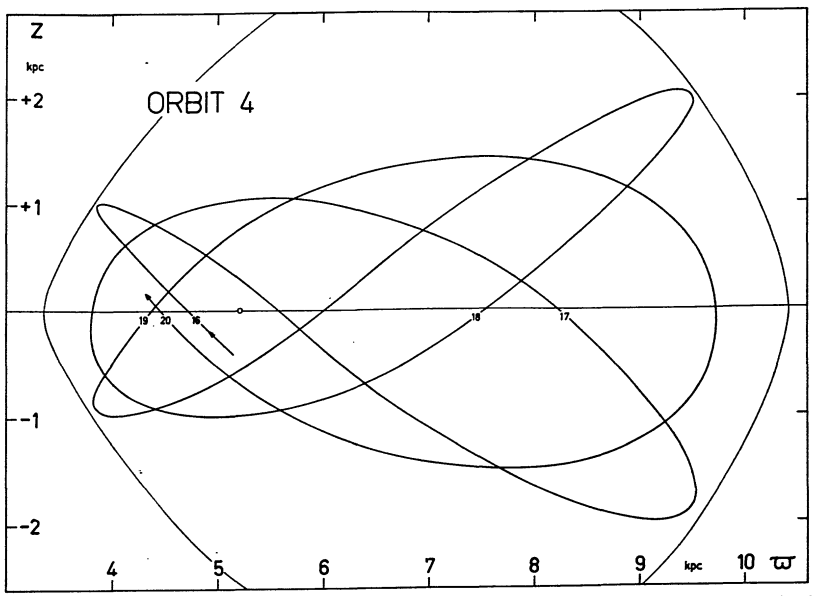

Revolutions 17 to 20 of orbit 4; the fundamental points A and B are approached.

FIGURE 23

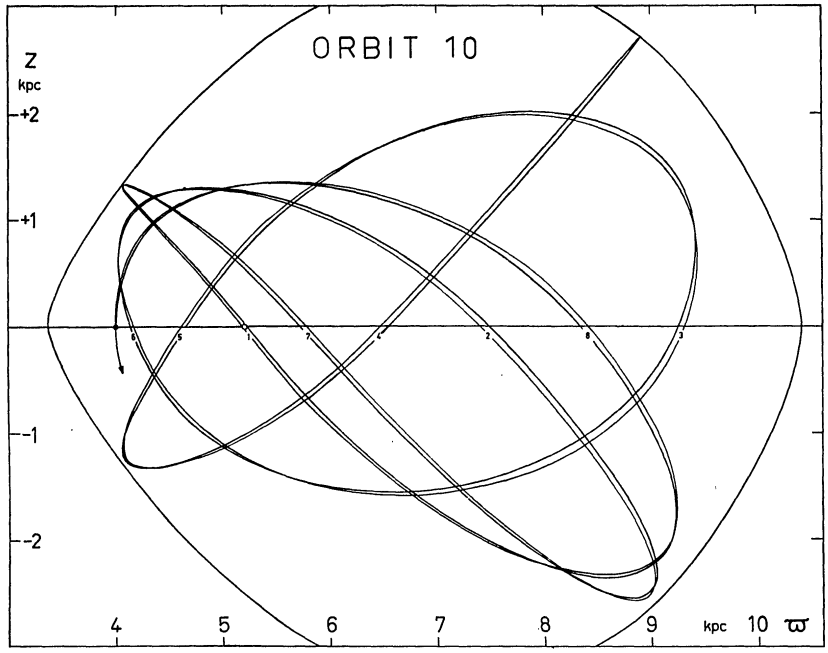

Orbit 10, *low, special*, frequency ratio near 14 : 17. In revolution 5 the fundamental point D is approached closely, after which the previous path is nearly retraced back to the starting point ($\varpi = \varpi_A$, $z = 0$).

FIGURE 24

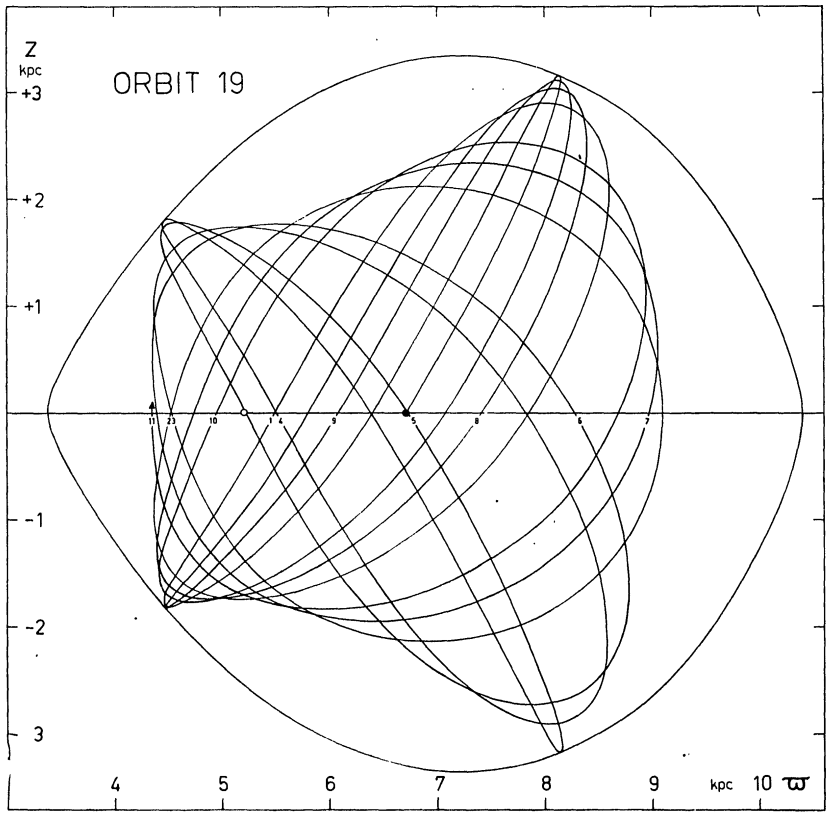

Orbit 19, *intermediate*. In revolution 11 the fundamental point A is approached closely. Motion of orbital plane is shown in Figure 33.

FIGURE 25

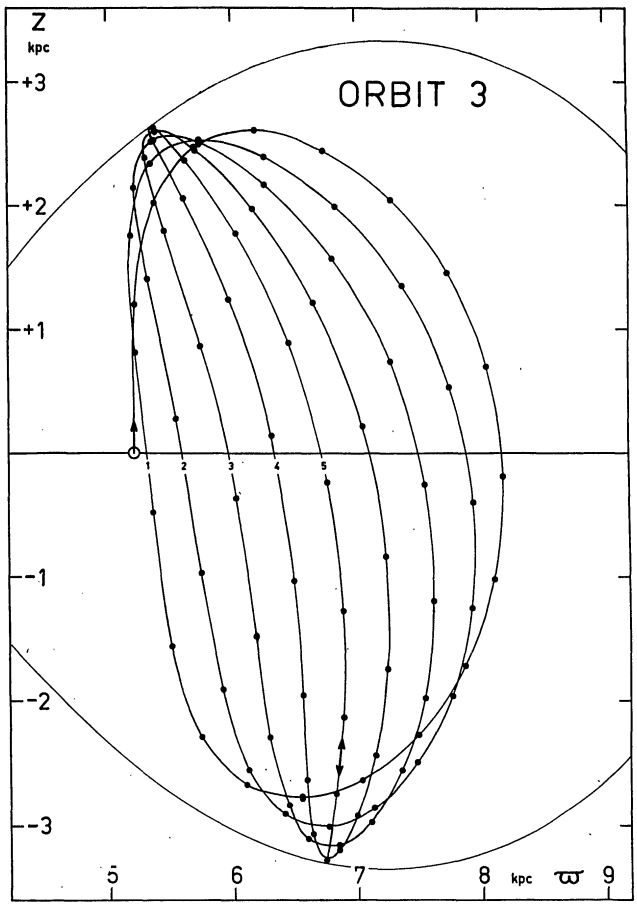

Orbit 3, *special, periodic*. Time interval between two dots: $7.8 \cdot 10^6$ years.

FIGURE 26

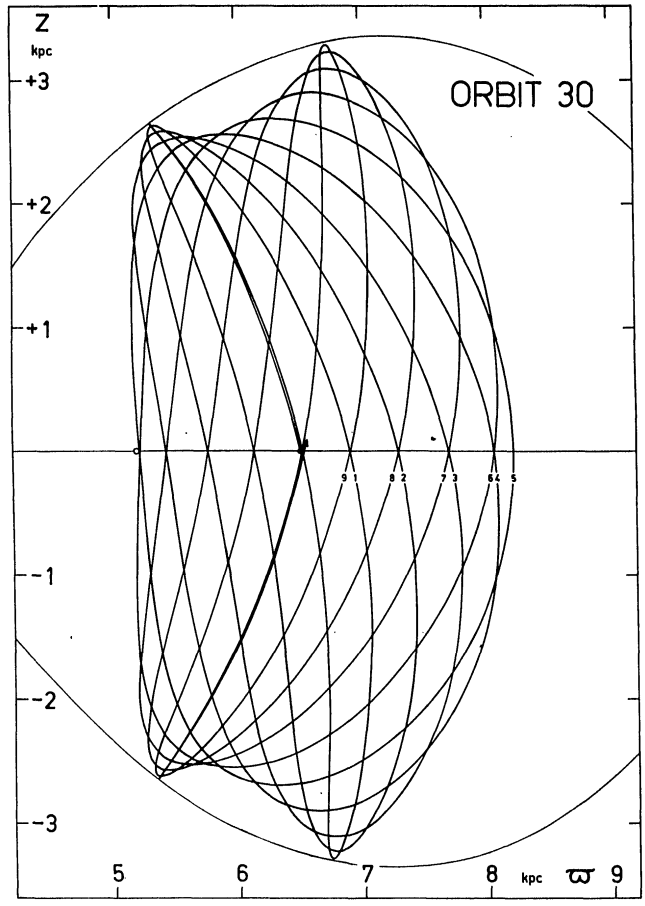

Orbit 30, *intermediate*, close to orbit 3. The trajectory departs only slowly from the trajectory of orbit 3.

lution. D is approached in the 15th revolution. In Table 15 some data, interpolated for $S^2 = \Pi^2 + Z^2 =$ minimum, are given for these three approaches. The table was prepared by Dr TORGÅRD.

From Table 15 it is seen that the numerical accuracy of computation is less than the accuracy of approach to the boundary: $E - E_0$ is in all three cases considerably larger than $S^2_{\min}$.

In Figure 25 the meridional trajectory for the first 5 revolutions of orbit 3 is drawn. The time interval between two dots in the figure is 0.08 units or $7.8 \cdot 10^6$ years.

Orbit 30 was computed in order to study the development of a box-type orbit "near" orbit 3. The starting data were obtained from an arbitrary point on the smooth curve joining the points in the inclination diagram corresponding to orbit 3 (see section 20). The development proved to be extremely slow. The orbit is not periodic, but after the 27 computed revolutions the meridional trajectory is still very much like that of orbit 3 (see Figure 26).

TABLE 15

Three successive approaches of orbit 3 to the boundary

	D′	D	D′
t	6.972503	20.917509	34.862521
S^2	$2 \cdot 10^{-8}$	$15 \cdot 10^{-8}$	$3 \cdot 10^{-8}$
Π^2	$1 \cdot 10^{-8}$	$14 \cdot 10^{-8}$	$41 \cdot 10^{-8}$
Z^2	$0 \cdot 10^{-8}$	$1 \cdot 10^{-8}$	$2 \cdot 10^{-8}$
$E - E_0$	$20 \cdot 10^{-8}$	$47 \cdot 10^{-8}$	$91 \cdot 10^{-8}$

Orbits 6 and 9 were both started perpendicularly to the ϖ-axis at $z = 0$ with $\varpi = 5.8$ and 6.0, so that $\varpi_A = 5.8$ and 6.0 respectively. For orbit 6 the meridional trajectory is shown in Figure 27; for orbit 9 no meridional figure is given as the computation was not completed owing to a failure of the BESK, which also destroyed the data needed for a continuation. The regions near the boundary for orbits 6 and 9 are drawn in some detail in Figures 28, 29 and 30. Broken lines are sections of the trajectory for negative z. For orbit 6 the numerical data do not show clearly

FIGURE 27

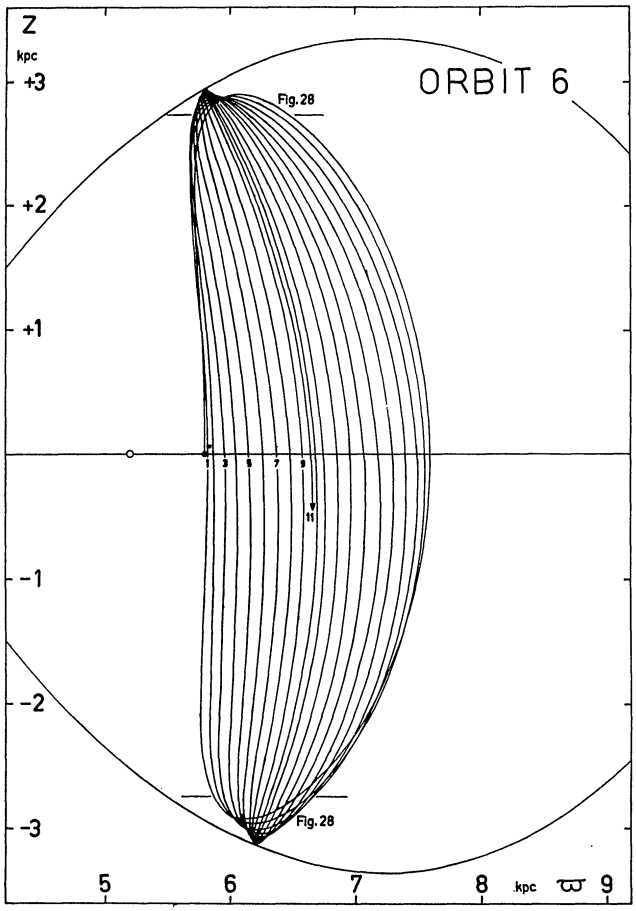

Orbit 6, *high, special*. Sense of rotation of all revolutions drawn is clockwise, except for revolution 11, which is of the switching type. Region within the boundary for $|z| > 2.75$ enlarged in Figure 28.

whether the envelope is folded or not, the figure was drawn on the assumption that it is not folded. For orbit 9 the fold in the envelope is clearly illustrated in Figures 29 and 30.

With increasing value of ϖ_A, the range in ϖ for $z = 0$, given by $(\varpi_B - \varpi_A)$ in Table 14, decreases. Also the length of arc along the boundary between the fundamental points C and D decreases. It is given by the values of Δs in the same table. We note, however, that Δs has almost vanished for orbit 9, whereas the fundamental points A and B are still 1.40 kpc apart. Therefore it may be expected that when Δs becomes zero in the limit, the quantity $(\varpi_B - \varpi_A)$ has not vanished but has attained a minimum value (see also Figure 31, where all envelopes of the orbits discussed here are sketched). Orbits which possess a perpendicular intersection with the ϖ-axis within this minimum range will be of a different type. Subsequent computations, not reported here, have shown this conjecture to be correct: the orbits of different type are the *shell-type* orbits, also mentioned in section 20. The orbit which separates the box-type orbits and the shell-type orbits will be called the *limiting* orbit. It is obtained by starting an orbit with $\Pi = 0$ at $(\varpi = \varpi_{A_{max}}, z = 0)$ or at $(\varpi = \varpi_{B_{min}}, z = 0)$. The corners C and D of the limiting orbit coincide. In Table 14 some data for this orbit are given; they were found by extrapolation of data obtained from numerical computations of orbits close to the limiting orbit. These computations will be discussed in a joint publication with Dr TORGÅRD.

With decreasing range $(\varpi_B - \varpi_A)$ the ratio P_c/P_a increases and approaches the value 1; this value is reached for the limiting orbit.

FIGURE 28

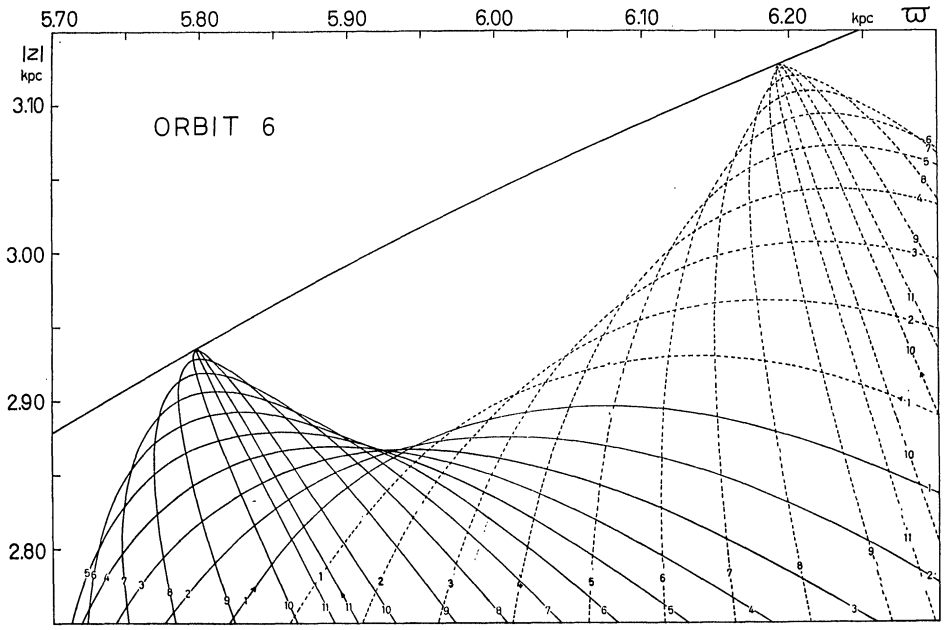

Orbit 6 near the boundary; solid lines: positive z, broken lines: negative z. Horizontal section of the envelope shows incipient dent, developed more fully in orbit 9.

FIGURE 29

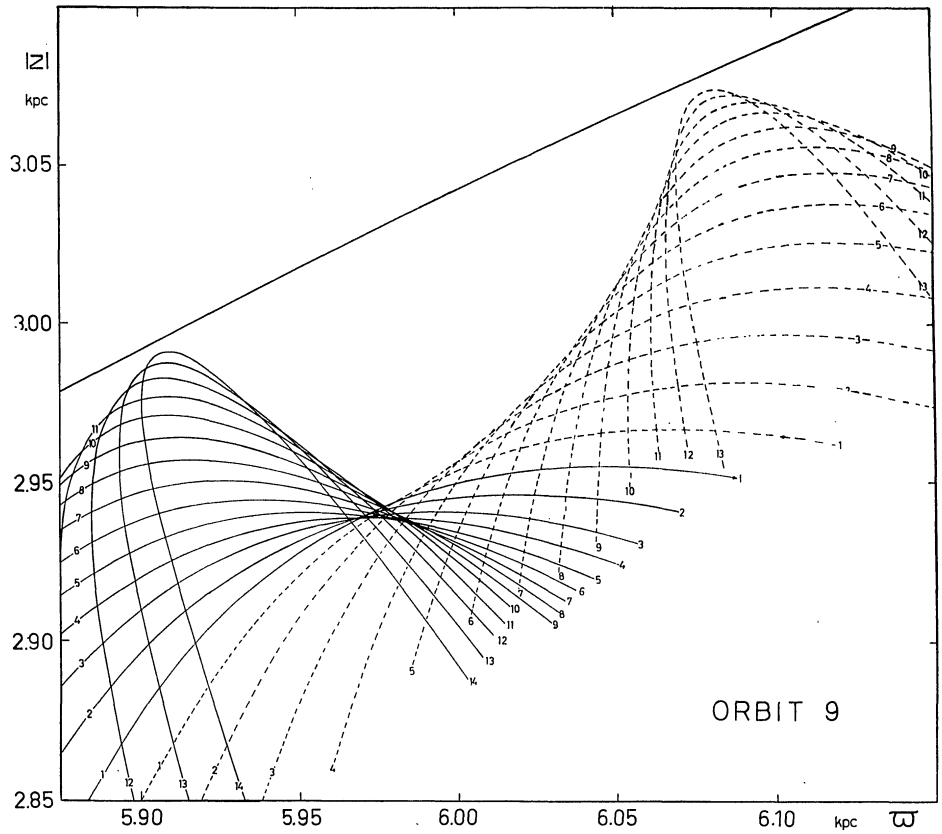

Orbit 9 near the boundary; solid lines: positive z, broken lines: negative z. Horizontal section of the envelope is folded. Computations carried out for revolutions 1 to 14 only.

FIGURE 30

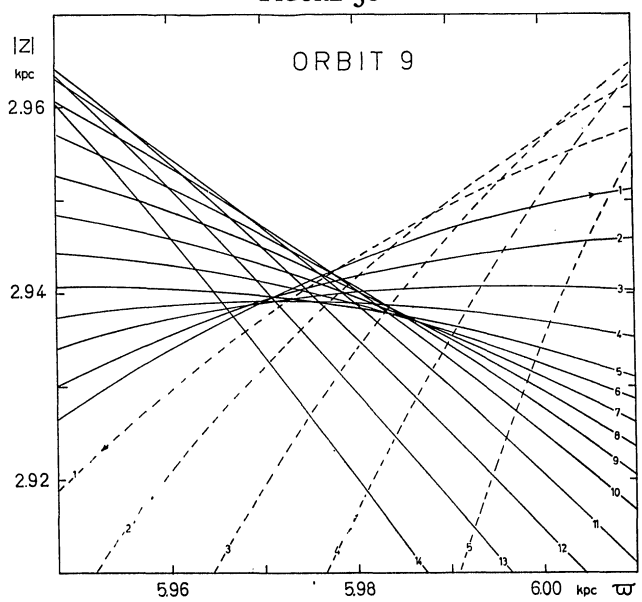

Enlargement of the triangular region formed by fold in envelope of orbit 9; within this region more than four directions of motion are permitted.

As shown in Table 14 the value of P_c increases as ϖ_A increases. The value given for orbit 9 is uncertain because of the small number of revolutions computed.

The periods of oscillation P_a° and P_c° for orbits of small amplitudes, given by $2\pi/\sqrt{a_0}$ and $2\pi/\sqrt{c_0}$ in section 8 (Table 4) depend only on the dynamical constants A, B and C (formulas (9.2) and (9.3)) and not on the initial conditions. Thus for all box-type orbits of a fixed low energy P_c/P_a is a constant. Lissajous figures corresponding to box-type orbits of this low energy have the same ratio $\frac{I}{C}\sqrt{-4B(A-B)}$, and if this is not a rational number, there are no closed Lissajous figures (excluding the periodic motions with $Z = 0$ and $\Pi = 0$ respectively).

The situation is very different for the box-type orbits of the family with the larger energy value considered here. From the estimates of the ratio P_c/P_a given in Table 14 it is seen that the ratio is not a constant for the various orbits in the family. Its value depends, as we have seen, on the value of ϖ_A; if this dependence is a continuous one, we may expect that

FIGURE 31

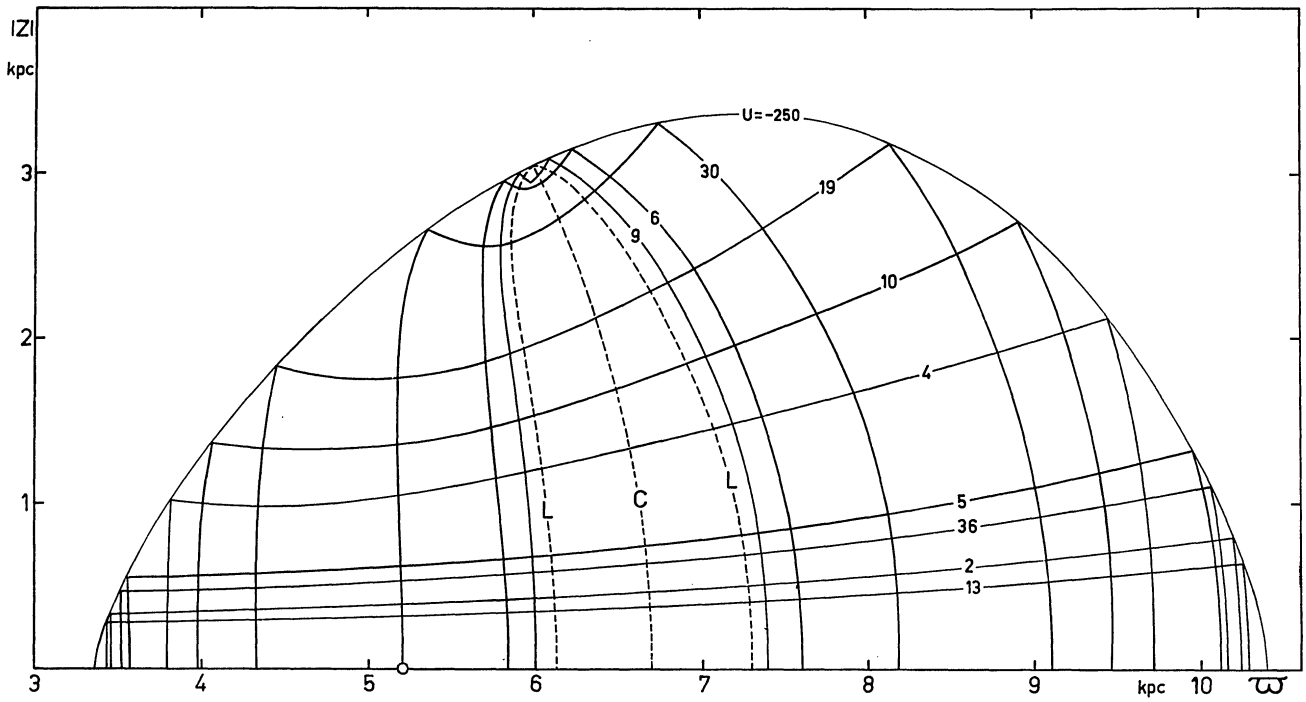

Envelopes of each of the orbits discussed in this thesis; corners of each envelope are rectangular, mutual intersections of the envelopes are not rectangular. Broken line marked L: limiting orbit. Broken line marked C: central orbit.

rational values for P_c/P_a also occur. An example of this is given by the case of orbit 3.

(c) Further properties of box-type orbits

Some general properties of meridional trajectories were formulated *prior* to numerical computation in section 17. After having reviewed the results of the numerical computations, we can now formulate some properties *a posteriori* for the meridional trajectories of box-type orbits.

Consider one box defined by any non-periodic box-type orbit. The six fundamental points of the box which belong to the envelope of the trajectory are:

the four corners (C, D, C′, D′) on the boundary $U = E$;

the two perpendicular intersections (A, B), of the envelope with the ϖ-axis. The defining orbit may not actually reach any of the fundamental points, as it does not reach a given point in general. If it does reach one of the fundamental points, it will be called a *special* orbit. The defining orbit cannot reach more than one fundamental point, for an orbit which reaches two (or three) fundamental points is a periodic orbit (with two or no end points).

Suppose the defining orbit is not a special orbit. Since it approaches arbitrarily closely to all points in the box and the two permitted directions of motion at each of these, it approaches arbitrarily closely to any fundamental point and to the one permitted direction of motion in the points A and B. This statement is equivalent to the statement that, by a suitable choice of the zero point in time, the defining orbit can be made to stay arbitrarily closely to any special orbit for a given length of time. This is also true if a periodic orbit passes through the fundamental point considered. Eventually, as time goes on, the defining orbit moves away from the special orbit; this means that periodic box-type orbits are unstable according to the definition given in section 17.

Consider now the singly infinite system of orbits generated by taking the points on a side of the envelope of a non-periodic box-type orbit and the one permitted direction of motion in each of these points as initial conditions. Again, by a suitable choice of the zero point in time, the defining orbit can be made to stay arbitrarily close to any orbit of the system for a given length of time. But then the trajectory of an orbit of the system cannot come outside the box, and (if it is not periodic) it defines the same box. Therefore each box contains a singly infinite system of trajectories. All trajectories of the box are included in this system of trajectories, which fills the box.

The property of the defining box-type orbit of approaching any special orbit arbitrarily closely for any given length of time, makes it possible to consider one of the non-periodic special orbits of the box as the defining orbit.

Let us consider the case of a box defined by the special orbit which passes through the fundamental point C. We must remark here that the results of the numerical computations discussed show that there exist such cases; however, it has not been shown, nor is it true, that any point on the boundary $U = E$ can be regarded as the fundamental point C of a box. Subsequent numerical computations, not reported here, have shown that there are certain "sections of avoidance" on the boundary, where no box-type orbit can approach the boundary. In the following we assume for the case considered that C lies well outside these sections of avoidance, as indeed lie all points C of the boxes discussed here.

If C is varied continuously along the boundary in the vicinity of the corner of the box considered, a system of ∞^1 boxes is generated. Therefore the system of all box-type orbits is doubly infinite.

The same conclusion is obtained by considering the fundamental point A on the ϖ-axis of the box considered, and varying it continuously in a small section of the ϖ-axis. We must restrict ourselves to such a section since the numerical computations have shown that a part of the ϖ-axis cannot be occupied by the fundamental point A of box-type orbits.

We conclude this section by giving a proof that the four corners of the envelope of a box-type orbit are rectangular.

One of the corner points on the boundary $U = E$ is taken as the origin of a cartesian coordinate system (x, y) with the x-axis tangent to the boundary and the y-axis perpendicular to the boundary, inwards being taken as positive. In a sufficiently small region containing the corner point, we may approximate U by the linear equation

$$U = E - ay, \tag{18.6}$$

so that

$$\Pi^2 + Z^2 = S^2 = 2ay. \tag{18.7}$$

Here E is the energy of the orbit and a is positive.

Further we assume that the points $S^2_{\min}$ lie on a straight line $x = py$. This assumption is justified on the same grounds as the assumption that there is an envelope to the orbit at all, namely by referring to the illustrations of the computed orbits, especially Figures 28 and 29. More detailed figures on the behaviour of the orbits near the boundary will be published later.

The equations of motion $\ddot{x} = 0$, $\ddot{y} = -a$ are solved by

$$\left.\begin{aligned} x &= \gamma \cdot t + \delta \\ y &= \tfrac{1}{2} a t^2 + \alpha t + \beta . \end{aligned}\right\} \tag{18.8}$$

By elimination of t the orbital equation is obtained

$$y = \tfrac{1}{2} a \left(\frac{x-\delta}{\gamma}\right)^2 + \alpha \frac{x-\delta}{\gamma} + \beta , \tag{18.9}$$

which shows that each loop of the orbit in this region may be approximated by a parabola. The minimum of S is reached at the same time as the minimum of y, namely in the vertex of the parabola, at time $t = -\alpha/a$. In this vertex we have

$$\left.\begin{aligned} x_{\text{vertex}} &= pc = -\frac{\alpha\gamma}{a} + \delta \\ y_{\text{vertex}} &= c = -\frac{\alpha^2}{2a} + \beta \\ \dot{x}_{\text{vertex}} &= S_{\min} = \gamma = \pm\sqrt{2ac} \\ \dot{y}_{\text{vertex}} &= 0 . \end{aligned}\right\} \tag{18.10}$$

These equations determine the integration constants α, β, γ and δ except for the value of α (which may be chosen arbitrarily to define the zero of t) and the sign of γ (which depends on the sense of motion in the parabola). From (18.10) we find

$$\beta = c\left(1 + \frac{\alpha^2}{\gamma^2}\right), \quad \delta = c\left(p + \frac{2\alpha}{\gamma}\right), \quad \gamma^2 = 2ac, \tag{18.11}$$

and upon substitution into (18.9) we find without ambiguity

$$y = \frac{1}{4c}(x - pc)^2 + c . \tag{18.12}$$

The two lines through the origin which are tangent to this parabola are found from the condition that the equations $y = bx$ and (18.12) have coincident roots. The condition is

$$b^2 + pb - 1 = 0 . \tag{18.13}$$

This equation shows that

(1) the values of b are real, so the tangents exist;

(2) the values of b are independent of c, so the tangents are common to all parabolas in this region and hence they form the envelope (more precisely: the tangents to the envelope close to the corner point);

(3) the product of the roots of (18.13) is equal to -1, so the tangents are mutually perpendicular.

This completes our proof.

19. *The energy check*

In the BESK programme, briefly described in section 16, the energy value is computed after each computed Runge-Kutta step, according to the formula

$$E_t = \tfrac{1}{2}(\Pi_t^2 + Z_t^2 + \Theta_t^2) + \Phi_t , \tag{19.1}$$

where the subscript t indicates instantaneous values at time t. For each printed point the energy value E_t was printed too, and therefore the energy of the orbits can be checked for constancy by plotting the printed values as a function of time. It appeared that for all computations treated here the energy *increased* gradually as a result of truncation errors; the dependence of E_t on the number of revolutions n_r after the start can be represented approximately by a linear relation (except in the case of orbit 6, where the values of E_t behaved erratically). We write for this relation

$$\frac{E_t - E_0}{E_0} = -k \,.\, n_r, \qquad (19.2)$$

in which k is a positive constant, n_r is a function of t and E_0 is the energy value at $t = t_0$.

If all computed revolutions are taken into account for the determination of k from relation (19.2), k is equal to the mean value of the relative error per revolution. For the orbits treated here, the constant k determined in this way is given in Table 16.

It is seen from the quoted values of k that the energy is constant with a high degree of approximation. For orbit 10, for instance, the value of k implies that the energy would differ by one percent from E_0 after about 14.10^5 revolutions—provided the approximate linear behaviour of the changes continued.

Also in Table 16 is given the maximum difference in energy found for the interval in time for which the orbit was computed. Usually this occurred shortly before or at the break-off value of t.

TABLE 16

Orbit no.	k (10^{-9})	$(E_t - E_0)_{max}$ (10^{-6} units)
13	4	21
2	5	16
36	6	45
5	23	400
4	10	83
10	7	32
19	7	26
3	13	97
30	8	56
6	—	122
9	5	15

20. *The inclination diagram*

Some properties of meridional orbits can be discussed conveniently by studying the representation of these orbits in the inclination diagram (see section 17). For practical purposes we shall not consider $(\Pi/Z)_{z=0}$ as a function of ϖ, but the quantity $I = (\sqrt{\Pi/Z})_{z=0}$, which we shall call the *inclination*. This means that the domain S used in section 17 is transformed into a domain bounded by the lines $\varpi = \varpi_l$ and $\varpi = \varpi_r$ for positive I only. When no confusion is possible we shall designate this domain also by S.

FIGURE 32

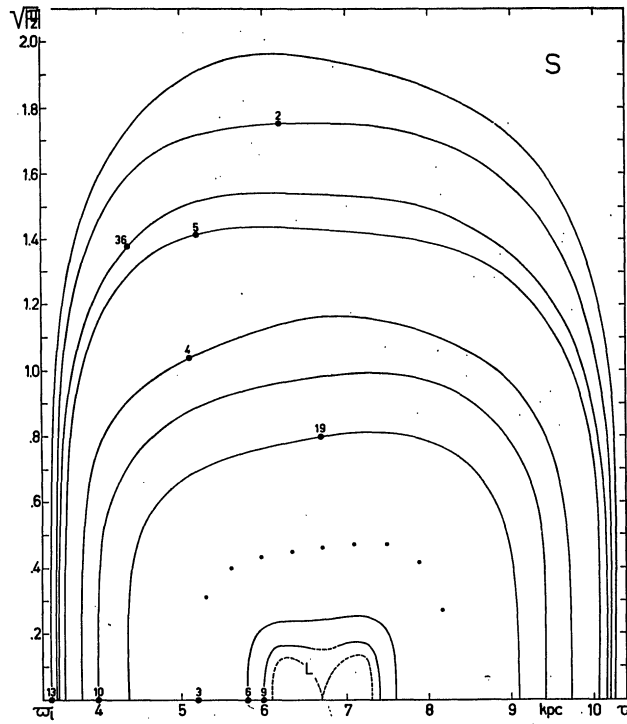

Inclination diagram for the box-type orbits. A filled circle indicates the starting point. Orbit 3 (periodic) is represented by a series of 10 points. Inclination curve of orbit 30 is not drawn but passes close to these points. For orbit 9, not computed long enough to give the entire curve, the broken line indicates the missing section. Broken lines marked L: limiting orbit.

For each of the box-type orbits computed the inclination curve (I, ϖ) is drawn in Figure 32. Each orbit gives a single simple curve in S. This curve intersects the ϖ-axis (perpendicularly) in two points only: $\varpi = \varpi_A$ and $\varpi = \varpi_B$, in which ϖ_A and ϖ_B are the values of ϖ for the two fundamental points of a box-type orbit on the ϖ-axis. No two curves intersect each other: this property was already mentioned in section 17.

The periodic orbit 3 gives a set of 10 invariant points in S. Orbit 30, which is a non-periodic orbit close to orbit 3, yields a simple curve in S passing close to the points representing orbit 3 (see Figure 32). According to the definition of stability of invariant points given in section 17, the invariant points of orbit 3 are unstable.

Later computations have shown that sets of stable invariant points in S also exist. Orbits which at a given time are in the vicinity of the corresponding periodic orbit, will stay near this orbit for all time. These orbits, which have characteristics fundamen-

tally different from those of the box-type orbits, have been called *tube orbits*. The discussion of these orbits is postponed to a future publication.

For each given inclination in S there are *two* corresponding values of ϖ in orbits 13, 2, ... 6. But for orbit 9 there are inclinations which occur for *four* values of ϖ. A suggestion of a minimum in the horizontal section of the inclination curve is also present in the case of orbit 6. With increasing value of ϖ_A (and, as we have seen, decreasing value of the arc-length along the boundary $U = E$ between the corners C and D of the boxes) the minimum deepens; for the maximum value of ϖ_A and coinciding points C and D, it reaches the ϖ-axis in a point $(\varpi_0, 0)$. Then the inclination curve has become two arcs corresponding to the limiting orbit (cf. section 18b). The point $(\varpi_0, 0)$ is an unstable single invariant point corresponding to the central orbit in the meridional plane (see section 17), which intersects the ϖ-axis perpendicularly in $(\varpi_0, 0)$ and reaches the boundary in the coincident corner points C and D of the limiting orbit. Orbits started perpendicularly to the ϖ-axis at $\varpi > \varpi_A$, give two arcs in the inclination diagram; they correspond to an orbit which has characteristics fundamentally different from those of box-type orbits. These orbits, which have been studied by subsequent numerical computation, not reported here, have been called *shell orbits*. The discussion of these orbits is postponed to a future publication.

Figure 32, in which only the inclination curves of box-type orbits have been drawn, is not a complete inclination diagram. Neither the sets of stable invariant points, nor the cases of inclination curves which are not simple single curves have been discussed. However, Figure 32 does show that the box-type orbits form an important class of meridional orbits in this family.

We cannot deduce the importance of box-type orbits in general from a discussion of one family of meridional orbits only. However, for smaller energies than considered here, box-type orbits must be increasingly important. For those cases of galactic stellar motion in which the meridional motion is separable only box-type orbits exist, as was shown in previous sections.

21. *The angular-momentum vector*

The three-dimensional orbit is completely specified by ϖ, z, ϑ, Π, Z and Θ as functions of t. The position of the meridional plane is given by ϑ, the angular velocity by $\dot{\vartheta} = \Theta/\varpi$. Until now we have been concerned with the two-dimensional meridional motion only; the third component may be included by studying the motion of the meridional plane. We shall instead study the motion of the *orbital plane*, defined by the position vector $\mathbf{r}$ and the velocity vector $\mathbf{v}$.

Let x, y and z be cartesian coordinates in a fixed frame of reference, with the galactic centre as origin and the galactic plane as the plane $z = 0$. Then

$$x = \varpi \cos\vartheta \quad y = \varpi \sin\vartheta$$

and the angular-momentum vector $\mathbf{R}$, defined as $\mathbf{r} \times \mathbf{v}$, has the components

$$\left.\begin{aligned} R_x &= \sin\vartheta\,(\varpi Z - z\Pi) - z\Theta\cos\vartheta \\ R_y &= -\cos\vartheta\,(\varpi Z - z\Pi) - z\Theta\sin\vartheta \\ R_z &= \varpi^2\dot{\vartheta} = h\,. \end{aligned}\right\} \qquad (21.1)$$

Denoting by Ω the longitude of the ascending node, and by ε the angle between the orbital plane and the galactic plane, we have further

$$\operatorname{tg}\Omega = -R_x/R_y \qquad (21.2)$$

$$\operatorname{tg}\varepsilon = (\sqrt{R_x^2 + R_y^2})/R_z\,. \qquad (21.3)$$

Usually at the starting point $\vartheta = 0$, and $z = 0$, whence

$$R_x = 0\,, R_y = -\varpi Z\,. \qquad (21.4)$$

When the orbit crosses the galactic plane ($z = 0$), ϑ and Ω are related by

$$\vartheta = \Omega + n_r \cdot 2\pi\,, \qquad (21.5)$$

in which n_r denotes the number of meridional revolutions since the start. For $z = 0$ the tilt ε of the orbital plane is determined by ϖ and Z only since

$$h \operatorname{tg}\varepsilon = \varpi Z\,. \qquad (21.6)$$

For orbit 19, the behaviour of the components R_x and R_y of the angular-momentum vector is shown in Figure 33 for 5 revolutions after the start. The values of Ω and tg ε can be found from the figure, as illustrated for the first passage through the galactic plane ($t \approx 1.0$). The sharp maxima of the curve for times of passage through the galactic plane are cusps, as

$$\frac{d\operatorname{tg}\varepsilon}{dt} = \frac{d\Omega}{dt} = 0$$

for these times.

As it can be proved that

$$\lim_{z\to 0} \frac{d\Omega}{d\varepsilon} = \frac{1}{\sin\varepsilon\cos\varepsilon} \frac{Z\Pi\ddot{\varpi}}{\Theta(\varpi\ddot{z} - Z\ddot{\varpi} + z\Theta^2/\varpi)}\,, \qquad (21.7)$$

the tangential line in the cusp passes through the origin of the coordinate system (R_x, R_y), for $\Pi = 0$. This is the case for $t = 0$ in orbit 19.

The motion of the meridional plane is direct since

FIGURE 33

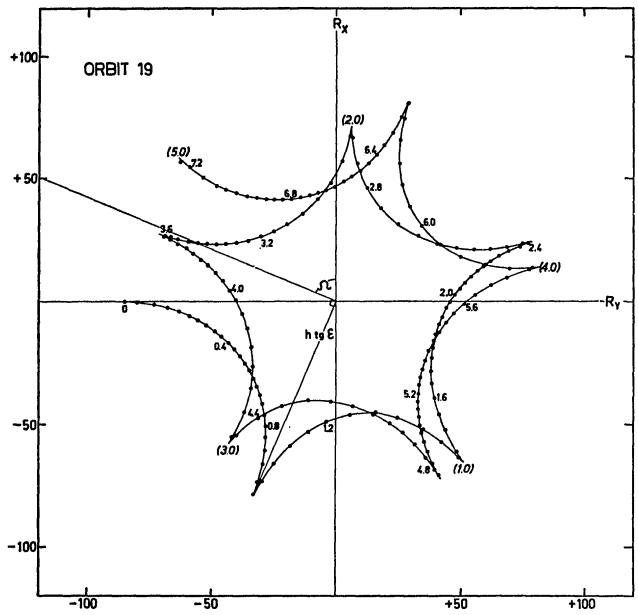

Projection of tip of angular-momentum vector on the galactic plane for orbit 19. Motion of orbital plane is retrograde. Time interval between two dots: 0.04 time units = $3.9 \cdot 10^6$ years. Every 10 time intervals the dot is marked with the time in time units. Longitude of ascending node ☊ can be found graphically as illustrated for the first passage through the galactic plane ($t \approx 1.0$). Length of line section in which $h \operatorname{tg} \varepsilon$ is written, is equal to this quantity. Units in both coordinates: 10 km.kpc/sec.

we have chosen the positive value of h which means that $\frac{d\vartheta}{dt} > 0$; it can be shown that the motion of the orbital plane is direct or retrograde according to the sign of

$$z\Theta \frac{d}{dt}(\varpi Z - z\Pi) - (\varpi Z - z\Pi)\frac{d}{dt}(z\Theta), \qquad (21.8)$$

the negative sign corresponding to retrograde motion. Figure 33 shows that the motion of the orbital plane of orbit 19 is retrograde in general.

IV. Provisional conclusions

22. *Theory of distorted Lissajous motion*

It was remarked in section 18 that the meridional trajectory of a box-type orbit is topologically equivalent to a Lissajous figure, i.e. it can be obtained from this figure by a continuous deformation. The rectangular envelope with straight sides is distorted into a rectangular envelope with curved sides, and in these sides folds may occur. The centre of the distorted Lissajous figure does not coincide with ϖ_c; in fact the whole range in ϖ for $z = 0$ may be contained in $\varpi > \varpi_c$ (see orbits 6 and 9, Figure 27 and Table 14).

The similarity between box-type orbits and Lissajous figures gave rise to the definition of the ratio of frequencies of oscillation in two directions (determined by comparison between box-type orbit and corresponding Lissajous figure, see section 18b). It was noted in section 18b that this ratio is not constant for the family of orbits of the energy value considered, contrary to the case of orbits of small energy (i.e. oscillations around ($\varpi = \varpi_c$, $z = 0$) with small amplitudes). The ratio increases with increasing value of ϖ_A, from about 0.5 to 1.0 (see Table 14).

These properties of the box-type trajectories have been formulated *after* numerical computation, and the question presents itself whether they could have been predicted *before*hand. The present section contains an attempt to discuss this question; the complete answer is not obtained, because we have been forced to introduce certain simplifying assumptions with which the results of the numerical computations do not comply.

We shall discuss the following aspect of the analytical prediction of the geometrical properties of box-type orbits: can motion occur in a given two-dimensional potential such that the trajectory is topologically equivalent to a Lissajous figure?

At the suggestion of Prof. VAN DE HULST this question is studied by "starting at the wrong end", considering at the outset a given Lissajous figure in the cartesian (X, Y)-plane, with time T. The given figure is deformed continuously in an arbitrary manner such that (X, Y) become curvilinear coordinates in the cartesian (x, y)-plane, and the time t is chosen as some function of T, so that the motion in the (x, y)-plane is fixed. We shall attempt to choose the various transformations in such a manner that the motion in the (x, y)-plane is a motion in a field of force which can be derived from a gravitational potential function.

Let the Lissajous figure in the (X, Y)-plane be given by

$$X = \sin a\,T \quad Y = \sin b\,T\,. \qquad (22.1)$$

As we shall distort the figure there is no loss of generality putting both amplitudes equal to unity and both phases equal to zero provided a and b are not commensurate. Let the transformations of coordinates and time be written

$$x = f(X, Y) \quad y = g(X, Y) \quad t = s(T)\,. \qquad (22.2)$$

On applying the transformations (22.2) to equations (22.1) the variables x and y are determined as functions of t, as are the velocities and the accelerations; we write for these last functions the vector equations

$$\begin{pmatrix} \dot{x} \\ \dot{y} \end{pmatrix} = \begin{pmatrix} \lambda(t) \\ \mu(t) \end{pmatrix} \qquad (22.3)$$

and

$$\begin{pmatrix} \ddot{x} \\ \ddot{y} \end{pmatrix} = \begin{pmatrix} d\lambda/dt \\ d\mu/dt \end{pmatrix}. \qquad (22.4)$$

If the particle passes through a point (x, y) at time t_1, and again at time t_2, the square of the velocities must be the same in both cases, i.e.

$$\lambda^2(t_1) + \mu^2(t_1) = \lambda^2(t_2) + \mu^2(t_2). \qquad (22.5)$$

This is the *first condition* which must be imposed.

The accelerations must also be the same in both cases i.e.

$$\left.\begin{aligned} \left(\frac{d\lambda}{dt}\right)_{t_1} &= \left(\frac{d\lambda}{dt}\right)_{t_2} \\ \left(\frac{d\mu}{dt}\right)_{t_1} &= \left(\frac{d\mu}{dt}\right)_{t_2}. \end{aligned}\right\} \qquad (22.6)$$

This is the *second condition* which must be imposed in order that the motion in the distorted figure may have physical meaning. When both conditions are fulfilled, $\frac{d\lambda}{dt}$ and $\frac{d\mu}{dt}$ can be written as functions of position and then the question can be considered whether the forces which govern the motion can be derived from a potential function.

Writing f_X for $\frac{\partial f}{\partial X}$, etc. we have for the velocities

$$\begin{pmatrix} \frac{dx}{dt} \\ \frac{dy}{dt} \end{pmatrix} = \left\{ \begin{pmatrix} f_X \\ g_X \end{pmatrix} a \cos aT + \begin{pmatrix} f_Y \\ g_Y \end{pmatrix} b \cos bT \right\} \frac{dT}{dt} \qquad (22.7)$$

and for the accelerations

$$\left.\begin{aligned} \begin{pmatrix} \frac{d^2x}{dt^2} \\ \frac{d^2y}{dt^2} \end{pmatrix} &= \left\{ \begin{pmatrix} f_X \\ g_X \end{pmatrix} a \cos aT + \begin{pmatrix} f_Y \\ g_Y \end{pmatrix} b \cos bT \right\} \frac{d^2T}{dt^2} - \left\{ \begin{pmatrix} f_X \\ g_X \end{pmatrix} a^2 \sin aT + \begin{pmatrix} f_Y \\ g_Y \end{pmatrix} b^2 \sin bT \right\} \left(\frac{dT}{dt}\right)^2 \\ &+ \left\{ \begin{pmatrix} f_{XX} \\ g_{XX} \end{pmatrix} a^2 \cos^2 aT + 2 \begin{pmatrix} f_{XY} \\ g_{XY} \end{pmatrix} ab \cos aT \cos bT + \begin{pmatrix} f_{YY} \\ g_{YY} \end{pmatrix} b^2 \cos^2 bT \right\} \left(\frac{dT}{dt}\right)^2. \end{aligned}\right\} \qquad (22.8)$$

In the expressions on the right-hand side in the latter formulae, we must eliminate t and T. This can be done by making use of the first condition. From (22.1) we find

$$\left.\begin{aligned} \cos aT &= \alpha\sqrt{1 - X^2} \\ \cos bT &= \beta\sqrt{1 - Y^2} \end{aligned}\right\} \qquad (22.9)$$

with $\alpha = \pm 1$ and $\beta = \pm 1$. The two values each of α and β correspond to the fact that a given point of a Lissajous figure can be passed in 2×2 ways.

Using (22.7) and (22.9) we find for the square of the velocity

$$v^2 = \left(\frac{dT}{dt}\right)^2 \left\{ (f_X^2 + g_X^2) a^2 (1 - X^2) + (f_Y^2 + g_Y^2) b^2 (1 - Y^2) + 2 (f_X f_Y + g_X g_Y) ab\, \alpha\beta \sqrt{(1 - X^2)(1 - Y^2)} \right\}, \qquad (22.10)$$

or

$$v^2 = \left(\frac{dT}{dt}\right)^2 (M + \alpha\beta N), \qquad (22.11)$$

where M and N are functions of position only. From the first condition we infer that

$$\left(\frac{dT}{dt}\right)^2 = P(M - \alpha\beta N), \qquad (22.12)$$

in which P is a function of position only.

At this stage we make a simplification, by supposing the curvilinear coordinates (X, Y) to form an *orthogonal* set of curves in the (x, y)-plane. Then N vanishes and the first condition means that $\frac{dT}{dt}$ is a function of position only. This simplification is not essential although it clarifies the mathematical treatment immensely. In fact the unsimplified case (22.12) has raised as yet unsolved analytical difficulties[1]). The

FIGURE 34

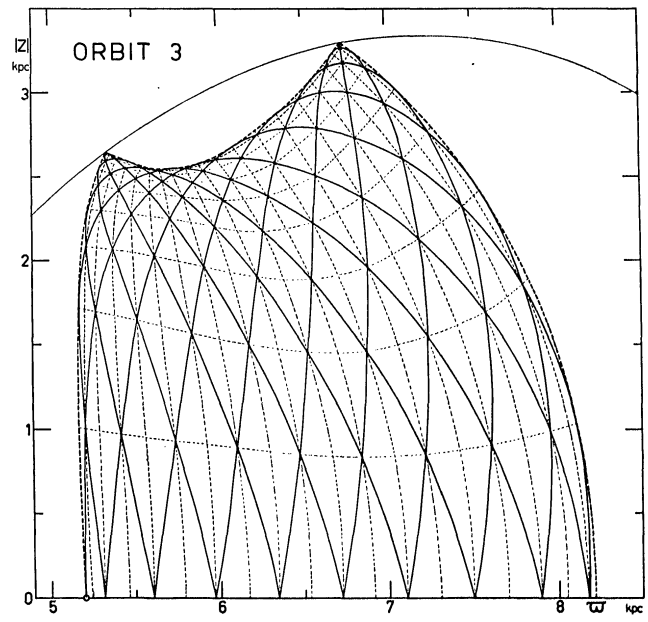

Curvilinear coordinates (X, Y), in the theory of distorted Lissajous motion (broken lines), obtained from the intersections of the periodic orbit 3 with itself.

[1]) Since this was written VAN DE HULST (1962b) has solved the general case (in which the assumption of orthogonality is not made) by a different method.

assumption of orthogonality can be checked by sketching the set of curves connecting intersections of a *periodic* orbit with itself. This has been done for orbit 3 in Figure 34, and it is seen that the broken lines do *not* form an orthogonal set of curves. Near the envelope at the vertical sections and near the corners, the broken-line curves are more nearly orthogonal than elsewhere, but near the horizontal line section, where the fold appears for higher orbits, the deviation from orthogonality is strongest.

Writing

$$\left(\frac{dT}{dt}\right)^2 = k(X, Y) \tag{22.13}$$

we have

$$\frac{d^2T}{dt^2} = \tfrac{1}{2}(k_X a \cos aT + k_Y b \cos bT) ,$$

and with (22.9), the right-hand side of (22.8) can be written as a function of X and Y, viz.

$$\begin{pmatrix} \frac{d^2x}{dt^2} \\ \frac{d^2y}{dt^2} \end{pmatrix} = \tfrac{1}{2}\left\{\begin{pmatrix} f_X \\ g_X \end{pmatrix} a\alpha\sqrt{1-X^2} + \begin{pmatrix} f_Y \\ g_Y \end{pmatrix} b\beta\sqrt{1-Y^2}\right\}(k_X a\alpha\sqrt{1-X^2} + k_Y b\beta\sqrt{1-Y^2}) - \tag{22.14}$$

$$-k\left\{\begin{pmatrix} f_X \\ g_X \end{pmatrix} a^2 X + \begin{pmatrix} f_Y \\ g_Y \end{pmatrix} b^2 Y\right\} + k\left\{\begin{pmatrix} f_{XX} \\ g_{XX} \end{pmatrix} a^2(1-X^2) + 2\begin{pmatrix} f_{XY} \\ g_{XY} \end{pmatrix}\alpha\beta ab\sqrt{(1-X^2)(1-Y^2)} + \begin{pmatrix} f_{YY} \\ g_{YY} \end{pmatrix} b^2(1-Y^2)\right\}.$$

From the second condition it follows that the coefficient of $\alpha\,\beta$ must vanish, so that

$$\left.\begin{aligned} f_X k_Y + f_Y k_X + 4 f_{XY} k = 0 \\ g_X k_Y + g_Y k_X + 4 g_{XY} k = 0 . \end{aligned}\right\} \tag{22.15}$$

These formulae are the final forms of the earlier imposed conditions for physical reality of the motion in a distorted Lissajous figure.

We may note a (trivial) solution of equations (22.15):

$$\left.\begin{aligned} k = \text{constant}\ (t \sim T) \\ f_{XY} = 0 \text{ and } g_{XY} = 0 . \end{aligned}\right\} \tag{22.16}$$

We have here the case that f and g are functions of X and Y respectively. The motion in the (x, y)-plane is then a distorted Lissajous figure consisting of mutually independent anharmonic oscillations in the x and y directions, having a rectangular envelope consisting of four straight line-sections.

Writing l_X and l_Y for k_X/k and k_Y/k respectively in (22.15), l_X and l_Y can be solved from the linear system to which (22.15) can be reduced. The solution is

$$\left.\begin{aligned} l_X = -4\frac{f_Y f_{XY} + g_Y g_{XY}}{f_Y^2 + g_Y^2} \\ l_Y = -4\frac{f_X f_{XY} + g_X g_{XY}}{f_X^2 + g_X^2} , \end{aligned}\right\} \tag{22.17}$$

for which we can write

$$\left.\begin{aligned} l_X = -2\frac{\partial}{\partial X}\log(f_Y^2 + g_Y^2) \\ l_Y = -2\frac{\partial}{\partial Y}\log(f_X^2 + g_X^2) . \end{aligned}\right\} \tag{22.18}$$

The necessary and sufficient condition for a solution of the latter equations to exist, is the compatibility relation

$$l_{XY} = l_{YX} . \tag{22.19}$$

Using (22.18) this condition can be written

$$\frac{\partial^2}{\partial X \partial Y}\{\log(f_Y^2 + g_Y^2) - \log(f_X^2 + g_X^2)\} = 0 , \tag{22.20}$$

from which it follows that

$$\frac{f_Y^2 + g_Y^2}{f_X^2 + g_X^2} = F(X) . G(Y) , \tag{22.21}$$

in which F and G are arbitrary functions of X and Y respectively.

Until now we have adapted the coordinate system (x, y) to the particular given Lissajous figure in the (X, Y)-plane and the corresponding given distorted Lissajous figure. We shall now remove this restriction by introducing a new coordinate system (ξ, η), defined by the (as yet unspecified) transformation

$$X = X(\xi) \quad Y = Y(\eta) \tag{22.22}$$

the derivatives of which are X_ξ and Y_η.

By application of this transformation, the Lissajous figure in the (X, Y)-plane defined by (22.1) is transformed into a distorted Lissajous figure in the (ξ, η)-plane. The latter is obtained from the original figure by *separate* distortions in the horizontal and vertical directions. We can now study the mapping of the (ξ, η)-plane into the (x, y)-plane. The mapping is given by the functions f and g and the transformation (22.22); f and g are functions of ξ and η by this transformation. The condition (22.21) is written in the coordinates ξ and η

$$\frac{f_\eta^2 + g_\eta^2}{f_\xi^2 + g_\xi^2} = \frac{Y_\eta^2}{X_\xi^2} . F\{X(\xi)\} . G\{Y(\eta)\} . \tag{22.23}$$

By a suitable choice of the transformation (22.22) we can make the right-hand side of this equation equal to unity. Then (22.23) reduces to

$$f_\xi^2 + g_\xi^2 = f_\eta^2 + g_\eta^2 = H(\xi, \eta) , \tag{22.24}$$

in which $H(\xi, \eta)$ is an arbitrary function. The condi-

tion (22.24) means that the mapping of the (ξ, η)-plane into the (x, y)-plane is *conformal.*

We have shown now that the conformal mapping of the (ξ, η)-plane into the (x, y)-plane is a necessary and sufficient condition for the existence of a solution to the equation (22.15) or to its equivalent (22.17). The distorted Lissajous figure in the (x, y)-plane will be bounded by simple curve sections which meet at right angles in the four corners of the box. This is indeed the case for the computed orbits. However, the sides of the box of high orbits are *not* simple curves whenever the phenomenon of a fold occurs. The description of these orbits is not possible on the basis of the theory of distorted Lissajous motion given here.

Before obtaining the potential function U as a function of ξ and η, we shall first give an existence theorem for it, in terms of the coordinates X and Y.

For (22.14) we write

$$\frac{d^2x}{dt^2} = -p(X, Y) \qquad \frac{d^2y}{dt^2} = -q(X, Y), \tag{22.25}$$

in which p (or q) is equal to the right-hand side of (22.14), without the term containing $\alpha\beta$. We must investigate now the question whether there exists a (potential) function $U(x,y)$, such that

$$\frac{d^2x}{dt^2} = -U_x \qquad \frac{d^2y}{dt^2} = -U_y$$

i.e.

$$U_x = p \qquad U_y = q \tag{22.26}$$

By the transformation (22.2), U is a function of X and Y written $u(X, Y)$, and

$$u_X = U_x f_X + U_y g_X$$
$$u_Y = U_x f_Y + U_y g_Y \tag{22.27}$$

or, with (22.26)

$$u_X = p f_X + q g_X$$
$$u_Y = p f_Y + q g_Y. \tag{22.28}$$

in which all functions are expressed in X and Y.

In order that the potential function U may exist, it must be solvable from equation (22.28), which entails the condition

$$p_Y f_X + q_Y g_X = p_X f_Y + q_X g_Y. \tag{22.29}$$

By fairly lengthy but straightforward analysis, it can be proved that this relation holds for p and q as defined in (22.14), making use of the conditions (22.15) and the orthogonality relation mentioned before.

The fact that motion in a distorted Lissajous figure is a physically possible motion in a field of force, provided that the (first) velocity condition and (second) acceleration condition hold, can also be obtained by deductive reasoning: along each part of the orbit $\int_P^Q \mathbf{a} \cdot d\mathbf{s} = \frac{1}{2}(v_Q^2 - v_P^2)$, in which $\mathbf{a}$ is the acceleration vector, $\mathbf{s}$ the position vector and $\mathbf{v}$ the total velocity. Therefore around a closed "loop" of the orbit $\oint \mathbf{a} \cdot d\mathbf{s} = 0$. Finally along any path which intersects itself this integral is also zero, as the path can be made up of orbit sections. But this means that $\mathbf{a}$ must be derivable from a potential function.

Having proved the existence of the potential function $U(x, y)$, we shall now obtain it as a function of ξ and η. In order to do so we use the definition

$$U = E - \tfrac{1}{2}v^2, \tag{22.30}$$

in which E is a constant equal to the total energy of motion in the (x,y)-plane, and v is the total velocity as before. By (22.11) we can write for this definition

$$u = E - \tfrac{1}{2}kM$$

and writing V for the function U expressed as a function of ξ and η, we have

$$V = E - \tfrac{1}{2}k\left\{\frac{f_\xi^2 + g_\xi^2}{X_\xi^2}a^2(1 - X(\xi)^2) + \frac{f_\eta^2 + g_\eta^2}{Y_\eta^2}b^2(1 - Y(\eta)^2)\right\}. \tag{22.31}$$

The function k is found from the solution of (22.18). The first of these equations can be written

$$l_\xi = -2\frac{\partial}{\partial \xi}\log H,$$

with the solution

$$l = -2\log H + \text{constant},$$

which gives

$$k = \frac{1}{H^2}$$

absorbing the constant into the arbitrary function H. Substituting this expression for k in (22.31), and using (22.24) we find finally for the potential function expressed in the coordinates ξ and η

$$V = E - \frac{1}{2H}\left\{\frac{a^2(1 - X(\xi)^2)}{X_\xi^2} + \frac{b^2(1 - Y(\eta)^2)}{Y_\eta^2}\right\}. \tag{22.32}$$

Van de Hulst (*op. cit.*), who obtained the same equation by different reasoning, has given the form of H for which the potential V takes Stäckel's standard form for separable systems. For such dynamical systems the form of the potential function is given in section 11 of the present work for various coordinate systems of interest in connection with the field of force of the galactic system.

However, not fully separable systems can also be described by the potential function (22.32). For the form of H for this case and further particulars the reader is referred to the article by Prof. VAN DE HULST already cited.

23. *Inferences for the velocity ellipsoid*

Since the present discussion of the orbits of particles of mass in the Galaxy is confined to one type of orbit and one energy value, any inferences concerning the velocity ellipsoid are necessarily provisional. The box-type orbits, however, would seem to form an important class of orbits, while on the basis of distorted Lissajous motion we have derived an existence theorem of box-type orbits in a field of force derivable from a potential function. Therefore a tentative review of the influence of this type of orbit on stellar statistics, does not seem out of place.

In section 18c it was pointed out that of the ∞^2 orbits in a family, ∞^1 are asymptotically equal because each of the ∞^1 orbits in a box will be reached asymptotically by an arbitrary non-periodic orbit of the box. Since all orbits of the box are thus obtained from the special orbit started at $(\varpi = \varpi_A, z = 0)$, with $\Pi = 0$ and $Z = \sqrt{2(E - \Phi)}$, the coordinate ϖ_A is a parameter, the value of which defines the ∞^1 orbits of the box.

That it is possible in this way to select ∞^1 asymptotically equal orbits, which are different from all other orbits in the family, is contrary to the *ad hoc* assumption of section 2 that the galactic potential function admits no other time-independent integrals of motion besides the integral of energy and angular momentum. Under that assumption, which was used in deriving JEANS' theorem of the equality of the meridional axes of the velocity ellipsoid, all ∞^2 orbits in the family are asymptotically equal.

The conclusion is that the *ad hoc* assumption is erroneous and must be replaced by the assumption that, if the potential function of the Galaxy can be represented by an analytical formula such as the formula IF discussed in section 15, it admits, besides the energy- and angular momentum integral, a *third integral of motion.* The analytical form of this integral for the formula IF has not been found, but the consequences of its existence, for the selected family of orbits, are found in the inclination diagram of Figure 32. The transformation T of the inclination diagram into itself, which was introduced in section 17 as a means of discussing properties of meridional trajectories, has the special properties described in section 20, and these reflect the existence of the third integral of motion.

The question, raised in section 6, whether and how conversion of energy from z-motion into ϖ-motion takes place for individual orbits of high-velocity stars, can also be answered now: there is temporary exchange during a revolution, but *no* systematic conversion. Stars which have low Π-velocities passing the galactic plane, will not gain Π-momentum at the cost of Z-momentum.

The inference for the velocity ellipsoid can now be drawn. As the proof of JEANS' theorem rests upon an erroneous assumption, the dispersions of the velocity-distribution function in the meridional plane need not be equal. Our result can also be formulated as follows: Numerical computations of orbits of particles of mass in the Galaxy indicate that the field of force of the Galaxy may for indefinite time admit of a tri-axial distribution of velocities in a large region of space.

A large part of the work connected with the investigation, such as the coding of the programme for the numerical computations, was done in collaboration with Dr INGRID TORGÅRD.

During an eight months' stay in Lund in 1959, the author enjoyed the hospitality of Prof. Dr C. SCHALÉN of Lund Observatory and his staff. At Lund Observatory many computations—all of those upon which the inclination diagram is based—were performed by Miss INGEBORG OLSSON; many photographic reproductions and some drawings were made by Mr M. VIELOCH.

Discussions with Dr P. O. LINDBLAD during the 1960 NUFFIC Summer School at Nyenrode Castle in the Netherlands, led to the formulation of section 21.

The Mathematisch Centrum, Amsterdam, has put the electronic computer ARMAC at the disposal of the author for many hours computing time, free of charge. At the Matematikmaskin Nämnd, Stockholm, the large Swedish electronic computer BESK was occupied for many hours with the computation of the orbits reported upon in this work, also free of charge.

Finally the author wishes to record his feelings of obligation to the Netherlands Organisation for the Advancement of Pure Research (Z.W.O.) for financial support.

REFERENCES

G. B. VAN ALBADA 1952, *Proceedings Koninkl. Nederl. Akademie van Wetenschappen*, Series B, **55**, No. 5, 620 (*Bosscha Contr.* No. 1).

G. D. BIRKHOFF 1922, *Act. Math.* **43**, 1.

G. D. BIRKHOFF 1927, "Dynamical Systems", *Am. Math. Soc. Coll. Publ.* IX.

G. D. BIRKHOFF 1927, *Am. Journ. of Math.* XLIX, 1.

A. BLAAUW 1961, *B.A.N.* **15**, 265 (No. 505).

G. L. CAMM 1941, *M.N.R.A.S.* **101**, 195.

G. L. CAMM 1955, "Vistas in Astronomy", Vol. I, p. 216. Beer, Pergamon Press, London and New York.

S. CHANDRASEKHAR 1942, "Principles of Stellar Dynamics", Univ. Chicago Press.

S. CHANDRASEKHAR and G. MÜNCH 1950, *Ap. J.* **112**, 380.

L. COLLATZ 1955, "Numerische Behandlung von Differentialgleichungen", 2 Ed., Springer-Verlag, Berlin, Göttingen, Heidelberg.

G. CONTOPOULOS 1957, *Stockholms Obs. Ann.* **19**, No. 10.

G. CONTOPOULOS 1958, *Stockholms Obs. Ann.* **20**, No. 5.

G. CONTOPOULOS 1960, *Zs. f. Ap.* **49**, 273.

A. S. EDDINGTON 1916, *M.N.R.A.S.* LXXVI, 37.

W. FRICKE 1951, *A.N.* **280**, 193.

H. GOLDSTEIN 1957, "Classical Mechanics", Addison-Wesley Publ. Comp., Reading, Mass., U.S.A.

E. R. HILL 1960, *B.A.N.* **15**, 1 (No. 494).

H. C. VAN DE HULST 1962a, *B.A.N.* **16**, 235 (No. 520).

H. C. VAN DE HULST 1962b, to be published in *B.A.N.*, shortly.

J. H. JEANS 1916, *M.N.R.A.S.* LXXVI, 70.

J. H. JEANS 1919, "Problems of Cosmogony and Stellar Dynamics", Cambridge, England; p. 230.

E. KASNER 1913, "Differential-geometric aspects of dynamics", *Lectures on Mathematics*, Princeton Colloquium; Am. Math. Soc.

B. V. KUKARKIN and P. P. PARENAGO 1948, "General Catalogue of Variable Stars", Moscow.

R. KURTH 1957, "Introduction to the Mechanics of Stellar Systems", Pergamon Press, London, New York and Paris.

G. G. KUZMIN 1953, *Tartu Astr. Obs.*, Teated No. 1.

G. G. KUZMIN 1956, *Tartu Astr. Obs.*, Teated No. 2.

G. G. KUZMIN 1956, *Astr. Journ. U.S.S.R.* **33**, 27.

T. LEVI-CIVITA 1927, *Abh. Math. Sem. Hamburg*, V. Band, 323.

B. LINDBLAD 1933, *Handb. d. Astrophysik* 5^2, 1047.

B. LINDBLAD 1959, *Handbuch der Physik, Band LIII, Astrophysik IV*, p. 21.

P. O. LINDBLAD 1960, *Stockholms Obs. Ann.* **21**, No. 4, 67.

H. NORDSTRÖM 1936, *Lund Medd.*, Ser. II, No. 79.

J. H. OORT 1928, *B.A.N.* **4**, 269 (No. 159).

J. H. OORT 1960, *B.A.N.* **15**, 45 (No. 494).

D. E. OSTERBROCK 1952, *Ap. J.* **116**, 164.

E. D. PAVLOVSKAYA 1953, *Variable Stars* **9**, No. 6 (84).

H. POINCARÉ 1892, "Les méthodes nouvelles de la mécanique céleste", Gauthiers-Villars, Paris.

M. SCHMIDT 1956, *B.A.N.* **13**, 15 (No. 468).

K. SCHWARZSCHILD 1907, *Nachr. Akad. Wiss. Göttingen, Math.-Physik. Kl.*, 614.

L. SPITZER JR. and M. SCHWARZSCHILD 1951, *Ap. J.* **114**, 385.

L. SPITZER JR. and M. SCHWARZSCHILD 1953, *Ap. J.* **118**, 106.

P. STÄCKEL 1890, *Math. Ann.* XXXV, 91.

P. STÄCKEL 1891, "Über die Integration der Hamilton-Jacobischen Differentialgleichung mittelst Separation der Variabeln", Habilitationsschr., Halle.

J. P. VINTI 1959a, *J. of Research* **63** B, No. 2.

J. P. VINTI 1959b, *Physical Rev. Letters*, **3**, No. 1.

A. N. VYSSOTSKY 1957, *P.A.S.P.* **69**, 109.

J. WEINACHT 1923, *Math. Ann.* **90**, 279.

E. T. WHITTAKER 1904, "A Treatise on the Analytical Dynamics of Particles and Rigid Bodies", Cambridge, England.

A. WINTNER 1947, "The analytical foundation of celestial mechanics", Princeton Univ. Press.

R. V. D. R. WOOLLEY 1960, "Vistas in Astronomy", Vol. III, p. 3, Beer, Pergamon Press, London and New York.